DOE/CONF-941022

Proceedings of the 5th International Conference on Stability and Handling of Liquid Fuels

Rotterdam, the Netherlands
October 3-7, 1994

Volume 2

Edited by Harry N. Giles
Office of Technical Management
Deputy Assistant Secretary for Strategic Petroleum Reserve
Assistant Secretary for Fossil Energy

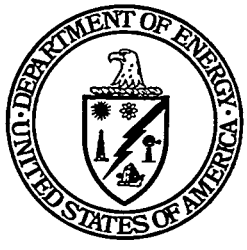

U.S. Department of Energy
Washington, DC

1995

Printed with soy ink on recycled paper

Previous Conferences

Conference on Long Term Storage Stabilities of Liquid Fuels, Tel Aviv, Israel, July 11-14, 1983. Proceedings published by the Israel Institute of Petroleum and Energy, Nahum Por, editor; Tel Aviv, Israel, December 1983.

2nd International Conference on Long-Term Storage Stabilities of Liquid Fuels, San Antonio, Texas, USA, July 29-August 1, 1986. Proceedings published by the Southwest Research Institute, Leo L. Stavinoha, editor; San Antonio, Texas, USA, October 1986.

3rd International Conference on Stability and Handling of Liquid Fuels, London, England, September 13-16, 1988. Proceedings published by the Institute of Petroleum (London), R. W. Hiley, R. E. Penfold, and J. F. Pedley, editors; London, England, November 1988.

4th International Conference on Stability and Handling of Liquid Fuels, Orlando, Florida, USA, November 19-22, 1991. Proceedings published by the U. S. Department of Energy, Harry N. Giles, editor; Washington, DC, USA, 1992.

Contents

*Author to whom correspondence should be addressed.

Session 2: Microbiology. Dr. R. A. Neihof, Chair.

Session 3-A: Jet Fuels - II. Dr. A. Roberts, Chair.

Session 4-C: Gasolines. A. E. Zengel, Chair.

Session 4-D: Heavy Oils and Refinery Processing. Dr. J. D. Bacha, Chair.

Session 5: Middle Distillate Fuels - I. Dr. B. Batts, Chair.

Poster Session: Dr. D. R. Hardy, Chair.

...

Contributors

Adiwar Research and Development Center for Oil and Gas Technology (Lemigas), P.O. Box 1089/JKT, Jakarta 10010, Indonesia

Agrawal, K.M. Indian Institute of Petroleum, Dehradun - 248 005, India

Anderson, S.D. USAF Wright Laboratory, 1790 Loop Road North, Wright-Patterson AFB, OH 45433-7103, USA

Arumugam, R. Fuel Science Program, Department of Materials Science and Engineering, The Pennsylvania State University, University Park, PA 16802, USA

Aswal, D.S. Indian Institute of Petroleum, Dehradun - 248 005, India

Bacha, J.D. Chevron Research & Technology Co., 100 Chevron Way, Richmond, CA 94802-0627, USA

Baker, C. BP Research and Engineering Centre, Chertsey Road, Sunbury-on-Thames, Middx. TW16 7LN, UK

Balster, W.J. Systems Research Laboratories, Inc., 2800 Indian Ripple Road, Dayton, OH 45400-3696, USA

Batt, R.J. The Associated Octel Company Ltd., Watling Street, Bletchley, Milton Keynes MK1 1EZ, UK

Batts, B.D. School of Chemistry, Macquarie University, Sydney, NSW 2109, Australia

Bauldreay, J.M. Shell Research Ltd., Thornton Research Centre, P.O. Box 1, Chester CH1 3SH, UK

Beal, E.J. Naval Research Laboratory, Code 6180, Washington, DC 20375-5342, USA

Beaver, B.D. Department of Chemistry and Biochemistry, Duquesne University, Pittsburgh, PA 15282, USA

Ben-Asher, J. The Israel Institute of Petroleum and Energy, P.O. Box 17081, Tel Aviv 61170, Israel

Beverdam, H.J. Netherlands National Petroleum Stockpiling Agency, Blaak 22, 3011 TA Rotterdam, the Netherlands

Binns, K.E. University of Dayton Research Institute, 300 College Park Drive, Dayton, OH 45469-0140, USA

Boneva, M.I. Institute of Organic Chemistry, Bulgarian Academy of Sciences, 1113 Sofia, Bulgaria

Chesneau, H.L. Fuel Quality Services, Inc., P.O. Box 1380, Flowery Branch, GA 30542, USA

Chin, L.P. Systems Research Laboratories, Inc., 2800 Indian Ripple Road, Dayton, OH 45400-3696, USA

Clark, R.H. Shell Research Ltd., Thornton Research Centre, P.O. Box 1, Chester CH1 3SH, UK

Crawford, J.D. Nalco/Exxon Energy Chemicals L.P., P.O. Box 87, Sugar Land, TX 77487-0087, USA

Dacre, B. Royal Military College of Science, Cranfield University, Shrivenham, Swindon, Wilts. SN6 8LA, UK
Daniels, D.A. Basic Fuel Services, 2 East Blackwell St., Ste. 29, Dover, NJ 07801, USA
David, P. BP Research and Engineering Centre, Chertsey Road, Sunbury-on-Thames, Middx. TW16 7LN, UK
Demunshi, R. Department of Chemistry and Biochemistry, Duquesne University, Pittsburgh, PA 15282, USA
Derst, P. Marie-Curie-Str. 64, D-76139, Karlsruhe, Germany
Dessens, C. W. M. Ministry of Economic Affairs, P.O. Box 20101, 2500 EC The Hague, The Netherlands
Dickout, S.J. National Defence Headquarters, DSE 6-2-2, MGen George R. Pearkes Bldg., Ottawa, Ontario K1A 0K2, Canada
Dieterle, G.L. University of Dayton Research Institute, 300 College Park Drive, Dayton, OH 45469-0140, USA
Edwards, T. USAF Wright Laboratory, 1790 Loop Road North, Wright-Patterson AFB, OH 45433-7103, USA
Eser, S. Fuel Science Program, Department of Materials Science and Engineering, The Pennsylvania State University, University Park, PA 16802, USA
Fass, R. Department of Biotechnology, Israel Institute for Biological Research, Ness Ziona 70450, Israel
Flohr, K.W. ARTECH Corp., 14554 Lee Road, Chantilly, VA 22021-1632, USA
Georgiev, P.T. SciBulCom, Ltd., P.O. Box 249, 1113 Sofia, Bulgaria
Gergova, K.M. Fuel Science Program, Department of Materials Science and Engineering, The Pennsylvania State University, University Park, PA 16802, USA
Geva, J. Department of Biotechnology, Israel Institute for Biological Research, Ness Ziona 70450, Israel
Giannini, R.M. Naval Surface Warfare Center, Carderock Division, 3A Leggett Circle, Annapolis, MD 21402-5067, USA
Giles, H.N. U.S. Department of Energy (FE-422), 1000 Independence Avenue, SW, Washington, DC 20585, USA.
Goss, L.P. Systems Research Laboratories, Inc., 2800 Indian Ripple Road, Dayton, OH 45400-3696, USA
Grinstead, R.R. University of Dayton Research Institute, Aerospace Mechanics Division/KL-463, 300 College Park, Dayton, OH 45469-0140, USA
Gutman, M. Internal Combustion Engines Laboratory, Faculty of Mechanical Engineering, Technion, Haifa 32000, Israel
Hardy, D.R. Naval Research Laboratory, Code 6180, Washington, DC 20375-5342, USA
Harrison, W.E, III USAF Wright Laboratory, 1790 Loop Road North, Wright-Patterson AFB, OH 45433-7103, USA
Hartman, J. Department of Mathematics, Israel Institute for Biological Research, Ness Ziona 70450, Israel

Hartstein, A.M. U.S. Department of Energy (FE-32), 1000 Independence Avenue, SW, Washington, DC 20585, USA
Heins, R.J. Shell Research Ltd., Thornton Research Centre, P.O. Box 1, Chester CH1 3SH, UK
Henry, C.P. Octel America, Inc., c/o DuPont, Petroleum Laboratory (P), Chambers Works, Deepwater, NJ 08023, USA
Heneghan, S.P. University of Dayton Research Institute, Aerospace Mechanics Division, 300 College Park Avenue, Dayton, OH 45469-0140, USA
Hetherington, J.I. Royal Military College of Science, Cranfield University, Shrivenham, Swindon, Wilts. SN6 8LA, UK
Hietkamp, S. CSIR, P.O. Box 395, Pretoria 0001, South Africa
Hill, E.C. ECHA Microbiology Ltd., Unit M210 Cardiff Workshops, Lewis Road, Cardiff, CF1 5EJ, UK
Hill, G.C. ECHA Microbiology Ltd., Unit M210 Cardiff Workshops, Lewis Road, Cardiff, CF1 5EJ, UK
Hughes, J.M. Naval Research Laboratory, Code 6180, Washington, DC 20375-5342, USA
Ishai, A. P.O. Box 7415, 31073 Haifa, Israel
Ivanov, Sl.K. SciBulCom, Ltd., P.O. Box 249, 1113 Sofia, Bulgaria
Jones, E.G. Systems Research Laboratories, Inc., 2800 Indian Ripple Road, Dayton, OH 45400-3696, USA
Joshi, G.C. Indian Institute of Petroleum, Dehradun - 248 005, India
Kalitchin, Zh.D. SciBulCom, Ltd., P.O. Box 249, 1113 Sofia, Bulgaria
Kamin, R. A. Naval Air Warfare Center, Aircraft Division, Trenton, NJ 08628, USA
Kassinger, R. DNV Petroleum Services, 111 Galway Place, Teaneck, NJ 07666, USA
Kauffman, R.E. University of Dayton Research Institute, Fluid Analysis Laboratory, 300 College Park Avenue, Dayton, OH 45469-0140, USA
Kelly, J.F. CANMET, Energy Research Laboratories, Natural Resources Canada, Ottawa, Ontario K1A 0G1, Canada
Kirzhner, Y. Internal Combustion Engines Laboratory, Faculty of Mechanical Engineering, Technion, Haifa 32000, Israel
Klinkhammer, M.D. Naval Surface Warfare Center, Carderock Division, Annapolis, MD 21402-5067, USA
Koenig, J.W.J. Erdölbevorratungsverband, Postfach 30 15 90, 20305 Hamburg, Germany
Krenis, G. The Israel Institute of Petroleum and Energy, P.O. Box 17081, Tel Aviv 61170, Israel
Lacey, P.I. Belvoir Fuels & Lubricants Research Facility, Southwest Research Institute, P.O. Drawer 28510, San Antonio, TX 78228-0510
Lavie, I. Bromine Compounds Ltd., P.O. Box 180, Be'er Sheva, 84101, Israel
Lavy, Z. Logistics Headquarters, Israel Defense Forces, Military P.O. 02306, Israel
Lenz, U. Rheinbraun A.G., Stüttgenweg 2, 5000 Köln (Lindenthal), Germany
Luria, D. The Israel Ministry of Energy, The Fuel Authority, P.O. Box 33541, Haifa 31334, Israel

Marais, B. National Petroleum Refiners of South Africa (Pty) Ltd., P.O. Box 234, Sasolburg 9570, South Africa
Marshman, S.J. Defense Research Agency, Fighting Vehicles and Systems/Fuels and Lubricants Department, Fairmile, Cobham, Surrey KT11 1BJ, UK
Martin, C.J. Defense Fuel Supply Center, Cameron Station, Alexandria, VA 22304-6160, USA
McInnis, L.A. Belvoir Fuels & Lubricants Research Facility, Southwest Research Institute, P.O. Drawer 28510, San Antonio, TX 78228-0510
McVea, G.G. Airframes and Engines Division, Aeronautical and Maritime Research Laboratory, 506 Lorimer Street, Fishermens Bend, Victoria 3207, Australia
Morris, R.E., Naval Research Laboratory, Code 6181, Washington, DC 20375-5342, USA.
Morris, R.W. U.S. Air Force, Wright Laboratory, 1790 Loop Road North, Wright-Patterson AFB, OH 45433-7103, USA
Morse, B.W. Nordre Ås, Jeløy, 1514 Moss, Norway
Motohashi, K. Chemical Inspection & Testing Institute, 4-1-1 Higashi-Mukojima, Sumida-ku, Toyko 131, Japan
Muth, C.L. Nalco/Exxon Energy Chemicals L.P., P.O. Box 87 Sugar Land, TX 77487-0087, USA
Nagpal, J.M. Indian Institute of Petroleum, Dehradun - 248 005, India
Nakazono, K. Chemical Inspection & Testing Institute, 4-1-1 Higashi-Mukojima, Sumida-ku, Toyko 131, Japan
Neihof, R.A. Naval Research Laboratory, Code 6180, Washington, DC 20375-5320, USA
Oki, M. Chemical Inspection & Testing Institute, 4-1-1 Higashi-Mukojima, Sumida-ku, Toyko 131, Japan
Pande, S.G., Geo-Centers, Inc., 10903 Indian Head Hwy., Ft. Washington, MD 20744, USA
Passman, F.J. Biodeterioration Control Associates, Inc., P.O Box 268176, Chicago, IL 60626-8176, USA
Petersen, S. Søren Schierbeck & Co. ApS, Sabroesvaj 15 A 2, DK-3000 Helsingør, Denmark
Pilviö, O. Neste Oy, R & D Services, P.O. Box 310, FIN-06101 Porvoo, Finland
Porlier, B.W. Nalco/Exxon Energy Chemicals L.P., P.O. Box 87, Sugar Land, TX 77487-0087, USA
Power, A.J. Airframes and Engines Division, Aeronautical and Maritime Research Laboratory, 506 Lorimer Street, Fishermens Bend, Victoria 3207, Australia
Propes, J. Department of Biotechnology, Israel Institute for Biological Research, Ness Ziona 70450, Israel
Rahimi, P.M. CANMET, Energy Research Laboratories, Natural Resources Canada, Ottawa, Ontario K1A 0G1, Canada
Roberts, A. Energy Plans & Policy Branch (N420), Strategic Sealift Programs Division, 2000 Navy Pentagon, Washington, DC 20350-2000, USA
Sarkar, G.N. Gujarat Refinery, Indian Oil Corp., Ltd., P.O. Jawaharnagar, Vadodara - 391 320, India
Saxena, G.C. R.B.S. College, Agra, India

Schobert, H.H. Fuel Science Program, Department of Materials Science and Engineering, The Pennsylvania State University, University Park, PA 16802, USA
Sharief, V. Department of Chemistry and Biochemistry, Duquesne University, Pittsburgh, PA 15282, USA
Sharma, Y.K. Indian Institute of Petroleum, Dehradun - 248 005, India
Shaver, B.D. Naval Surface Warfare Center, Carderock Division, 3A Leggett Circle, Annapolis, MD 21402-5067, USA
Shouse, D.T. USAF Wright Laboratory, 1790 Loop Road North, Wright-Patterson AFB, OH 45433-7103, USA
Shuftan, M. Logistics Headquarters, Israel Defense Forces, Military P.O. 02306, Israel
Siegert, W. Schülke & Mayr GmbH, Robert-Koch-Straße 2, D-22840 Norderstedt, Germany
Singh, I.D. Indian Institute of Petroleum, Dehradun - 248 005, India
Skoog, P.-Å. Celsius Materialteknik AB, Box 13 200, S-580 13 Linköping, Sweden
Sommer, S. "Delek" - The Israel Fuel Corporation, P.O. Box 50250, Tel Aviv 61500, Israel
Stavinoha, L.L. Belvoir Fuels & Lubricants Research Facility, Southwest Research Institute, P.O. Drawer 28510, San Antonio, TX 78228-0510
Strauss, K. H., 69 Brookside Road, Portland, ME 04103-4609, USA.
Street, J.P. Nalco/Exxon Energy Chemicals L.P., P.O. Box 87, Sugar Land, TX 77487-0087, USA
Strucko, R. Naval Surface Warfare Center, Code 859, 3A Leggett Circle, Annapolis, MD 21402-5067, USA
Sufrin, Y. Logistics Headquarters, Israel Defense Forces, Military P.O. 02306, Israel
Tanielyan, S.K. Seton Hall University, South Orange, NJ 07079-2694, USA
Tartakovsky, L. Internal Combustion Engines Laboratory, Faculty of Mechanical Engineering, Technion, Haifa 32000, Israel
Taskila, S.M. Amoco Oil Company, Research Center, P.O. Box 3011, Naperville, IL 60565-7011, USA
Taylor, S.E. BP Research and Engineering Centre, Chertsey Road, Sunbury-on-Thames, Middx. TW16 7LN, UK
Teng, Y. Department of Chemistry and Biochemistry, Duquesne University, Pittsburgh, PA 15282, USA
Terebenina, A. Institute of Inorganic Chemistry, Bulgarian Academy of Sciences, 1113 Sofia, Bulgaria
Thomsen, E.S. Søren Schierbeck & Co. ApS, Sabroesvaj 15 A 2, DK-3000 Helsingør, Denmark
Tian, D. Department of Chemistry and Biochemistry, Duquesne University, Pittsburgh, PA 15282, USA
Todorova, O. Institute of Inorganic Chemistry, Bulgarian Academy of Sciences, 1113 Sofia, Bulgaria
Torres-Ordonez, R.J. Amoco Oil Company, Research Center, P.O. Box 3011, Naperville, IL 60565-7011, USA

Turner, L. M. Defense Fuel Supply Center, Cameron Station, Alexandria, VA 22304-6160, USA

Venter, J.J. National Petroleum Refiners of South Africa (Pty) Ltd., P.O. Box 234, Sasolburg 9570, South Africa

Viljoen, C.L. Sasol Oil R&D, P. O. Box 1, Sasolburg 9579, South Africa

Waynick, J.A. Amoco Oil Company, Research Center, P.O. Box 3011, Naperville, IL 60565-7011, USA

Wechter, M.A., Department of Chemistry, The University of Massachusetts, Dartmouth, North Dartmouth, MA 02747, USA

Weiss, A. Logistics Headquarters, Israel Defense Forces, Military P.O. 02306, Israel

Westbrook, S.R. Belvoir Fuels & Lubricants Research Facility, Southwest Research Institute, P.O. Drawer 28510, San Antonio, TX 78228-0510

White, E.W. Naval Surface Warfare Center, Code 632, 3A Leggett Circle, Annapolis, MD 21404-5067, USA

Whitesmith, P.R. Conoco Ltd., Conoco Centre, Warwick Technology Park, Gallows Hill, Warwick CV34 6DA, UK

Williams, T. University of Dayton Research Institute, 300 College Park Drive, Dayton, OH 45469-0140, USA

Woodward, A.J. BP Research and Engineering Centre, Chertsey Road, Sunbury-on-Thames, Middx. TW16 7LN, UK

Zabarnick, S. University of Dayton Research Institute, Aerospace Mechanics Division/KL-463, 300 College Park, Dayton, OH 45469-0140, USA

Zengel, A.E. Coordinating Research Council, Inc., 219 Perimeter Center Parkway, N.E., Atlanta, GA 30346-1301, USA

Zvirin, Y. Internal Combustion Engines Laboratory, Faculty of Mechanical Engineering, Technion, Haifa 32000, Israel

• • •

Author Index

...

Preface

Two measures of the success of an international conference are the number of attendees and the number of countries that they represent. Based on these criteria, the 5th International Conference on Stability and Handling of Liquid Fuels was very successful, with 203 attendees from 28 countries. This is the largest number of countries ever represented at these conferences. These figures are highly gratifying to me, in my role as conference chairman. Because of the continuing recession that began before the 1991 conference, many companies and organizations have curtailed or eliminated attendance at international conferences. These cutbacks have especially affected attendance at specialized conferences such as this.

From the papers presented at this conference, jet fuels and other middle distillates continue to be the subject of considerable study. The microbial aspect of petroleum degradation is another subject that still attracts much attention. The use of computer-based expert systems for monitoring storage stability and predicting when products should be used or replaced is on the increase. The causes of fuel degradation apparently are better understood, and less attention was devoted to this topic than in previous years. Interest continues in quality of refined products stored in strategic stockpiles. Test rigs and simulators are now widely used in evaluating stability. New methods for measurement of deposits formed during degradation have been developed and older methods revised. The effects of metals and heterocompounds on gasoline storage stability also continue to be studied.

A broad topic coming to the forefront is that of environmentally-friendly or *green fuels*. Within the United States, legislative initiatives and an enlightened environmental awareness have resulted in stricter practices at fuel handling and storage facilities. The Clean Air Act Amendments of 1990 are requiring refiners to reformulate their fuels or turn to alternate compositions. For marketing in certain ozone nonattainment areas, gasoline must contain at least 2 percent oxygen, and less benzene and other aromatics than previously allowed. By the year 2000, the entire U.S. gasoline pool may be reformulated. Diesel fuel must have an ultra-low sulfur content, and it is possible that even home heating oil may eventually have to conform to this new standard. Product imports must also meet current environmental and statutory requirements. This is compelling offshore refineries to upgrade their processes to produce cleaner fuels for the U.S. market. Because reformulated fuels have only recently appeared in the marketplace, little is known how many of them will withstand the rigors of handling and storage, or succumb to microbial attack. In Europe as well, changes are taking place in the composition of fuels in response to a growing environmental awareness. Many countries are beginning to adopt more stringent policies regarding fuel composition. The world crude oil stream is getting heavier and higher in sulfur, which is complicating the need to produce cleaner fuels. More severe processing is necessary, therefore, to obtain specification products. Moreover, there is a greater tendency to upgrade the bottom of the barrel to provide more transportation fuels in response to rapid growth in demand. These trends are exacerbating problems with product quality and stability.

We are witnessing one of the most dramatic changes in the composition of fuels in more than 50 years. Consequently, the timing of the 5th conference probably could not have been better. Several papers were presented that discussed various aspects of the new fuels that are appearing. I expect the stability and handling of these "future fuels" will be a major theme of the 6th conference. Whatever their composition, we will continue to face the same problems identified by the National Petroleum Council more than 50 years ago, namely: instability, incompatibility, and contamination.

I thank the following who provided generous support for this conference: U.S. Al-Ghamdi; Chevron; Biodeterioration Control Associates; Ethyl; Fuel Quality Services, Inc.; Fina Nederland; KLM, Royal Dutch Airlines; Nalco/Exxon Energy Chemicals, L.P.; Octel America; Paktank International BV; and Rohm and Haas. The Dutch Ministry of Economic Affairs was the conference host and provided invaluable support to the organizers. I am also grateful to the many people that helped me in organizing this conference. I am especially indebted to Mrs. Shirley Bradicich and Mrs. Jan Tucker of the Coordinating Research Council who so admirably handled many arrangements and administrative details. Finally, I thank everyone that attended the conference. Their interest and support ultimately make these conferences successful.

Harry N. Giles
Conference Chairman

5TH INTERNATIONAL CONFERENCE ON STABILITY AND HANDLING OF LIQUID FUELS
Rotterdam, the Netherlands
October 3-7,1994

THICKNESS MEASUREMENT OF JFTOT TUBE DEPOSITS BY ELLIPSOMETRY

Clive Baker, Peter David, Spence E Taylor, Andy J Woodward*
(Co-sponsored by BP Oil and UK MOD (PE))

BP Oil
Chertsey Road
Sunbury-on-Thames
Middx, TW16 7LN
UNITED KINGDOM

ABSTRACT

Thickness measurement of Jet Fuel Thermal Oxidation Test (JFTOT) tube deposits has long been a desirable goal to characterise better the thermal stability of jet fuels. The current visual rating method used for specification purposes suffers from the drawback of operator subjectivity and provides little information on the thickness and volume of deposits, parameters which are far more meaningful for characterising fuels for users and suppliers. Ellipsometry has been identified as a suitable technique for measuring the thickness of JFTOT tubes. Such a system would be robust and non-destructive; cover the important thickness range with regard to visual ratings; provide quick and easy absolute measurement of thickness; enable single spot and profiling measurements; and there would be no restriction on minimum deposit thickness.

1. INTRODUCTION

Previous work[1] has shown that the current visual rating method for JFTOT tube deposits used for specification purposes suffers from the drawback of operator subjectivity which is the main cause of lack of reproducibility of visual rating of tubes between laboratories. The visual rating method also provides little or no information on the thickness and volume which are far more meaningful for characterising fuels especially for aircraft and engine manufacturers. Poor reproducibility was also observed for JFTOT breakpoint measurement (ie the highest temperature for a pass rating) with maximum variations of 15°C and associated errors of 6.5° C which was considered unacceptable for a research tool.

In order to achieve a better understanding of the chemistry of jet fuel degradation, BP Sunbury has used SEM/EDX (Scanning Electron Microscope/Energy Dispersive Analysis of X-Ray) for chemical characterisation of JFTOT tubes[2]. However, one of the restrictions of the

technique was that elemental concentration was expressed in terms of ratios of the specific element to aluminium from the tube itself, eg C/Al, Cu/Al. In order to build up an improved picture of thermal degradation mechanism as related to the JFTOT tests, it is important to combine film thickness with deposit compositional information. Ellipsometry has been identified as a suitable technique for measuring the thickness of JFTOT tube deposits. This paper describes the principles of ellipsometry and demonstrates the relationship between visual rating and deposit thickness / volume for a range of fuels. The potential of ellipsometry for quality assurance purposes, as an alternative to the current requirement of visual rating, and for research applications is also discussed.

2. EXPERIMENTAL

2.1 Ellipsometry

The principles of ellipsometry were first laid down by Drude in 1889, but it is only recently that the technique has found more widespread use, particularly in the semi-conductor industry, as computing systems have become more available to solve the extremely complex mathematical equations necessary. The ellipsometric measurement is based on the change in state of polarisation of light reflected from a surface and is dependent on the substrate refractive index and absorption coefficient, and the film absorption coefficient, refractive index and thickness (see Figure 1). Ellipsometry is capable of measuring film thickness in the range of 1 - 6000 nm, but does require a reflecting (smooth) surface.

The instrument used in the present study was a Plasmos SD2000 system designed principally for examining semiconductors (eg silicon) wafers, but modified slightly to enable profiling of JFTOT tubes. There are several different techniques for the determination of polarisation changes upon reflection, each yielding different information. The present instrument operates on the rotating analyser principle, enabling the ellipsometric parameters tan Ψ, the intensity of reflection of radiated light compared with that of the incident light, and Δ, the relative phase difference of the material under test to be determined. From these parameters, film thickness and refractive indices can be computed. Two different cases can be considered. In the first case, the incident light is reflected directly from the substrate surface with no film on the surface, for which the Drude equation is of the type

$$\tan \Psi \exp(\Delta) = f\,(N_{sub}, N_o, \phi\ )$$

where N_{sub} and N_o are the refractive indices of the substrate and medium, respectively, f is a function of N_{sub} and N_o, and ϕ is the angle of incidence. Since N_o the refractive index of air is 1 and ϕ is known, N_{sub} can be determined.

In the presence of a thin film deposited on the surface of the substrate, the corresponding Drude equation is of the form

$$\tan \Psi \exp(i\Delta) = f \quad (N_o, N_{film}, k, N_{sub}, \lambda, \phi, t)$$

where N_{film} is the refractive index of the film, λ is the wavelength of the incident light, k is the relevant absorption coefficient and t the film thickness. This represents the situation for a homogeneous film of uniform thickness. In reality, however, these circumstances are rarely encountered, and rough films of non-uniform (optical) properties are more likely to be the case. The parameters determined under these conditions should therefore be regarded as being *effective* values.

The Plasmos SD2000 instrument comprises a HeNe-laser providing a source of monochromatic light (wavelength 632.8 nm). This is polarised before passing through a quarterwave plate to convert the linearly polarised (at 45°) light into circularly polarised light prior to impinging the sample. Upon reflection, a constant rotating analyser allows the detector to sample the state of polarisation of the reflected beam. This information is fed into the purpose-made software to allow computation of the refractive index and film thickness[3].

2.2 Analysis of JFTOT tubes

For analysis of JFTOT tubes, some of the warnings alluded to the previous section should be borne in mind. Firstly, the surfaces under scrutiny are not ideal, both in terms of uniformity of thickness and chemical composition. Thus, variation of surface composition varies from purely metallic, with arguably no surface film, to highly carbon-rich film. Thick films will also provide little reflection of the light beam. A further complication is the shape of the surface to be analysed. Since JFTOT tubes are highly curved, it was envisaged initially that some alignment difficulties could be experienced. However, this potential difficulty was easily overcome.

To perform the analysis , tubes are mounted on a moveable measuring stage of the ellipsometer, which allows typically 200 measurements to be made along 30 mm length of the "hot" part of the tube (ie a resolution of 150 μm). Several tests had to be conducted to ensure the correct configuration of the tube.

In tests on a new tube, the parameters for the aluminium alloy tube substrate were determined by iterative calculations which gave average values of N_{sub} and k_{sub} of 2.0 and -4.3 respectively. Whilst values for pure aluminium are quoted in the literature, no values are quoted for the particular aluminium alloy employed for JFTOT tubes. In other tests on JFTOT deposits where the film was sufficiently thick as to represent a substrate in its own right, again the film parameters were determined by iterative calculation. A film refractive index of 1.45 has been determined, which agrees well with values quoted in the literature for carbonaceous materials. In subsequent tests on normal tube deposits, these measured values have been used to enable film thickness to be calculated.

The ellipsometric technique can be used to measure deposit thickness at a single spot on the tube and by performing measurements along the length of the tube, a thickness profile (Figure 2) can be obtained. Additional information on deposit volume and mass may also be obtained from the thickness profile data. Deposit volumes may be calculated by integrating the area under the deposit profile, assuming the deposit is distributed symmetrically around the tube. Limited tests have been performed to demonstrate the distribution of deposits around a JFTOT tube (Figure 3) and these results suggest that film thickness deposition is symmetrical, although only quartile measurements have been made so far. If further information on deposit density is available, then the mass of deposit may be estimated from the deposit volume.

3. RESULTS AND DISCUSSION

3.1 Validation of ellipsometric technique

In order to confirm the accuracy of the ellipsometry measurements performed at BP Sunbury laboratories, it was necessary to examine deposits with known thickness, as characterised by other techniques. Two approaches were followed. In the first, films of known thickness were prepared using Langmuir-Blodgett controlled deposition techniques[4] (Figure 4), such that monomolecular films of cadmium behenate (C_{22}) were deposited onto the surface of a new aluminium JFTOT tube. The thickness of the monomolecular film can be determined by X-Ray diffraction[5] and the value quoted in the literature is 3.2 nm. Using this approach, a series of multiple films (in stages of 16 molecular layers) of known thickness, increasing from 0 to 450 nm were produced on a JFTOT tube and examined by ellipsometry; the thickness profile along the length of the tube is shown in Figure 5. Knowing the number of molecular layers deposited allows the thickness of the films to be calculated; the results do indeed confirm the accuracy of the ellipsometric measurement.

In the second approach, JFTOT tube deposits previously characterised by interferometry[6] measurements performed by Naval Research Laboratory, NRL Washington DC, USA were

examined by ellipsometry. The results are shown in Figure 6 and show reasonable agreement between the two techniques in the thickness range common to both methods, although for the thicker deposit, there was some discrepancy between the location on the tube of maximum deposition.

Thus it was demonstrated that ellipsometry can provide absolute measurement of deposit film thickness.

3.2 Effect of time on JFTOT tube deposition

In order to study the effect of increasing test time on deposit thickness, a series of JFTOT deposits were generated for Merox and hydrofined fuels for increasing time periods (15 to 150 minutes at 15 minute intervals). Tests were performed at the fuels' respective breakpoint temperatures (ie Merox 287°C and hydrofined 302°C) using aluminium tubes. Ellipsometry analysis of these tubes gave deposit film thickness profiles giving maximum thickness and enabling calculation of deposit volume. These results are given in Table 1 and show that tube deposition increases with time, although further work is needed to establish whether the increase is linear or exponential. The results also show that ellipsometry distinguishes between different fuel types as there are significant differences in thickness for the two fuels with the same visual ratings. The results for the Merox treated fuel are shown in Figure 7.

3.3 Effect of temperature on JFTOT deposition

Ellipsometry has also been used to study the effect of temperature on JFTOT tube deposition for two Merox fuels. JFTOT deposits were generated at 270, 285, 287 and 290°C for one Merox fuel and 260, 270, 275 and 285°C for the other fuel to give visual ratings of 1, 2, 3 and 4 respectively. Both fuels were run for 150 minutes using aluminium tubes. These results are given in Table 2 and suggest that deposition increases gradually until a point is reach where deposition occurs at a much faster rate. This change in deposition rate may provide an alternative meaningful definition of breakpoint than that currently used involving visual rating. Deposit profiles for fuel 1 are shown in Figure 8.

3.4 Relationship between visual rating and thickness

The results in Table 1 show that there are significant differences in deposit film thickness for fuels with the same visual rating. This aspect is demonstrated further in Figure 9 which shows the relationship between visual ratings and deposit thickness/volume for two Merox fuels; there are significant differences in thickness and volume for the deposits with a 4 visual rating.

For all fuels examined so far, deposits of visual rating 3 have maximum thickness in the range of 100 - 140 nm. The results highlight the drawback of the current visual rating used for quality assurance purposes, ie that the rating is so dependent on the physical nature of the deposit surface and does not reflect the true characteristics of the film. Ellipsometry has the potential to replace the visual rating method for specification purposes by providing absolute measurement of JFTOT deposit thickness, a parameter which would be far more meaningful information for the engine designer and manufacturer. In addition, the problems associated with visual rating subjectivity and poor precision of measurement would also be overcome.

3.5 Assessment of "abnormal" and "peacock" deposits

Previous work[1] has shown that "abnormal" coloured tube deposits which are either pale blue or white require a high degree of personal judgement to interpret and rate, resulting in difficulty in achieving good reproducibility between laboratories. Ellipsometric analysis of an abnormal deposit is shown in Figure 10. These results suggest there is a discontinuity in the deposit profile, believed to be due to the uneven nature of the deposit causing scattering of the reflected light. Ellipsometry can provide an absolute measurement of thickness for abnormal deposits which are difficult to rate. In addition, abnormal deposits which in current specifications are classified as failures, may be sufficiently thin such that in terms of engine /airframe operation, they are acceptable. Ellipsometry would allow more meaningful identification of "acceptable" fuel.

Ellipsometric analysis of a "peacock" deposit is also shown in Figure 10 and confirms that peacock type deposits are continuous films with thickness greater than that observed for normal deposits with visual rating 1 to 4.

3.6 Effect of substrate on JFTOT tube deposition

The ellipsometric measurement is based on the change in state of polarisation of light reflected from the surface and is dependent on the substrate refractive index and absorption coefficient and the film absorption coefficient, refractive index and thickness. Previous work[7] has shown that magnesium migration occurs at prolonged, elevated temperatures and will change the metallurgy of the tube surface which could effect the substrate refractive index and absorption coefficient. If this occurs, new values for these parameters will have to be determined for each temperature. The extent of magnesium migration is dependent on the temperature of testing. To examine the effect of substrate on JFTOT tube deposition, JFTOT tests were run at 260 and 300°C for 150 minutes using aluminium tubes and alumina treated dodecane to simulate fuel (but which would not give a deposit). Scanning Electron Microscopy/Energy Dispersive

Analysis of X-rays (SEM/EDX) was used to confirm that there were substrate differences between the two tubes; Figure 11 shows the variation in magnesium concentration along the length of the tube. The tubes produced were examined by ellipsometry to generate data on refractive index and absorption coefficient; these data are shown in Figure 12 and indicate that there were slight differences between the two tubes. In order to determine whether the variation was sufficient to affect actual thickness measurement, the values obtained were used in the calculation of thickness for a normal JFTOT tube deposit. For the extremes of substrate refractive index and absorption coefficient employed, deposit thickness varied by a maximum of only 5%. Thus it is concluded that standard values may be employed for deposit analysis with no need to determine substrate parameters for each temperature examined.

4. CONCLUSIONS AND POTENTIAL FOR ELLIPSOMETRY

The work so far has demonstrated that ellipsometry can provide absolute measurement of JFTOT deposit thickness. The technique has potential for quality assurance purposes, as a replacement for visual rating for assessment of tube deposits, thereby overcoming the problems of operator subjectivity associated with the current rating procedure and also providing information on thickness and volume of deposits, parameters which are far more meaningful for engine designers and manufacturers. This aspect is being investigated further by extending the database of samples studied (from in-house programmes and industry round robins). Such a system would be robust and non-destructive; cover the important thickness range with regard to visual rating; provide absolute measurement of thickness; enable single spot and profiling measurements; and there would be no restriction on minimum deposit thickness.

5. REFERENCE

1. The thermal stability working group; Factors influencing JFTOT breakpoint measurement and implications for test procedure, March 1990, MOD (PE) Aviation Fuels Committee.

2. Baker, C.; David, P.; Hall, D.E.; "Characterisation of Degradation Products from Thermally Stressed Aviation Fuels and Influence of MDA on Their Formation," Conference Proceeding of 4th International Conference on Stability and Handling of Liquid Fuels, Orlando, Florida, USA, November 1991.

3. Azzam, R.M.A.; Bashara, N.M.; Ellipsometry and Polarised Light, Elsevier Science Publishers B.V

4. Fromherz, P.; Oleschlagel,U.; Wilke, W.; Thin Solid Films **1988**, 159, 421-427

5. Bettarini, S.; Bonosi, F.; Gabrielli, G.; Martini, G.; Am. Chem. Soc. **1991**, 7, 1082-1087.

6. Mitchell, C.S.; Morris, R.E.; Wagner, R.L.; "An Automated Device for Quantitative Measurements of JFTOT Deposits by Interferometry," Conference Proceeding of 4th International Conference on Stability and Handling of Liquid Fuels, Orlando, Florida, USA, November 1991.

7. Baker, C.; David, P.; Hazell, L; Surface and Interface Analysis 1986, 9, 507-513

6. ACKNOWLEDGEMENTS

The authors would like to thank BP Oil and UK MOD(PE) for their sponsorship of this work.

Schematic view of ellipsometer

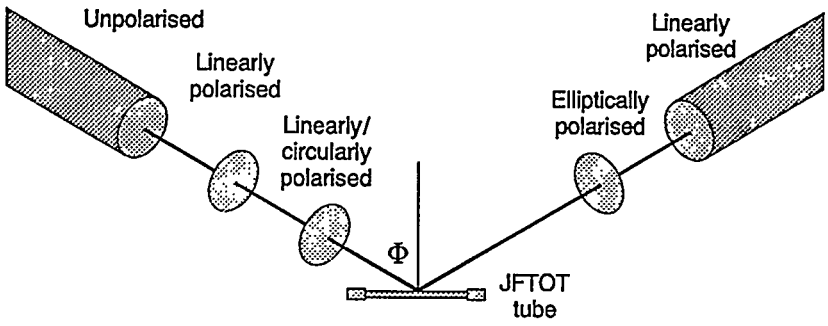

Based on the change in state of polarisation of light reflected from a surface, affected by:

- surface refractive index and absorption coefficient
- film refractive index absorption coefficient and thickness

CG 40233

FIGURE 1

Deposit profile as a function of JFTOT run time (Merox fuel at 287°C)

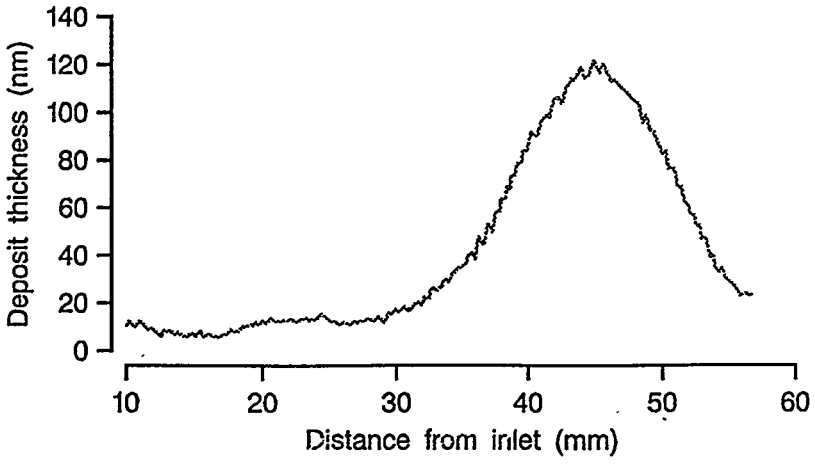

CG 40982

FIGURE 2

Tube #244 ellipsometric '4-slice' profile

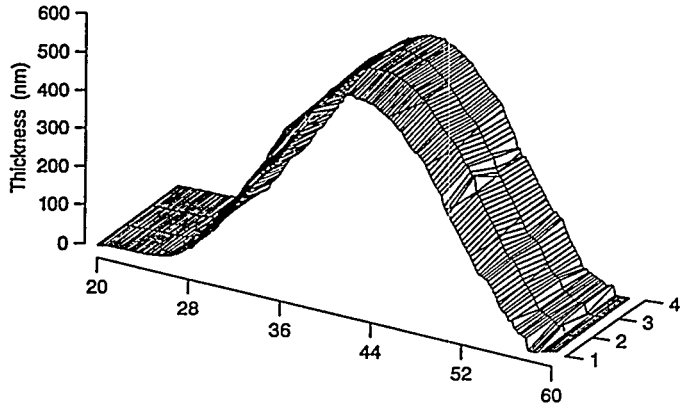

FIGURE 3

'Simulated' model deposit studies

Use monomolecular cadmium behenate (C_{22}) films deposited on a clean JFTOT tube using Langmuir-Blodgett controlled deposition technique

Advantages

- Known film thickness
- Known film composition

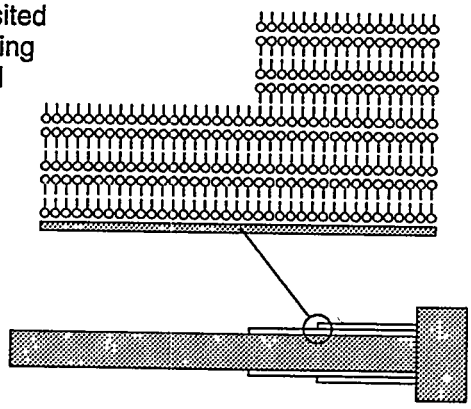

FIGURE 4

Thickness profile for a JFTOT tube coated with multiple cadmium behenate films

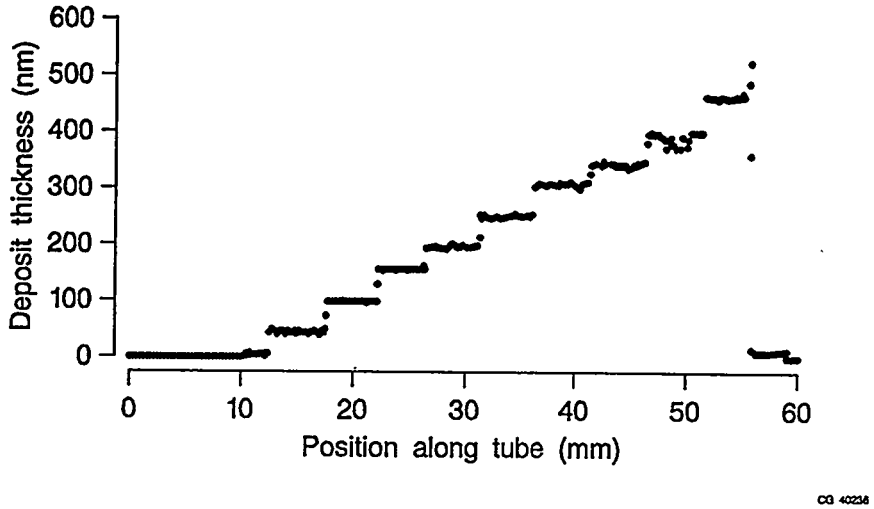

FIGURE 5

Comparison between interferometry (NRL) and ellipsometry

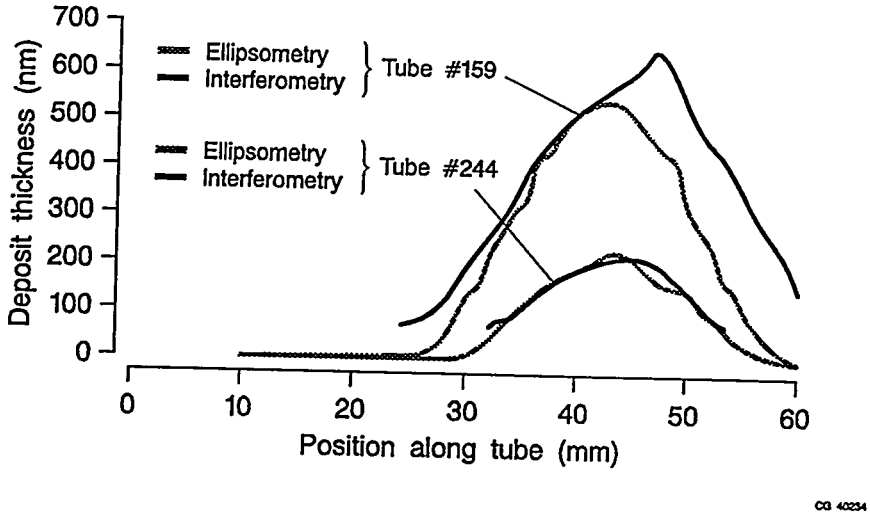

FIGURE 6

Deposit profiles as a function of JFTOT run time (Merox fuel at 287°C)

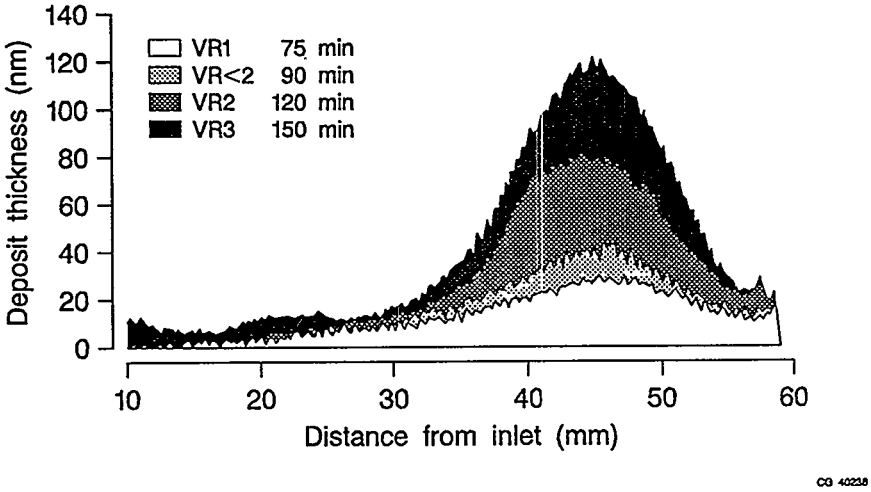

FIGURE 7

Deposit profiles as function of JFTOT temperature

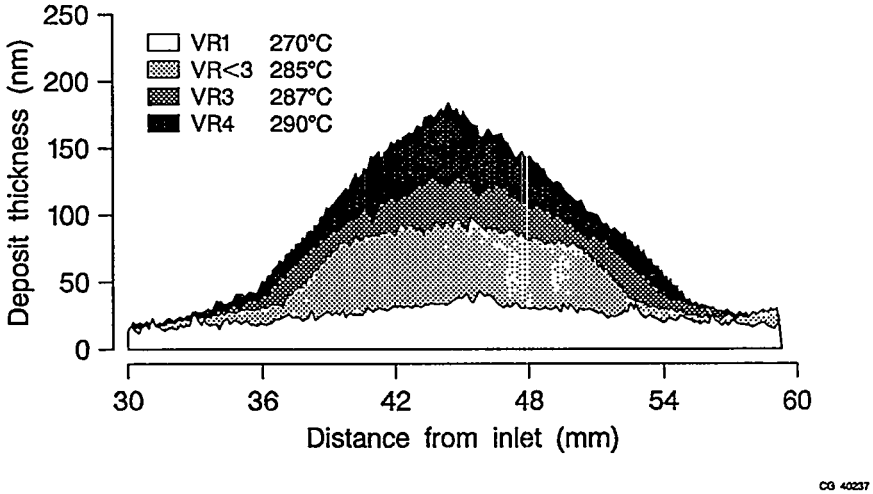

FIGURE 8

Visual rating comparisons

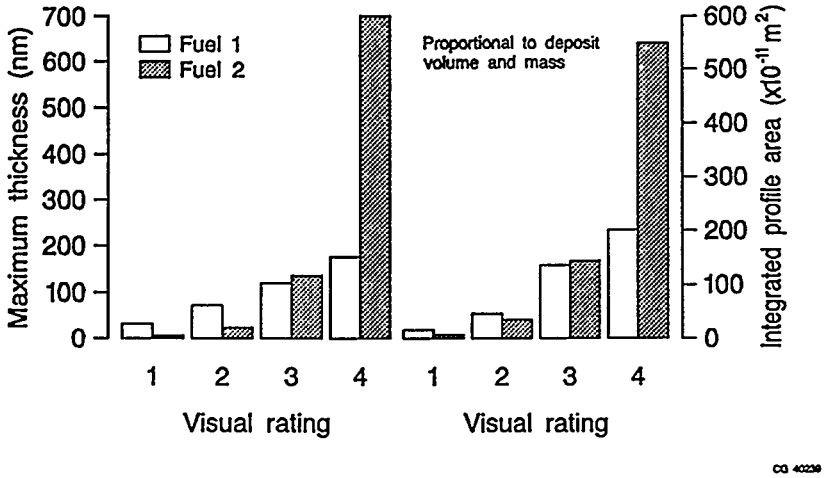

FIGURE 9

Ellipsometric analysis of 'abnormal' deposit

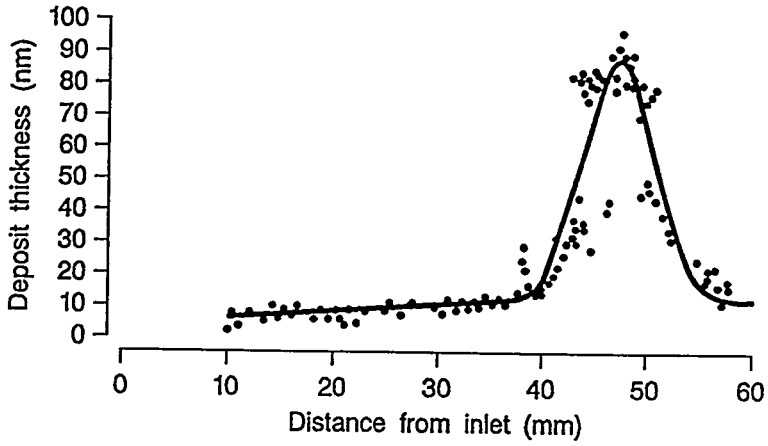

FIGURE 10

Ellipsometric analysis of 'Peacock' deposit

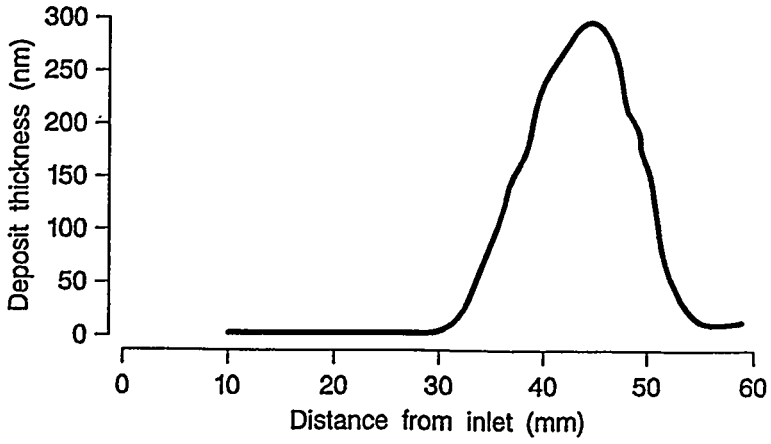

FIGURE 11

SEM / EDX analysis of tube substrate

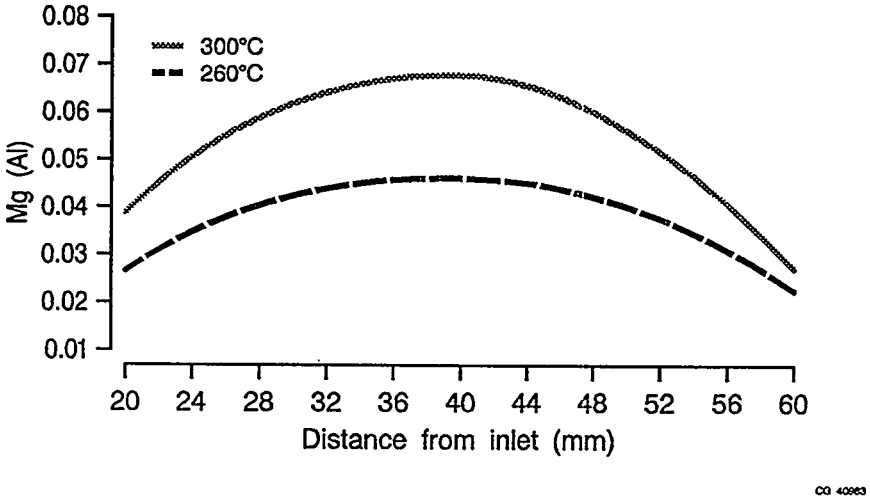

FIGURE 12

Effect of temperature on JFTOT tube substrate parameters

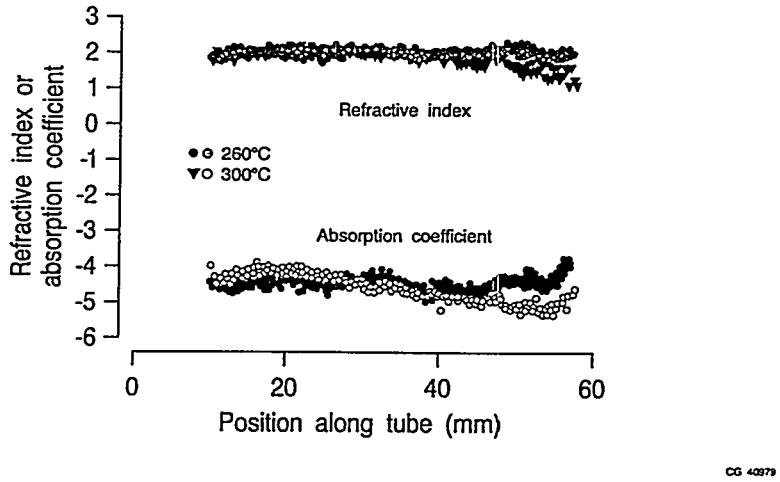

FIGURE 13

TABLE 1

DEPOSIT FILM THICKNESS AND DEPOSIT VOLUME AS A FUNCTION OF JFTOT RUN TIME

(Merox Fuel at 287°C, Hydrofined Fuel at 302°C)

Time Duration (mins)	Visual Rating		Thickness (nm)		Volume ($x10^{-11}m^2$)	
	Merox	Hydrofined	Merox	Hydrofined	Merox	Hydrofined
15	1	1	11.3	4.2	2.3	0.9
30	1	1	20.8	6.4	5.1	2.0
45	1	1	23.8	15.0	5.8	2.4
60	1	<2	20.7	18.0	4.1	4.2
75	1	2	29.9	38.1	8.2	8.6
90	<2	2	43.7	83.6	8.6	7.7
105	2	<3	78.5	78.5	12.0	9.6
120	2	<3	80.7	83.5	14.0	10.6
135	<3	<3	90.6	89.5	17.1	12.3
150	3	3	121.8	97.5	24.0	14.0

TABLE 2

DEPOSIT FILM THICKNESS AND DEPOSIT VOLUME AS A FUNCTION OF TEMPERATURE

Temperature °C	Visual Rating		Maximum Thickness (nm)		Volume ($x10^{-11}m^2$)	
	Merox 1	Merox 2	Merox 1	Merox 2	Merox 1	Merox 2
260		1		10		7
270	1	2	39	26	19.3	36
275		3		140		149.2
280	2		80		48.6	
285		4		700		550
287	3		127		142.9	
290	4		180		205.2	

5th International Conference
on Stability and Handling of Liquid Fuels
Rotterdam, the Netherlands
October 3-7, 1994

WEIGHING BY STOPWATCH - SORTING OUT THE VARIABLES IN FILTER BLOCKING TENDENCY

Dennis R. Hardy*, Erna J. Beal and Janet M. Hughes

Naval Research Laboratory, Code 6181, 555 Overlook Ave., Washington DC 20375-5342

Abstract

This paper first reviews the work reported in the early 1960's on the major variable governing rate of flow of a liquid through a membrane filter - viscosity. Ignoring this major variable leads to both confusing interpretation of filter blocking tendency (FBT) experiments in the laboratory and also for FBT standard tests which cannot adequately or correctly assess FBT from fuel to fuel. Next, the paper will establish a protocol for correctly assessing any given liquid FBT by first calibrating given porosity membrane filters for viscosity and then for solids content. The technique can then be used to measure not only existent solids in various liquid samples but also solids formed during typical accelerated tests such as the gravimetric JFTOT test (for aviation fuels) or ASTM D5304 (for diesel fuels) using only a stopwatch and graduated cylinder. Accuracy and precision of this "weighing" technique will be compared with direct gravimetric determinations.

Introduction

Since the advent of mid distillate fuel usage in turbine engine applications, filterability has been an important fuel property. Early systematic work in this area is well summarized in a paper by Chiantella and Johnson. Unfortunately this work has been largely ignored by all subsequent workers in the field. This is especially evident in the abandonment of a proposed ASTM standard test method for filtration time in about 1960 in favor of a gravimetric filtration test (ASTM D2276). The earlier ASTM work on filtration time which dates to about 1954 is also summarized in the Chiantella paper.

A constant flow rate variation of the filtration test was next attempted in the mid 1980's by the UK MOD. This ultimately resulted in ASTM adoption of an equivalent method (ASTM D2068). This type of test was very critically examined by the US Navy engineering test facilities and was judged to be unacceptable for its intended use.

For a variety of reasons it would be very desirable to be able to adopt a useful filtration test. These include the ability to automate the test for quality assurance and for field test kit use, and the possibility of adopting the test in the laboratory as a replacement for weighing small concentrations of particulates.

In this paper we review the earlier work by Chiantella and Johnson where the major effects of liquid viscosity on filterability, which are well known to filtration experts but essentially ignored by fuel handlers, are reexamined. We apply these earlier results to the current ASTM D2068 filter blocking tendency (FBT) method. In addition we incorporate the more recent work of McVea, Power and Solly which made important comparisons of particulate size hold up through a variety of laboratory and real world filter media.

Finally, a set of recommendations can be made based upon a critical review of the ASTM D2068 method which should lead to a realistic and useful new method for filterability of both jet and diesel fuels. This would also have the potential of replacing the sometimes dangerous ASTM D5452 particulate contamination test for aviation fuels and the cumbersome ASTM D2276 field test for filterability of aviation fuels.

Experimental

The apparatus to measure filtration time by gravity head is simply a Millipore filter funnel capable of holding a 47 mm diameter filter and a reservoir of 300 mL. This is placed above a 100 mL graduated cylinder and a stopwatch is used to measure flow times. After the filter pad is wetted, the graduated cylinder is placed below and 200 mL is added to the reservoir. The first 100 mL of effluent is timed.

The apparatus to measure the FBT is commercially available from EMCEE Electronics, Inc. and conforms to the criteria established in ASTM D2068. It consists of a pump capable of pumping 20 mL/min at an initial delta pressure of 0 psi. The flow timer is set to deliver 300 mL through the filter or up to a delta pressure reading of 15 psi. Thus each test takes up to 15 minutes to complete. If the delta pressure remains below 15 psi after 15 minutes, the

fuel is considered to have particulates below 10 mg/L and to be suitable for marine turbine engine filtration system usage. The filter medium specified in ASTM D2068 is glass fiber GF/A with a nominal pore size of 1.5 microns.

For the gravity flow work the membrane filters of 0.45, 0.8, 3.0, and 15.0 microns were obtained from Millipore Corp. All had a stated porosity of about 60%. GF/A filters were obtained from Whatman Corp. All filters were 47 mm diameter. Unused filter/coalescer elements were obtained from two manufacturers and represent the great majority of all marine fuel filtration media. A paper final filter from an auxiliary power gas turbine was obtained from the USS Arleigh Burke.

Results and Discussion

Using typical, actual flow rates, cross sectional filter areas, and pressure differentials it is possible to assess the scale down factors for a FBT such as ASTM D2068. As noted in previous work[2] the flow rate in D2068 is really about an order of magnitude too great for the cross sectional area employed (about 1 cm^2). The net effect of improperly scaling the D2068 test is that it essentially becomes too sensitive to variables such as solid contamination concentration.

In order to maintain the comparability between the laboratory test and full scale with regards to the actual meaning of the delta pressure, it would be preferable for future FBT tests to increase the cross sectional filter area to about 10 cm^2 rather than decreasing the flow rate of the test. Decreasing the flow rate would make the test inordinately long. Increasing the filter cross sectional area would maintain the fine discrimination possible in the 0 to 15 psi delta pressure range.

The other major problem with the D2068 FBT test is the selection of GF/A glass fiber depth filter medium (with a nominal or effective pore size of 1.5 microns). Typical paper filters for diesel filtration have nominal pore sizes of about 8 to 10 microns. The choice of GF/A as a test filter in many laboratory scale tests has historically been due to the fact that

a "standard", chemically inert medium which is a depth type filter is preferable to the membrane filter type.

In order to select a filter medium to properly simulate the real world paper filters it is necessary to sort out the influence of both filter porosity and filter pore size. This is straightforward for membrane filters. The pore size is the diameter of the holes in the membrane and the porosity is the percent of total open space or holes per unit area of filter.

These two concepts can become quite muddled when considering typical depth filters. Most paper filters show some sort of cut-off when plotting % retention on the filter vs particle size (for reasonable monodisperse test particles). Thus the depth paper filters can be describe by a relative or nominal pore size. The concept of porosity of depth filters must be measured empirically, however.

In order to better define the concept of depth filter relative or nominal porosity, we employed the concept of first measuring the flow rate of a standard liquid through membrane filters of varying pore size and constant, known porosity. First, n-tetradecane was filtered through a 0.45 micron nylon filter to remove any particulate matter. Then, using a gravity head, the time to pass the first 100 mL of a 200 mL sample through various pore size membrane was determined. Figure 1 shows the results for 0.45 micron and 0.8 micron filters which both have about 60% porosity. Even though the total amount of open pore area is identical, the flow time for the model system chosen (typical for most diesel fuels) varies over the entire measured volume range.

Figure 2 also includes the data for the 0.8 micron membrane along with two additional 60% porosity membranes of 3.0 and 15.0 microns. In all of these cases, filter porosity is constant and the n-tetradecane filtrate contains no particulate material. Thus the effect of pore size on flow time per unit volume is easily seen. When the GF/A filter with the nominal 1.5 micron pore size is tested it can be seen that its porosity is similar, although slightly higher than, the membrane filters value of 60%.

Subjecting three typical filters to the test conditions above gives the results shown in Figure 3. Since these filters have a nominal pore size of 8 to 10 microns, we see that their porosity values are also somewhat above 60%. Thus the choice of the GF/A filter medium for a test such as the D2068 FBT test is acceptable from the point of view of similar porosity to actual paper depth filters. Nevertheless, as the work of McVea, et al[2] shows the GF/A filter is unacceptable from the point of view of nominal pore size.

On the other hand, many standard laboratory test methods for filtration and gravimetric determination of solids (either hold up or through put) are based on an 0.8 micron membrane filter. Again, although this material is acceptable from a porosity point of view, it is not acceptable from a pore size point of view.

From the results in Figure 2 it appears that the best choice to measure either FBT or fuel solids hold up would be a membrane filter with a pore size of about 10 microns and a porosity of about 60%. This type of filter medium should be able to simulate reality very well.

Despite the discussion above regarding the proper choice of filter medium for the ASTM D2068 FBT test, it was decided to continue the evaluation of the test in a systematic fashion. The results would then be extended to alternative test filter media at a later time.

In order to test the earlier conclusions of Chiantella and Johnson[1] that viscosity was playing a major role in FBT tests, a number of n-decane and silicone oil mixtures were prepared which would span the stated operating range of D2068 and also the range of distillate diesel fuels found in reality. This viscosity range is about 1.8 to 8.5 cSt at about 22°C. It can be clearly seen in Figure 4 that there is the expected increase in FBT with viscosity for this test. It should be noted that for the higher viscosity fluids the delta pressure at the end of the 300 mL filtration is close to the allowed maximum of 15 psi. Of course, all of the fluids contain no particulate matter above 0.45 microns in all cases.

It is well known that on a weight per unit volume of fuel basis the fuel derived sludge/solids from ageing are the primary cause of filter blocking over time. It is also well known that regardless of the source of this sludge, it forms an elastic hydrocarbonaceous sphere which is noted for its monodispersity. The isolated spheres are almost always about 1 micron in diameter. It is also well known that large aggregates of these spheres can form which are sometimes up to tens or hundreds of microns across.

Because of this it was decided to use a typical diesel sludge material which had been washed and dried as a "standard" contaminant source. This sludge can be accurately weighed into the silicone oil/n-decane mixtures described above. The sludge is insoluble in this mixture.

Initial attempts to suspend this solid material at concentrations of 2, 10, 15 and 20 mg/L were made by vigorous shaking. Visual observation of the suspension showed that the sludge was not homogeneously distributed. This was also noted when aliquots were filtered and the filter pad was not smoothly covered but showed "clumps" of the sludge. This problem was overcome by sonicating the samples after shaking. The resulting solution was a very homogeneous solid suspension.

The sludge was added to a low, medium and high viscosity liquid as shown in Figure 5. In the case of the 1.92 cSt liquid the test correctly passes the 2 mg/L sample, but incorrectly passes the 10, 15 and 20 mg/L sample. The highest concentration sample would be representative of a very problematic field sample.

For the 4.09 cSt (at 22°C) sample, which is quite typical of most distillate diesel fuels the 2 mg/L sample just passes the test (correctly), and although the 10 and 15 mg/L samples are correctly failed (at very short test times/volumes), it is obvious that the acceptable range between 2 and 10 mg/L would also incorrectly be failed by this test. For the 6.18 cSt liquid this is shown in the very rapid failure (incorrectly) of the 2 mg/L sample.

Thus problems previously encountered by the US Navy test facilities in correlating this FBT test to real world vessel filtration systems are not surprising. In its current state the test

method allows both gross false passes and gross false fails, since liquid viscosities are not taken into account.

Conclusions

This work points to the need to incorporate standard filtration industry concerns such as liquid viscosities, filter media porosities, and scaling effects into any future FBT test methods. Once this is done, it should be possible to easily correlate such a FBT test with real world marine diesel filtration equipment.

This kind of testing should then prove to be useful in the aviation fuel cleanliness area both as a field test and for laboratory quality assurance testing.

If the 10 micron pore size (with 50 to 60% porosity), 47 mm membrane filter can be incorporated into the FBT test as suggested above, this should have implications in the laboratory regarding the real engine performance and filtration equipment performance correlations. This implication will probably require changes in the laboratory test criteria for filter blocking and also concentration of sludge in a given sample.

Finally, if useful and realistic correlations between contamination level and pressure can be established as a function of liquid viscosity, it should be possible to substitute this type of FBT test for the filtration/gravimetry step in many standard laboratory fuel tests. Thus a fuel sample from an accelerated stress test such as ASTM D5304 (static, diesel test) could be assessed for solid concentration by subjecting it to this type of FBT test. This eliminates the need for the error fraught and labor intensive weighing step. An alternative, of course, would be to use a simple variation such as the gravity head/filtration technique described above. This would allow one to essentially weigh the solid by means of a stopwatch.

References

(1) Chiantella, A. J. and Johnson, J. E., "Filterability of Distillate Fues", Journal of Chemical and Engineering Data, Vol. 5, No. 3, p. 387-389, July 1960.

(2) McVea, G. G., Power, A. J. and Solly,. K., "The Effect of Vehicle Filter Media Characteristics Upon the Filterability of Automotive Diesel Fuel," Fuel, Vol. 69, p. 1298-1303, October 1990.

Effect of Pore Size on Filtration Time
"Equivalent" Porosity Membrane Filters

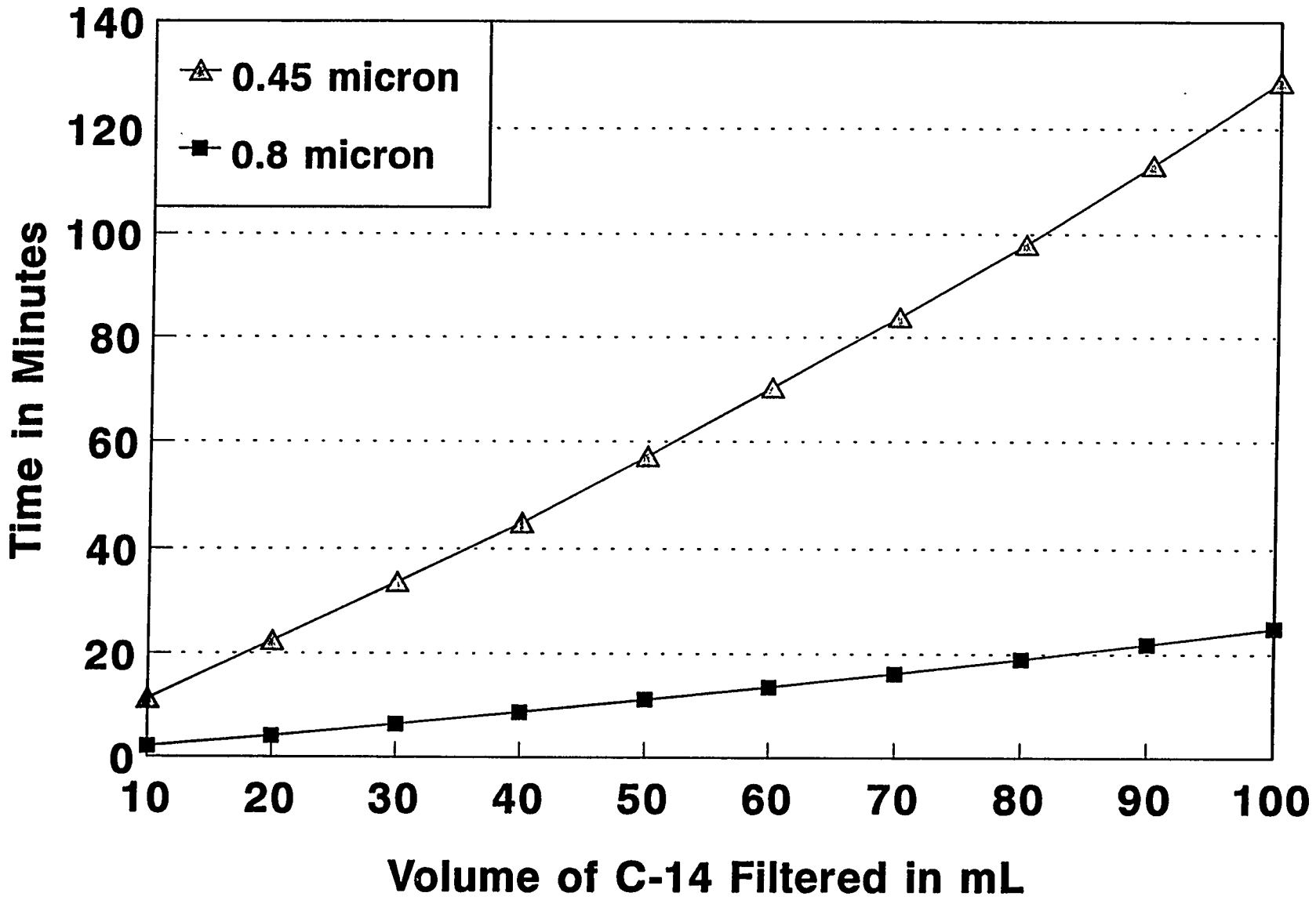

FIGURE 1. See text for details. C-14 = n-tetradecane (99 mol %)

FIGURE 2. See text for details.

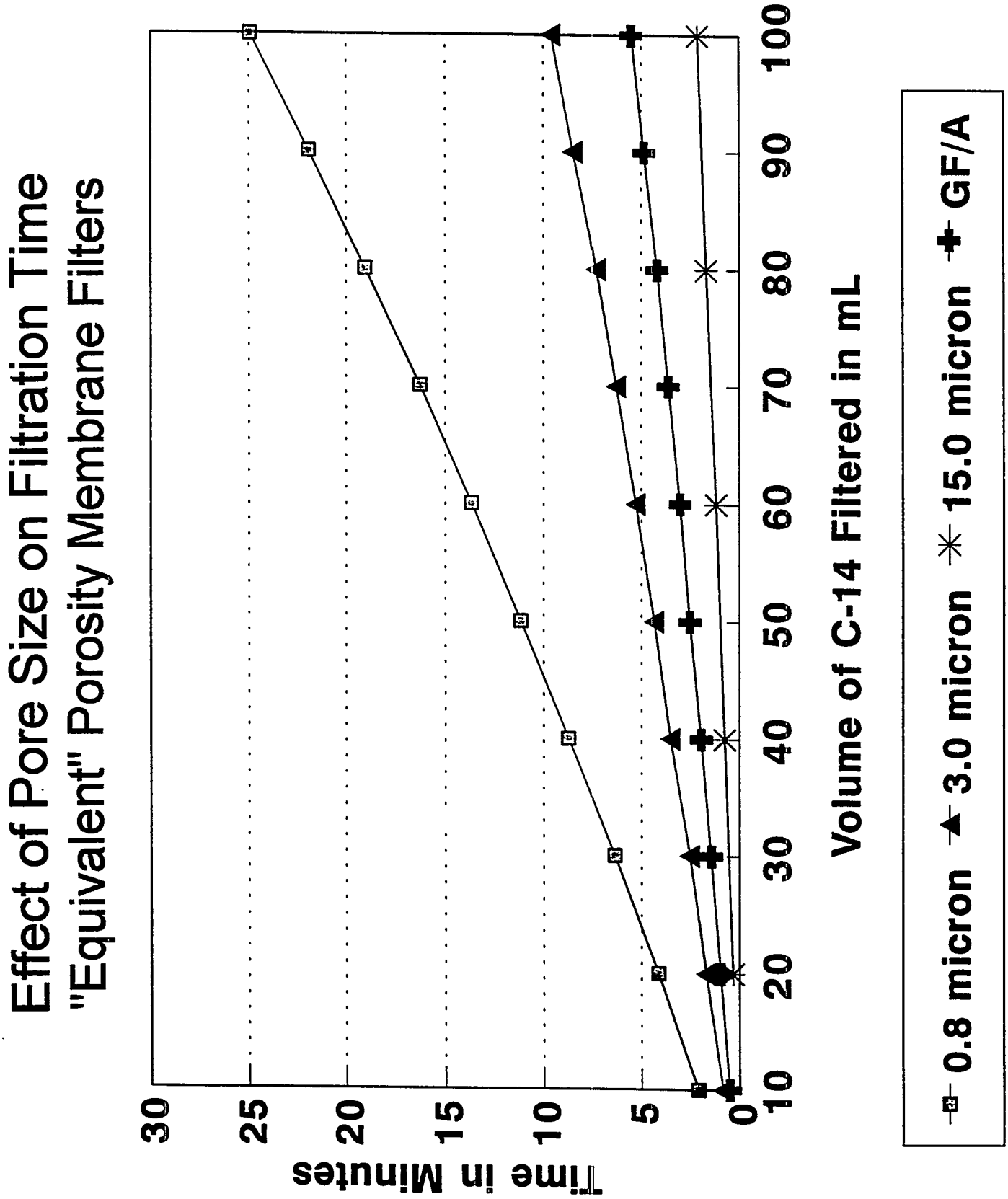

FIGURE 3. See text for details.

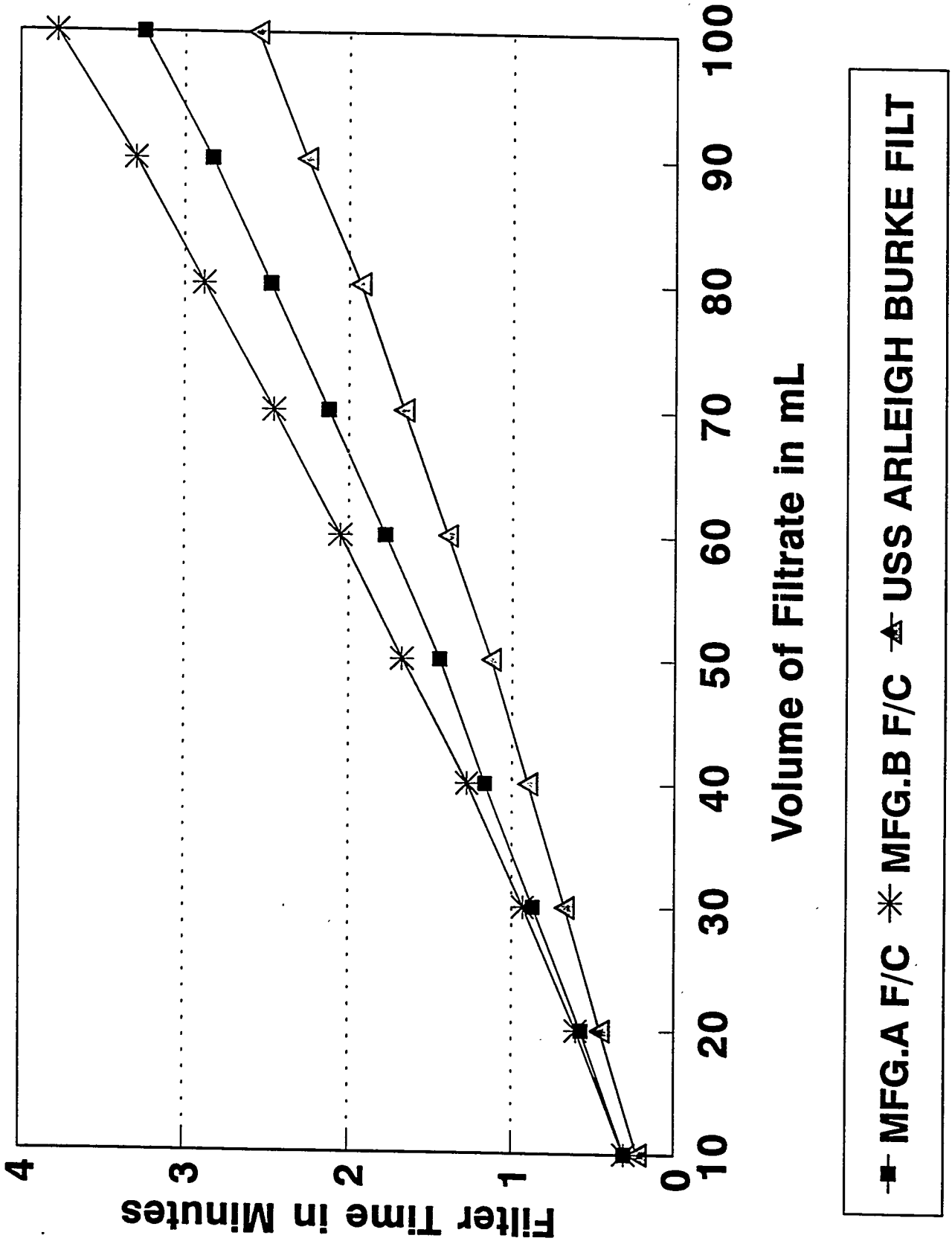

Filter Pressure vs Viscosity Using D2068
Mixtures of Silicone Oil and n-Decane

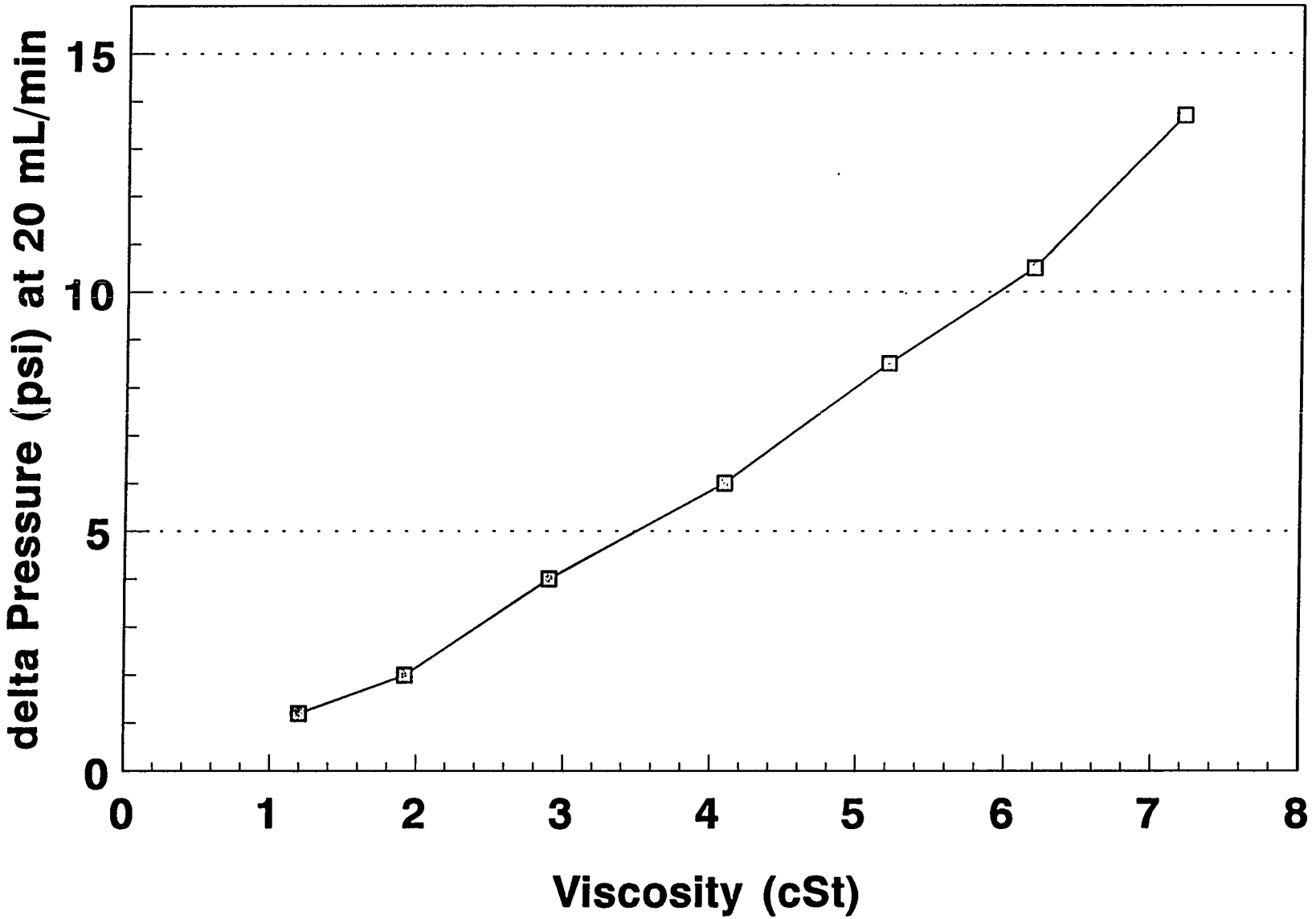

FIGURE 4. See text for details. Viscosity measured at 22° C.

Pressure vs Contamination Using D2068
Mixtures of Silicone Oil and n-Decane with Pet. Sludge at 22°C

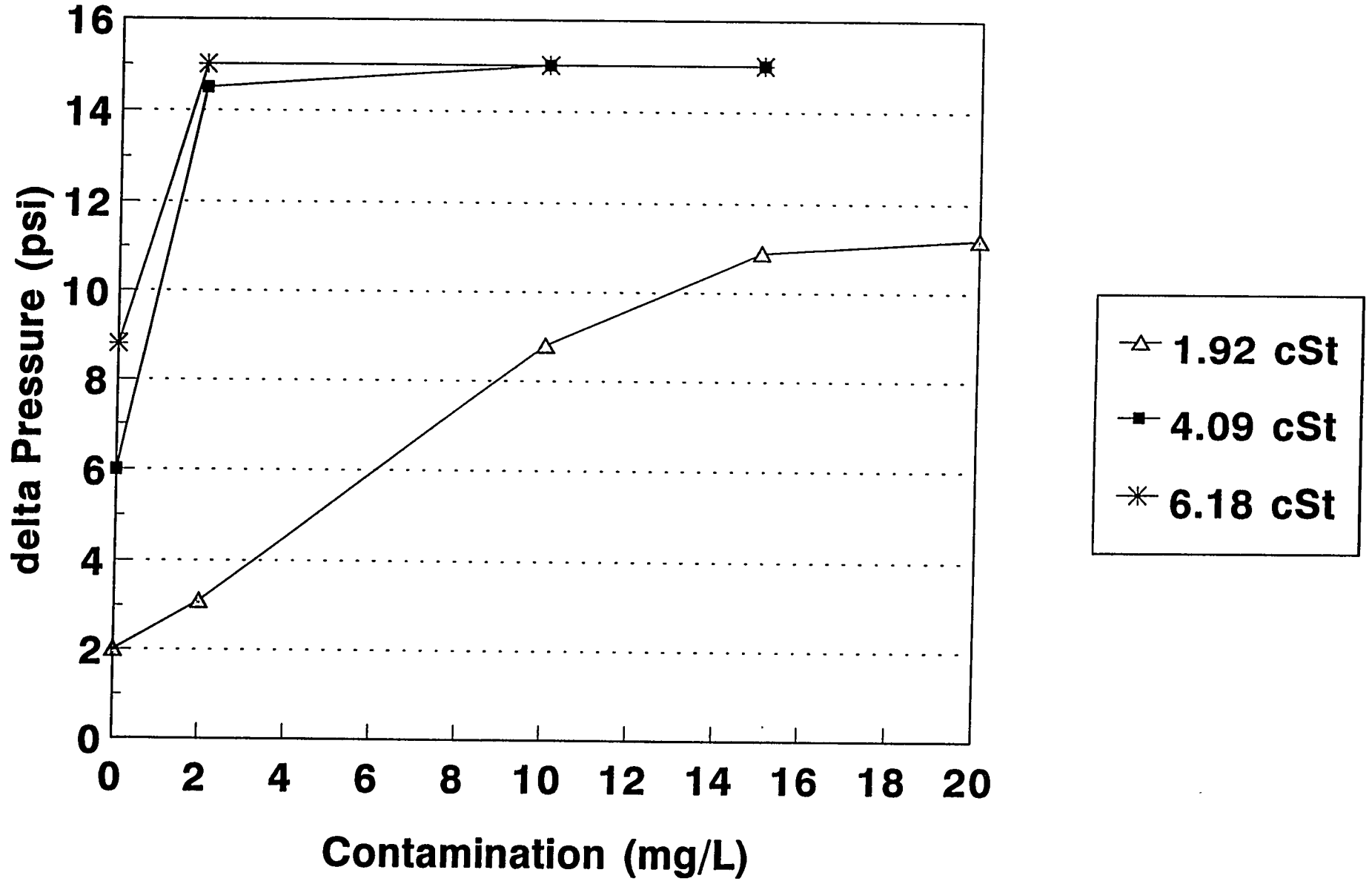

FIGURE 5. See text for details.

5th International Conference
on Stability and Handling of Liquid Fuels
Rotterdam, the Netherlands
October 3-7, 1994

MONITORING THE FORMATION OF SOLUBLE DEPOSIT PRECURSORS IN FUELS WITH LIGHT SCATTERING PHOTOMETRY

Robert E. Morris*[a], Dennis R. Hardy[a], Seetar Pande[b] and Margaret A. Wechter[a,c]

[a]Naval Research Laboratory, Code 6181, 4555 Overlook Avenue, S.W., Washington, DC 20375, USA; [b]Geo-Centers, Inc., Indian Head Hwy., Ft. Washington, MD 20744, USA. [c]The University of Massachusetts, Dartmouth, North Dartmouth, MA 02747, USA..

Abstract

The reactions that can take place in hydrocarbon fuels often manifest themselves as an increase in the propensity to form thermally induced insoluble reaction products. This is not a one-step process but the result of a multitude of intermediate processes. These intermediate processes will produce a range of soluble products that differ considerably in structure and functionality from the fuel itself. Since these soluble "precursors" can, upon further thermal stress, lead to insoluble products, a method for following their formation could form the basis of a useful predictive measurement. It would also serve as a research tool for following the discrimination between soluble and insoluble product formation. Light scattering photometry was evaluated as a means of monitoring the formation of large soluble product molecules as they are formed in fuels. Changes in light scattering properties were measured after thermal stressing in the presence of dissolved copper and a metal deactivator additive. These results correlated well with the amounts of soluble and insoluble products formed. Fuel changes were detected by light scattering before detectable quantities of insoluble products were produced.

Introduction

It has never been clearly demonstrated why a proportion of the reaction products formed in fuel become insoluble. Historically, this phenomenon has been attributed to changes in molecular size and / or polarity. The presence of soluble gums in fuels has been interpreted[1] as evidence that there is an ongoing process of growth in the sizes of soluble reaction products. This process can either precede or accompany the precipitation of insolubles. In the Flory[2] model, a dissolved macromolecule becomes insoluble in a given solvent if the molecular size becomes a factor in its interaction with the solvent. As the molecular diameters of the solute molecules increase, the

solvating power of the fuel-solute interactions decreases. The solute molecules begin to assume a more spherical configuration until the excluded volume approaches zero and they precipitate out as spheres of nearly uniform size. The uniformly spherical morphology of fuel particulates often observed suggests that in those cases this process may be responsible for their precipitation from solution. The chemical complexity of fuel and the multiplicity of potential reaction pathways involved would be expected to result in a variety of solute sizes. Therefore, if the fuel particulates behave as macromolecules in solution, a distribution of products having increasing molecular dimensions would be established. Fuel stability assessment traditionally has been based on measuring insoluble products. However, an analytical method that responds to these soluble macromolecules during the onset of fuel degradation and before measurable deposition could prove valuable. Such a measurement could reveal the extent to which the process has progressed toward the eventual deposition of insoluble reaction products. Assessment of fuel stability through such monitoring of solute size changes would be possible under less severe conditions of stress than those required to produce measurable quantities of insolubles. A means for monitoring average changes in solute sizes may also be useful in assessing storage stability. Another potential benefit would be a means of estimating levels of soluble reaction products that can be reached in a fuel before precipitation occurs.

An analytical technique that has been investigated for this purpose is light scattering photometry. The angular dependence of monochromatic light scattered by dilute solutions of macromolecules in pure solvents has long been used[3] to gain information about molecular configurations and sizes. The applicability of light scattering to monitor thermal degradation of diesel fuels was studied by Johnson, et al[4,5] at NRL, using blends of straight run and catalytically cracked stocks. They were able to monitor changes in particle sizes and the number of particles in fuels during relatively mild thermal stress. These findings were interpreted as evidence that this method had the potential to evaluate stability additives in Naval distillate fuels. In a subsequent NRL study[6], light scattering was used to monitor chemical changes in JP-4, JP-5 and hydrocarbon mixtures after stressing from 150° to 370°C in a bomb. Phenyl disulfide was added to produce insoluble products. The large sizes of the products revealed the limitations of light scattering with dispersions of particles having average dimensions significantly larger than the wavelength of the incident light. Laser

light scattering measurements were applied[7] to the study of storage stability of upgraded H-coal, solvent refined coal (SRC-II) process products in addition to samples of oil shale and petroleum derived JP-5. Measurements of scattering intensities as a function of stress times were obtained in samples doped with 2,5-dimethyl pyrrole (DMP) and thiophenol. Synergistic effects between the co-dopants were observed. Light scattering was used[8] to measure the kinetics of reactions induced by DMP during storage stability testing of a stable shale-derived diesel fuel. DMP depletion rates measured by gas chromatography were found to correlate well with the rates of soluble product formation from turbidity measurements. In this instance, the highly reactive DMP was simply polymerizing without significant interaction with the fuel. Kinetic measurements have also been obtained with nephelometric studies[9] using visible light (500 - 800 nm). Together with conventional gravimetry, the degradation of diesel fuels during thermal stress was characterized in the presence of oxygen in the ASTM D2274 procedure. By measuring nephelometric changes, it was possible to characterize the kinetics of the induction period during the test.

Experimental

Measurements of scattered light intensity were obtained by the method of Brice, et al[10] , using a Brice-Phoenix Universal Light Scattering Photometer (Phoenix Precision Instrument Co.). Samples were measured in a 25mL semi-octagonal light scattering cell at angles of 135°, 90°, 45° and 0°. A mercury lamp with bandpass filters at 436 and 546nm was used as the light source. To minimize interferences from absorption and fluorescence, light at the longer wavelength (546nm) was used. Measurements of transmitted light at 0° were obtained by the insertion of an opal glass working standard in the path between the light source and the sample. The linearity of photomultiplier response was insured by keeping the measured light intensity within a narrow range with neutral filters. The instrumental parameters were verified by molecular weight determinations of known polymers dissolved in pure solvents. Oxygen uptake experiments were carried out by thermally stressing fuels in the modified JFTOT apparatus that has been described previously[11,12] using 127mm stainless steel heater tubes. Samples for light scattering and dissolved oxygen measurements were taken as the heater tube temperature was raised in discrete increments. The modified JFTOT apparatus allows sampling of stressed samples after passing over the heater tube and before returning to the reservoir. To prevent restoration of the

equilibrium oxygen concentration of the sample, contact with air was avoided by directly routing the JFTOT effluent to a gas chromatograph via a liquid sampling valve. The permanent gases were separated from the liquid with a 6 ft. x 1/8 in. stainless steel 42/60 mesh alumina column and resolved by a 6 ft. x 1/8 in. stainless steel column packed with 42/60 mesh 5X molecular sieves. Column and transfer line temperatures were maintained at 100° C. Entrapped organics were periodically removed from the alumina column by backflushing at an elevated temperature. Permanent gases were detected with a Gow-Mac model 24-600 helium discharge detector. The helium carrier gas was purified with a helium diffusion cell to attain sufficient oxygen sensitivity.

Gravimetric measurements of insoluble reaction products were obtained from fuel samples stressed in the gravimetric JFTOT (GravJFTOT) device[13,14]. An Isco model 2350 reciprocating piston HPLC pump was used to deliver fuel at a flow rate of 3 mL/min over a stainless steel strip maintained at 260°C. All tests were conducted for 2.5 hr at a pressure of 4 mPa (500 psig), maintained by a micrometer valve at the fuel outlet. After passing through the heated section, the fuel effluent was collected and filtered through two pre-weighed 0.8μ nylon membrane filters. The filters were washed with filtered hexane, dried in an oven at 70°C for 30 minutes, cooled and weighed to obtain the particulate weight. The stainless steel strips were weighed directly to determine the weight of adherent deposits.

Fuel aging during ambient storage was simulated by stressing in an Oxygen Overpressure Reactor, also known as the Low Pressure Reactor (LPR). Overpressure tests were conducted for 24 hours at 90°C under 720 kPa (90 psig) and 400 kPa (50 psig) air, following the procedures in ASTM D5304-92[15]. These conditions were chosen to approximate six months of ambient storage.

Copper was added as copper (II) ethylacetoacetate ($[CH(COOCH_3)COOC_2H_5]_2Cu^{II}$; Eastman Kodak) and used without purification. N,N'-disalicylidene 1,2-propanediamine (Pfaltz & Bauer), the active ingredient in the metal deactivator additive (MDA), was also used without further purification. A specification Naval distillate (F-76) and two specification JP-5 fuels, designated as JP-5 fuels A and B were used in this work. The properties of JP-5 fuel A are described[16] elsewhere.

Results and Discussion

Theoretical Considerations. The calculation of absolute turbidity is determined from the ratio of the scattered light intensity at 90° to that at 0° and includes various instrumental parameters and corrections. The apparent turbidity (τ) is obtained by reducing many of the parametric values to constants in accordance with Eq. (1).

$$\tau = Kn^2 a \left[\frac{I_{90}}{I_0}\right] \qquad 1)$$

Where, K and a are experimentally determined instrumental correction factors, n is the refractive index of the solution, I_{90} and I_0 are the light intensities measured by the photomultiplier at 90 and 0 degrees, respectively. Turbidity will generally increase as the number of scattering centers increases. A parameter referred to as the excess turbidity (τ') can be obtained which represents the change in turbidity with respect to the unstressed fuel. Solute molecules with diameters smaller than 1/20 the wavelength of the incident light will scatter the light in all directions with equal intensities, so that the envelope of scattered light intensity is nearly spherical or symmetrical. As illustrated schematically in Figure 1, if molecular diameters increase beyond this size, the distances between the scattering centers within each molecule are sufficient to produce interference between the scattered light waves. In this experiment, light with a wavelength of 546 nm was employed. Thus, solute molecules with mean diameters greater than 280 angstroms (ca. 0.3μ) would produce dissymmetry in the scattering envelope, causing a greater proportion of light to be scattered in the forward direction. Under these conditions, an increase in dissymmetry is interpreted as an indication that the sizes of the scattering molecules in solution have increased above this threshold of 0.3μ. Experimentally, the dissymmetry (z) is obtained from the ratio of light scattered at 45° to 135°. The excess dissymmetry would be the change compared with some reference value. In pure polymer solutions, the measurements are referenced to those of the pure solvent. In fuels, the unstressed fuel could be used as a reference. However, this often leads to misleading results due to initial decreases in solute size at the start of the stress regimen. In this study, excess light scattering properties were not used since the fuels were not fresh and rapid initial changes in dissymmetry were observed.

Limitations of Light Scattering in Complex Media. In the presence of a solute that has a refractive index greater than that of the solvent, a phenomenon known as multiple scattering occurs. In multiple scattering, reflected light from particle surfaces acts as secondary light sources, which excite other scattering centers. This serves to enhance the light scattered back toward the source, resulting in erroneously low dissymmetry values. In this manner, multiple scattering would decrease the sensitivity of dissymmetry measurements used to monitor changes in solute sizes. Since the light is scattered as a result of induced dipole oscillations in the solute molecules, the intensity of the scattered light is greatly influenced by the dielectric properties of the surrounding medium. As the solute size increases, solvent molecules are expelled from the interior of the particles. In a multicomponent solvent such as fuel, various morphological and electronic properties of the solute particles will cause preferential expulsion of certain fuel constituents. This would result in the establishment of local gradients in solvent dielectric properties around the solute molecules.

Therefore, the analyst must exercise restraint in the application and interpretation of light scattering data in fuel when using these methods. It might therefore not be practical to attempt the determination of molecular configurations or sizes of soluble products in a fuel, since the principles upon which these methods are based might not apply. However, it may be possible to estimate intrinsic properties of solute molecules if they can be isolated and redissolved in a pure solvent. We have had some initial success in measuring polymer molecular weights in pure solvents containing various concentrations of fuel-generated insolubles. This will be discussed in a future publication.

JFTOT Oxidation. Since fuel is oxidized in an oxygen-limited environment in the JFTOT, it was anticipated that this would limit the extent of oxidation to a point before the formation of products larger than the wavelength of the incident light. The Naval distillate (F-76) and JP- 5 fuel A were stressed in the JFTOT. Samples of the stressed fuel were examined at discrete maximum heater tube temperatures to determine the temperature dependence of autoxidation and changes in fuel properties[12]. After each desired maximum heater tube temperature was attained, the oxygen concentration in the fuel effluent was allowed to equilibrate. The dissolved oxygen

content was then measured and a sample was then collected and examined by light scattering photometry. The results of these measurements are summarized in Figures 2 and 3, where the oxygen content, turbidity and dissymmetry are plotted against stress temperature.

The autoxidation of the diesel fuel, as shown by the oxygen content in Figure 2, begins between 80 and 170°C and gradually increases up to the maximum temperature of 350°C. The increases in turbidity and dissymmetry are consistent with autoxidation. The reaction rates of diesel fuels under these conditions are typically more gradual than the rates of jet fuels, as illustrated by the oxygen consumption profiles. This is probably due to a greater number of free radical pathways and the presence of natural oxidation inhibitors in the diesel fuel. The JP-5 oxidation rate begins at 200°C and increases until nearly all the available oxygen is consumed at 280°C. Accordingly, starting at 120°C, the turbidity and dissymmetry both begin to increase. At 220°C, they reach maximum values, at which point they begin to decrease. This peak in the light scattering properties corresponds to the outset of autoxidation. As the stress temperature increases, the dissymmetry values continue to fall until 280°C, at which point, all the available oxygen has been consumed. In the region where rapid autoxidation ensures, the turbidity again increases and continues to do so even after all the oxygen has been depleted.

It's difficult to definitively interpret light scattering measurements in a complex fuel medium but these findings imply that there is an initial increase in the number of larger product molecules before the autoxidation rate increases. As the temperature increases further and rapid autoxidation ensues, the production of large molecules does not predominate. After the oxygen is consumed, products are formed which have distinct light scattering properties by a process that does not require free oxygen. Thus, it may be entirely possible to form insoluble particulate in jet fuel after the oxygen has been consumed. It is not known if the presence of oxidized products is a prerequisite for these anaerobic changes. This will be answered by repeating the experiment with deoxygenated fuel.

Effects of Copper and Metal Deactivators. Oxygen overpressure (i.e., LPR) testing is used to simulate extended ambient storage. LPR stressing of JP-5 fuel A was conducted to illustrate the

effects of long-term storage on light scattering properties. As shown in Figure 4, significant changes in turbidity and dissymmetry were measured over a test period of 100 hours. Soluble reaction products are formed after 22 hours and continue to accumulate for up to at least 60 hours. The light scattering properties then decrease until the values return to the pre-stress level. This could indicate the presence of soluble products that accumulate until they precipitate from solution. The increases in both turbidity and dissymmetry would suggest that these products are increasing in both size and number. Similar periodicity in light scattering properties has also been observed in vented bottle tests conducted at lower temperatures[17].

It is well known that trace quantities of dissolved copper can act to enhance autoxidation in hydrocarbon fuels. This has been shown[18] to lower the temperature at which rapid autoxidation occurs in the JFTOT and to catalyze the decomposition of hydroperoxides. This is usually (but not always) accompanied by an increase in the quantities of fuel-insoluble reaction products. It has also been shown[12,16,19] that the metal deactivator additive (MDA) is extraordinarily effective in suppressing thermal deposition onto JFTOT heater tubes. Using light scattering measurements, it was possible to monitor the influences exerted by copper and MDA on fuel during thermal stress.

The impact of increasing soluble copper content on changes in the JP-5 fuels during LPR stress is shown in Tables I - III. The turbidity was measured after the stressed fuel samples had been in the dark for 3, 6 and 24 hours to assess the impact of post-stress residence time. In addition, the three hour samples were vacuum filtered through a 0.8μ membrane filter and remeasured. The turbidity of the unstressed fuel was 16×10^{-4}. Comparison of this value with the turbidity of the neat fuel stressed in the LPR illustrates the changes induced by stressing the fuel without copper. The data in Tables I and II show that, when JP-5 fuel A was stressed under these conditions, the impact of soluble copper on turbidity was negligible at concentrations as high as 100ppb. This is reflected in the amounts of total insolubles obtained gravimetrically. As discussed above, at 546nm, any scattering centers with a mean diameter greater than approximately 0.3μ should produce dissymmetry in the scattering envelope. Since filtration through a 0.8μ filter reduced both turbidity and dissymmetry values to levels near the unstressed fuel, the scattering particles in solution were larger than 0.8μ, even though the samples appeared clear before filtering. Turbidity

is also shown to decrease with time after stressing. This could be a consequence of precipitation of products from the fuel, or other continuing changes undergone by the soluble products. The lower turbidity value at 3 hours with 1000ppb Cu could be due to precipitation, as in the long-term LPR data depicted in Figure 4. The gravimetric data indicate that 1000ppb of copper did increase the quantity of insoluble products formed. As shown in Table III, increasing the copper content in the less thermally stable JP-5 fuel B had the same effect as the stress time was increased from 16 to 24 hours. Fuel B was more responsive to low levels of copper, as shown in the unfiltered turbidity values and in the corresponding gravimetric data. Note that in this fuel, significant increases in product formation were observed with as little as 10ppb added copper. This illustrates the variability in response to copper that is often observed among different fuel samples which may exhibit high thermal stabilities in the absence of copper.

Pande and Hardy[16] have evaluated the effects exerted by copper on thermal stability of jet fuels and how these effects were mediated by the presence of MDA. They used LPR stress to simulate long-term storage and the Gravimetric JFTOT (GravJFTOT) to evaluate the subsequent thermal stability. Gravimetric determinations of filterable and adherent insoluble products were obtained from the GravJFTOT. In addition to the GravJFTOT samples, aliquots before stressing and after LPR stress were also examined by light scattering photometry before filtration. Table IV summarizes light scattering measurements taken on JP-5 fuel B and the available GravJFTOT results. Recall that turbidity increases generally reflect an increase in the number of larger molecules formed and that dissymmetry increases as the molecular size increases. Subjecting the neat fuel to LPR stress increased both the number and size of the products. Following LPR stress with GravJFTOT stress produced substantial increases in both dissymmetry and turbidity. When MDA was added to the fuel at 5.8mg/L, there was a large increase in insoluble products formed whenever the fuel was subjected to thermal stress in the GravJFTOT. This was consistent with increases in light scattering properties that indicated the presence of large products in solution. While reproducible in this specification JP-5, this MDA-induced thermal instability is not considered typical and was not observed in other fuels similarly examined.

The addition of 94ppb Cu to JP-5 fuel B did not result in significant increases in light scattering

properties or in the total insolubles. MDA was effective in suppressing any catalytic activity exerted by the presence of 410ppb of copper in the LPR, which simulates long-term storage. However, MDA did not reduce the formation of insoluble reaction products during GravJFTOT stress with 410ppb copper. The light scattering data indicate that MDA was not effective in reducing the accumulation of *soluble* products when the copper-bearing fuel was subjected to simulated long-term storage (i.e., the LPR) before thermal stressing in the GravJFTOT. Pande and Hardy have measured[16] filterable insolubles from GravJFTOT stressing of several other copper-doped JP-5 fuels. They also found that MDA was effective in suppressing deposition from copper-bearing fuels only when it was added before LPR stress. These findings suggest that when a copper-bearing fuel is allowed to stand for an extended period of time, copper-mediated reactions can occur to such an extent that the products of these reactions exert a deleterious effect on thermal stability. Deactivation of the copper by the later addition of MDA would therefore have no impact on these soluble reaction products since they would not necessarily contain copper. Despite the controversial benefits of MDA at elevated temperatures, the addition of MDA to an aged copper-rich fuel would halt any further copper induced degradation in storage by chelating the soluble copper.

Summary

There are fundamental limitations to the extent that light scattering photometry can be used to determine intrinsic solute properties in fuels. Measurements of scattered light were, however, shown to correlate well with other observed changes in fuel stability in several stress regimens. This suggests that qualitative evaluations of fuels by light scattering may be possible. Light scattering measurements of stressed fuels also revealed changes in soluble fuel constituents which were not evident from measurements of insoluble products. This was illustrated by the fact that chemical reactions do not cease in the JFTOT after all the available oxygen has been consumed. Light scattering revealed significant increases in soluble products when the fuel was subjected to simulated long-term storage in an LPR before thermal stress. It may be possible to develop these techniques to determine intrinsic properties of the soluble products themselves. At the very least, the method provides additional information about the soluble products that serves to compliment, if not add another dimension to, what we can learn from examinations of the insoluble products.

Literature Cited

(1) Mayo, F. R.; Richardson, H. and Mayorga, G. D., "*The Chemistry of Ruel Deposits and Their Precursors*", Stanford Research Institute, final report prepared under Naval Air Propulsion Center contract N0019-73-0318, **1973**.

(2) Flory, P. J. *J. Chem. Phys.*, **1949**, *17*(3), 303.

(3) Debye, P. *J. Physical and Colloid Chem.*, **1947**, *51*(1), 18.

(4) Johnson, J. E.; Chiantella, A. J; and Carhart, H. W., "*Light Scattering in Fuels: Part I-Preliminary Studies on Diesel Fuel Stability*". Naval Research Laboratory Report No. 4422, **1954**.

(5) Johnson, J. E.; Chiantella, A. J. and Carhart, H. W. *I&EC*, **1955**, *47*(6), 1226.

(6) Shyuler, R. L.; Krynitsky, J. A. and Carhart, H. W. "*A Study by Light Scattering of the Effect of High Temperature on the Formation of Insolubles in Jet Fuels*". Naval Research Laboratory Report No. 5553, **1960**.

(7) Li, N. C.; Hazlett, R. N.; Ge, J. and Yaggi, N. F. *Fuel*, **1984**, *63*, 1285.

(8) Hazlett, R. N.; Hardy, D. R.; Cooney, J. V.; Beal, E. J.; Morris, R. E.; Beaver, B. D.; Mushrush, G. W. "*Mechanisms of Syncrude / Synfuel Degradation*". Naval Research Laboratory, final report DOE/BC/10525-16 (DE87001232), **1987**.

(9) Kalitchin, Zh. D.; Ivanov, Sl. K.; Tanielyan, S. K.; Boneva, M. I.; Georgiev, P. T., Ivanov, A and Kanariev, K. *Fuel*, **1992**, *71*, 437.

(10) Brice, B. A.; Halwer, M. and Speiser, R. *J. Opt. Soc. Amer.*, **1950**, *40*(11), 768.

(11) Hazlett, R. N.; Hall, J. M. and Matson, M. *Ind. Eng. Chem., Prod. Res. Dev.*, **1977**,*16*(2), 171.

(12) Morris, R. E.; Hazlett, R. N. and McIlvaine, C. L. *Ind. Eng. Chem. Res.*, **1988**, *27*, 1524-1528.

(13) Beal, E.J.; Hardy, D.R.; Burnett, J.C. *Proceedings of the 4th International Confernence on Stabilty and Handling of Liquid Fuels*; Giles, H.N., (Ed.); U.S. Department of Energy, Washington, DC, **1992**, 245-59.

(14) Beal, E.J.; Hardy, D.R. and Burnett, J.C. "*Aviation Fuel: Thermal Stability Requirements*", ASTM STP 1138; Kirklin, P.W. and David, P. (Eds.); American Society for Testing and Materials, Philadelphia, PA, **1992**, 138-50.

(15) ASTM "*Standard Test Method for Assessing Distillate Fuel Storage Stability by Oxygen Overpressure*", in Annual Book of ASTM Standards; ASTM: Philadelphia, **1993**; Volume 05.03, ASTM D5304-92.

(16) Pande, S. G. and Hardy, D. R. "*The Effect of Copper, MDA and Aging on Jet Fuel Thermal Stability as Measured by the Gravimetric JFTOT*". In the Proceedings of this meeting.

(17) Morris, R.E. and Wechter, M.A. *Prepr.- Am. Chem. Soc., Div. Petr. Chem.* **1994**, *39*(1), 58.

(18) Morris, R. E.; Turner, N. H.; Fuel Sci. & Tech. Int. **1990**, *8*(4), 327.

(19) Clark, R. H. *Proceedings of 3rd International Conference on Stability and Handling of Liquid Fuels*, R.W. Hiley, R.E. Penfold; J.F. Pedley, Ed., The Institute of Petroleum: London, UK, **1989**, 283.

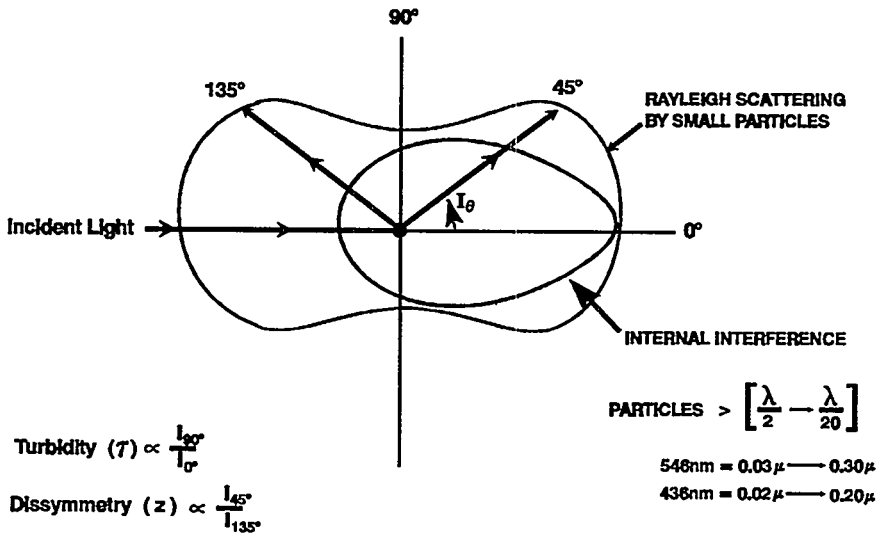

Figure 1. The effect of secondary scattering by large particles to produce dissymmetry in the scattered light.

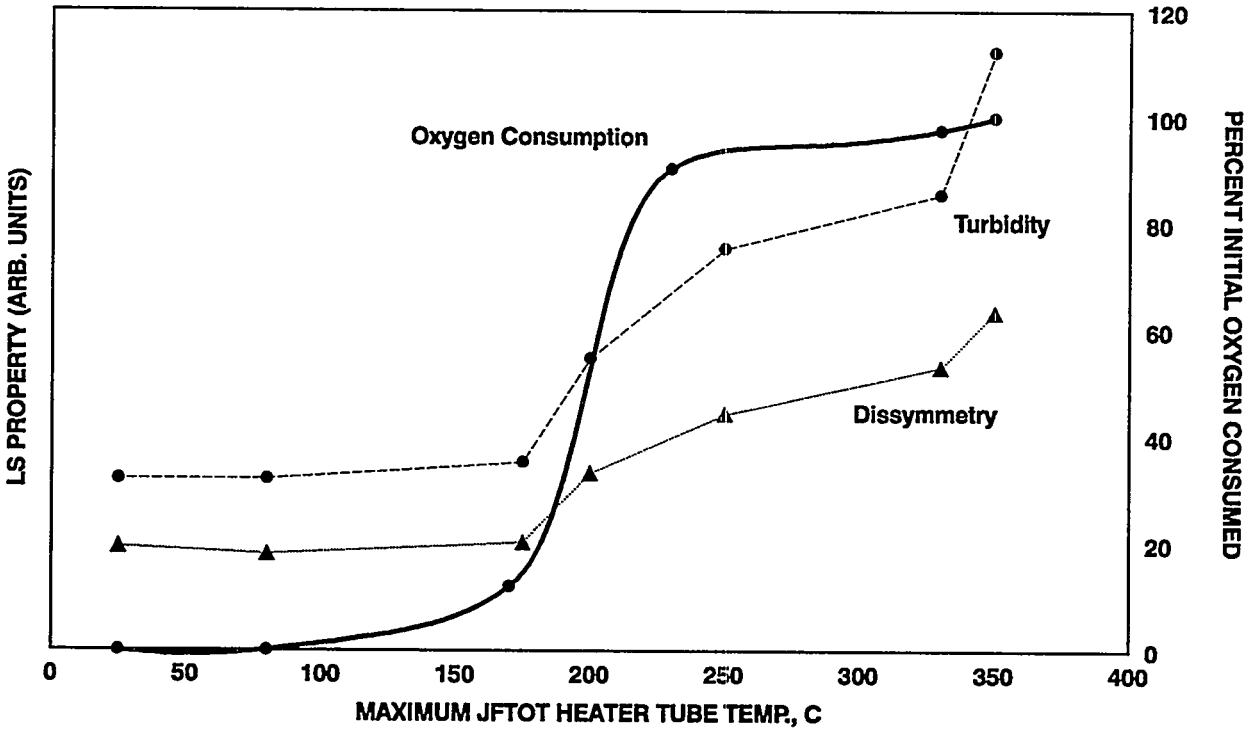

Figure 2. Correlation of light scattering properites with autoxidation of a naval distillate fuel during thermal stress in a JFTOT.

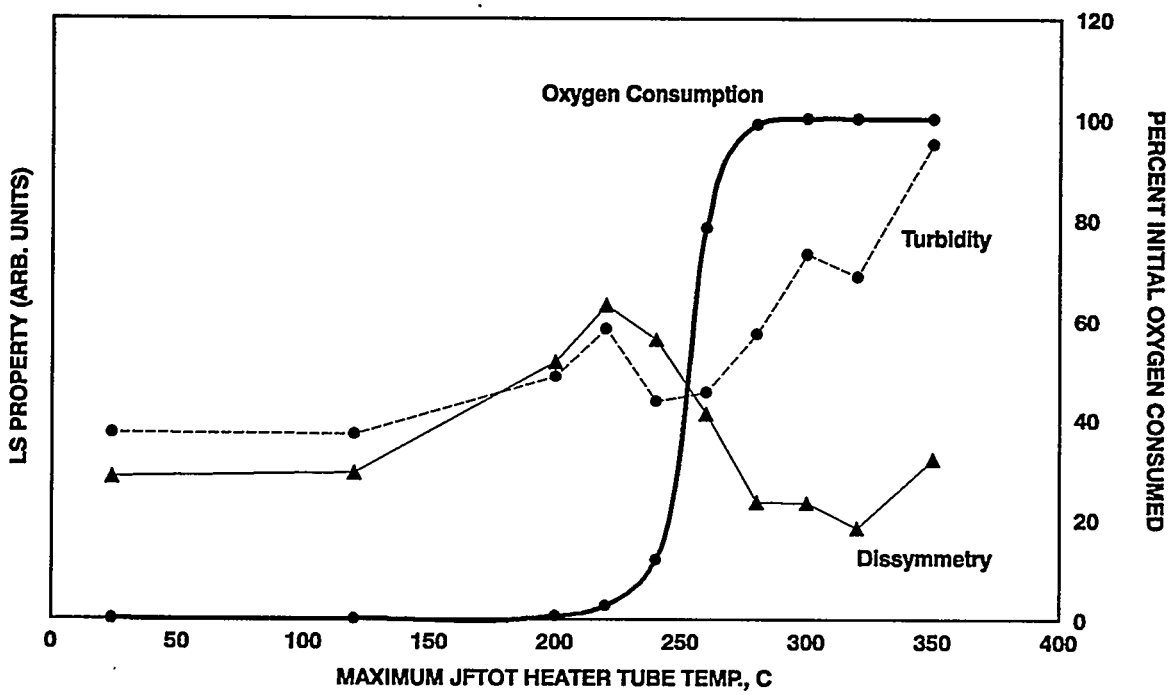

Figure 3. Correlation of light scattering properites with autoxidation of a JP-5 fuel during thermal stress in a JFTOT.

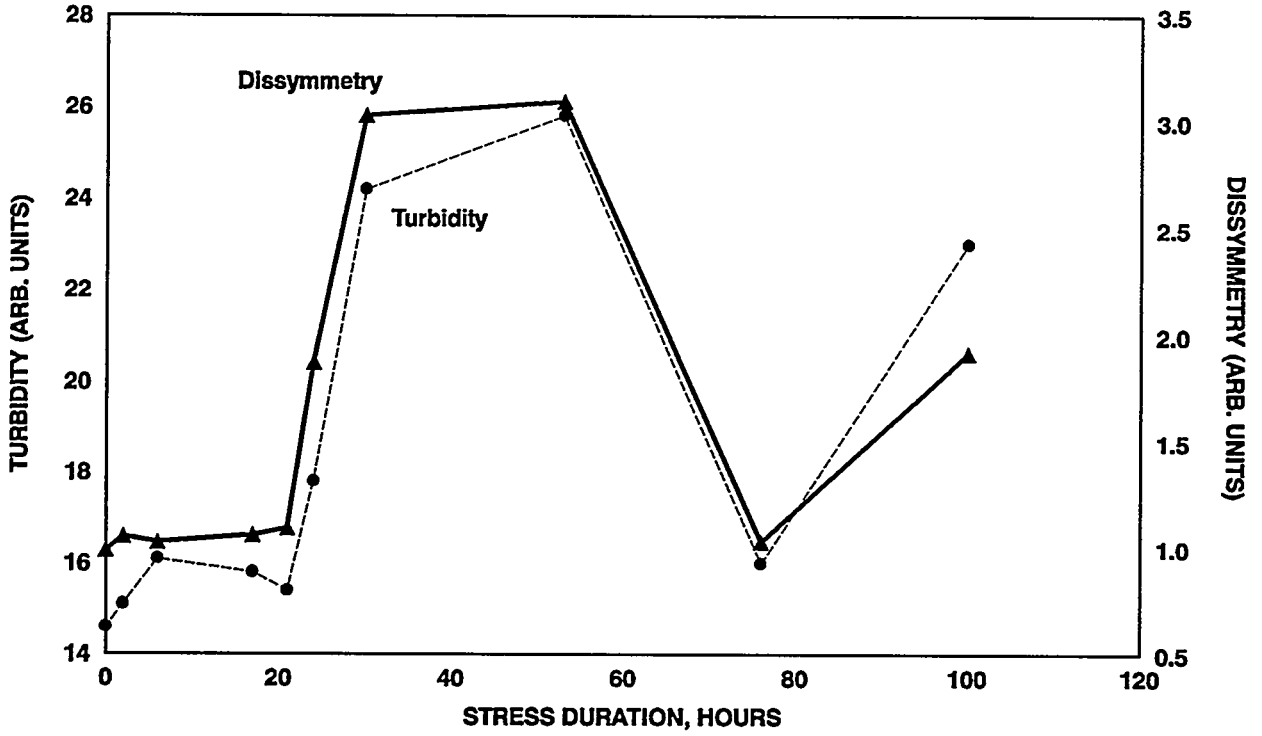

Figure 4. Changes in light scattering properties in a JP-5 fuel during extended stress in the oxygen overpressure (LPR) test at 90°C under 720 kPa air.

TABLE I. Turbidity measured in JP-5 fuel A at 3, 6 and 24 hours after LPR stress at 90°C under 720 kPa air.

16 hours LPR stress

Cu, ppb	Turbidity (τ), x 10^4				Total Insolubles, mg/L
	3hrs	3hrs, filtered 0.8μ nylon	6 hrs	24 hrs	
0	19.3	20.7	22.0	21.6	0
10	18.9	20.1	21.6	21.3	1
100	20.9	20.8	20.1	21.6	1
1000	149.7	10.8	84.3	52.0	7

TABLE II. Turbidity measured in JP-5 fuel A at 3, 6 and 24 hours after LPR stress at 90°C under 720 kPa air.

24 hours LPR stress

Cu, ppb	Turbidity (τ), x 10^4			Total Insolubles, mg/L
	3hrs	3hrs, filtered 0.8μ nylon	24 hrs	
0	20.7	21.5	21.1	1
10	21.1	21.1	28.8	0
100	41.6	20.9	32.8	5
1000	84.9	24.1	78.4	9

TABLE III. Turbidity measured in a less thermally stable JP-5 fuel B after LPR stress at 90°C under 720 kPa air for 16 and 24 hours.

Cu, ppb	16 hours LPR			24 hours LPR		
	$\tau \times 10^4$ unfiltered	$\tau \times 10^4$ filtered	Total Insolubles, mg/L	$\tau \times 10^4$ unfiltered	$\tau \times 10^4$ filtered	Total Insolubles, mg/L
0	51.1	19.6	1	65.8	20.4	7
10	79.8	21.0	6	79.2	21.1	9
100	117.8	22.0	9	77.6	22.5	14
1000	151.9	23.1	18	58.2	23.4	23

Table IV. The influences of copper and MDA on JP-5 fuel B as detected by light scattering and gravimetry after LPR* and Gravimetric JFTOT stressing.**

Stress Regimen	Cu, ppb	MDA, ppm	$\tau \times 10^4$	z	Total Insol., mg/L
none			22	0.8	
LPR			43	0.6	
LPR + GravJFTOT			62	2.7	8.1
GravJFTOT	94		28	2.2	8.3
LPR + GravJFTOT	94		33	2.1	7.4
none		5.8	12	1.2	
LPR		5.8	17	1.9	
GravJFTOT		5.8	180	3.0	11.8
LPR + GravJFTOT		5.8	111	2.8	7.4
none	410	5.8	13	1.3	
LPR	410	5.8	23	2.1	
GravJFTOT	410	5.8	33	0.8	10.4
LPR + GravJFTOT	410	5.8	183	3.0	10.2

*24 hrs at 90°C under 400 kPa air. **2.5 hrs at 260°C and 4 mPa pressure.

5th International Conference
on Stability and Handling of Liquid Fuels
Rotterdam, the Netherlands
October 3 - 7, 1994

AN IMPROVED REFERENCE FUEL SYSTEM: PART 2 - A STUDY OF ADHERENT AND FILTERABLE INSOLUBLES FORMATION AS FUNCTIONS OF TRIMETHYLPYRROLE CONCENTRATION IN DODECANE

Edmund W. White* and Michael D. Klinkhammer

Naval Surface Warfare Center, Carderock Division, 3A Leggett Circle, Annapolis, MD 21402-5067

ABSTRACT

At the 4th International Conference on the Stability and Handling of Liquid Fuels, a trimethylpyrrole (TMP)/dodecane reference fuel system for use with ASTM Test Method D2274 was presented. It was concluded that the TMP/dodecane system would have sufficient reproducibility of total insolubles values to serve as a reference fuel system. In this paper, the filterable and adherent insolubles from the same data base are examined. Like the total insolubles, the FY 91 results for both adherent and filterable were less scattered than the FY 90 data. Both adherent and filterable insolubles were found to be adequately represented as linear functions of the initial TMP concentration. Further, the data support a hypothesis that filterable insolubles do not form in the 16 hours of stress unless the initial TMP concentration is greater than about 25 mg/100 mL. A plot of the FY 91 ratio of adherent insolubles to filterable insolubles as a function of the initial TMP concentration approaches 0.6 at TMP concentrations in excess of 75 mg/100 mL.

INTRODUCTION AND BACKGROUND

Following World War II, the Navy developed a stability test method to limit the quantities of unstable cracked stocks being blended with straight run gas oils to produce diesel fuels. The method was accepted, with modifications, by ASTM as Test Method D2274 for Oxidation Stability of Distillate Fuel Oil (Accelerated Method) and first published in 1964.

The test method starts with aging a 350 mL sample of filtered fuel at 95°C for 16 hours during which oxygen is bubbled through the fuel at a rate of 3 L per hour. After aging, the sample is cooled in the dark to about room temperature and is then filtered to obtain the quantity of filterable insolubles. Adherent insolubles are removed from the oxidation cell and associated glassware using an equal volume blend of toluene, acetone, and methanol (TAM trisolvent). The trisolvent is evaporated to obtain the quantity of adherent insolubles. The sum of the filterable and adherent insolubles, expressed in mg/100 mL, is reported as the total insolubles.

Unfortunately, the repeatability and the reproducibility of the method were poor. In the late 1960's, the precision statements for the method indicated that, for fuels with total insolubles of 1.0 mg/100 mL or below, the repeatability was 0.3 and the reproducibility was 1.0 mg/100 mL. Interlaboratory testing in the early 1970's indicated that, for total insolubles above 1.0 mg/100 mL, the repeatability was 0.9 and the reproducibility was 3.0 mg/100 mL.

Partly as a consequence of this poor precision, the U. S. Navy found it necessary to reduce the maximum total insolubles permitted by the specification MIL-F-16884 for its NATO F-76 Naval Distillate ship fuel from 2.5 to 1.5 mg/100 mL, to insure the acquisition of stable fuels. Also, in 1983 the Quadripartite Navies (the United States, the United Kingdom, Canada, and Australia) expressed concern over the adequacy of the method for measuring instability and requested ASTM Committee D02 on Petroleum Products and Lubricants to address the poor precision.

Papers presented at the Third (London) and Fourth (Orlando) International Conferences[1,2,3,4] discussed some of the efforts undertaken by ASTM Committee D02 and by Carderock Division, Naval Surface Warfare Center (CARDEROCKDIV), to explore the variables

which affect results and to improve Test Method D2274. In summary:

* Committee D02 circulated a questionnaire developed by CARDEROCKDIV to ascertain how the test method was being run. Responses revealed serious departures from the standard, so the test method was revised to emphasize the more important criteria, e.g. use of reagent grade solvents and pure oxygen vis-a-vis reported technical grade solvents and compressed air.

* As a result of the wide use of membrane filters rather than the specified glass fiber filter medium in a Gooch crucible, a cellulose ester membrane filter was specified as the standard filter medium.

* The jet gum apparatus (ASTM Test Method D381) used for evaporating trisolvent from the adherent insolubles was replaced with evaporation on a hot plate at 135^{o}C under a hood. It is a faster method that gives comparable results.

* CARDEROCKDIV ascertained that different heating baths yielded statistically different results. Consequently, Committee D02 made a survey to determine the variations in heating baths being used for the test method. Responses showed wide ranges in the volume of heating oil per oxidation cell (from 2.5 to 6.7 L/cell) and in the wattage available for heating per oxidation cell (from 125 to 367 watts/cell). A standard heating bath requirement is being developed and use of dummy oxidation cells to fill vacant slots is being specified.

* It was discovered that different analysts were starting the 16-hour stress period at different times. The zero time has now been defined as the time the first of a

batch of oxidation cells is placed in the heating bath.

* CARDEROCKDIV is developing a reference fuel system for use in conjunction with D2274 for training analysts, for use as a blind sample in quality control laboratories, for use in qualifying new apparatus, and for use in certifying a laboratory.

This paper addresses the quantities of adherent and filterable insolubles formed as functions of the concentration of active ingredient in the base reference fuel.

OVERVIEW OF REFERENCE FUEL DEVELOPMENT

Details of the development of a reference fuel system were presented at the 3rd and 4th International Conferences.[3,4] The original base fuel consisted of 75% dodecane, 22.5% t-amylbenzene, and 2.5% dodecene. The components were commercial grade chemicals and various concentrations of 1,2,5-trimethylpyrrole (TMP) were added as the active ingredient. When commercial grade t-amylbenzene became unavailable following the 3rd International Conference, we converted to a system consisting only of TMP in dodecane.

The FY 90 tests of the simplified system yielded total insolubles results with an unsatisfactory scatter. Experimentation indicated this resulted from the use of aged TMP by several of the analysts. TMP concentrations ranged from 16.5 to 150 mg/100 mL of dodecane. In the FY 91 tests, fresh TMP from a newly-opened 5-gram bottle was used for each batch of test fuels. This practice reduced the scatter of the total insolubles. TMP concentrations ranged from 10 to 80 mg/100 mL of dodecane. Other details of the program were presented at the Orlando Conference.[4]

In the previous papers, results were expressed as milligrams of total insolubles per 100 mL of reference fuel. In this paper, we examine the two types of insolubles which, when added together, yields "total insolubles," i.e. the adherent insolubles and the filterable insolubles. The data were obtained as part of the total insolubles obtained in FY 90 and FY 91 with the dodecane as base reference fuel.

RESULTS AND DISCUSSION

Adherent Insolubles - Figures 1 and 2, drawn to the same scale, show averages of the adherent insolubles values obtained by each operator in the FY 1990 and 1991 programs. (Different operators used different sizes of replicates in some instances. A normal replicate was a duplicate, but some replicates consisted of six independent determinations.) Note the smaller degree of scatter in the FY 1991 data. Linear fits obtained by regression analysis are shown. The equations for the lines are:

$$AI_{90} = 0.065[TMP] - 1.15 \quad (1)$$

$$AI_{91} = 0.016[TMP] + 0.05 \quad (2)$$

where AI stands for "adherent insolubles," and [TMP] stands for the "trimethylpyrrole concentration." The subscripts 90 and 91 indicate the fiscal year the data were obtained. The correlation coefficients are 0.96 and 0.98 respectively, so the empirical equations represent good fits of the data. The standard errors of estimate, indicative of the degree of scattering, were 0.930 for the FY 90 data and 0.214 for the FY 91 data, i.e. the FY 90 scattering was over 4.3 times that of the FY 91 scattering.

It is evident that the slope of the line for the FY 90 data is over four times that of the slope of the line for the FY 91 data. We ascribe this to the use of somewhat aged TMP by several of the analysts participating in the FY 90 program. The aged TMP would have contained oligomer at the time it was introduced into the dodecane base fuel. Hence, it is postulated that the higher concentration of oligomer in the fuel would have caused more diffusion, hence greater adherent insolubles deposition.

The deposition of adherent insolubles onto the wetted surfaces of the apparatus used in Test Method D2274 is postulated as an adsorption process after diffusion of the oligomer through a boundary layer of fuel.[5] The classical Freundlich isotherm equation[6] relates the quantity of material adsorbed at equilibrium to the concentration of the material in the fluid:

$$m = kc^{1/n} \qquad 3)$$

where m is the mass absorbed per unit mass of adsorbent, c is the concentration in the fluid, and k and n are constants for the temperature and the system.

Although the D2274 system represents a dynamic condition rather than the static equilibrium situation to which the Freundlich equation applies (the reaction to form the oligomer is a continuing one while unreacted TMP remains in solution), we decided to check the applicability of such an exponential equation to the experimental data:

$$AI = a[TMP]^{b} \qquad 4)$$

where AI represents the quantity of adherent insolubles in mg per 100 mL of fuel, [TMP] represents the original TMP concentration, and a and b are constants.

Using the averages of all data for each TMP concentration, we developed the following equations:

$$AI_{90} = 0.0028\ [TMP]^{1.62} \quad 5)$$

$$AI_{91} = 0.0224\ [TMP]^{0.91} \quad 6)$$

The correlation coefficients were 0.97 and 0.83 respectively, hence the exponential fit was as good as the linear fit for the FY 90 data but appreciably worse for the FY 91 data.

Up to this point, we have examined the total adherent insolubles data for FY 90 and 91. However, the data of the individual analysts can also be expressed in similar ways. To illustrate this, we will consider only the linear regressions which yield the following equations for the four analysts who participated in the program in FY 1991:

$$AI_1 = 0.015[TMP] + 0.18 \quad 7)$$
$$AI_2 = 0.012[TMP] + 0.18 \quad 8)$$
$$AI_3 = 0.019[TMP] + 0.06 \quad 9)$$
$$AI_4 = 0.017[TMP] + 0.00 \quad 10)$$

The coefficients of correlation ranged from 0.82 to 0.93, i.e. generally slightly poorer than obtained with the total set of data. The standard errors of estimate ranged from 0.173 to 0.267 whereas the overall body of FY 91 data yielded a standard error of estimate of 0.214.

Filterable Insolubles - Figures 3 and 4 show the operator averages for filterable insolubles in FY 90 and FY 91 respectively. In consonance with the theory that filterable insolubles do not form until the fuel is saturated with oligomer, the data are correlated using two straight lines, - one essentially congruent

with the TMP-axis and one fitting the data generated at the higher initial TMP concentrations.

The FY 90 average filterable insolubles for initial TMP concentrations from 0 to 33 was 0.20 with a standard deviation of 0.14, whereas the FY 91 average filterable insolubles for initial TMP concentrations from 0 to 25 was 0.07 with a standard deviation of 0.04. Considering the standard deviations, both averages were sufficiently low to support the theory of no filterable formation prior to saturation of the fuel with oligomer.

The equations for the filterable insolubles formed at higher TMP concentrations were:

$$FI_{90} = 0.168[TMP] - 7.06 \quad (11)$$

$$FI_{91} = 0.043[TMP] - 1.07 \quad (12)$$

The correlation coefficients were both 0.96 and the standard errors of estimate were 1.98 and 0.25 for FY 90 and 91 respectively. It is obvious from a comparison of figures 3 and 4, which were drawn to the same scale, that there was less scatter of FY 91 data than of FY 90 data; the standard errors of estimate support this conclusion.

By setting the filterable insolubles to zero in equations 11 and 12, we can calculate the point at which the regression line crosses the TMP-axis. The FY 90 TMP-axis (initial TMP concentration) intercept was about 42 mg/100 mL, which was appreciably higher than roughly 25 mg/100 mL intercept for the FY 91 data.

In FY 91, the four analysts each obtained very low filterable insolubles averages from initial TMP concentrations below 20 to 30 mg/100 mL. Their individual filterable insolubles averages for this low end of TMP concentrations ranged from 0.03 to 0.09 with standard deviations of 0.04 to 0.10. This further supports our hypothesis that no filterable insolubles are formed below the

point at which the fuel is saturated with oligomer. It is postulated that any filterable insolubles measured below the threshold (intercept) value can be accredited to small amounts of adherent insolubles that are physically displaced from the glassware, e.g. during rinsing with the isooctane hydrocarbon solvent, or else to oligomer which is adsorbed by the filter medium.

The empirical linear equations obtained for each analyst by regression analysis of filterable insolubles obtained from the higher initial TMP concentrations (above 20 to 30 mg/100 mL) were:

$$FI_{91-1} = 0.041\ [TMP] - 0.83 \quad (13)$$

$$FI_{91-2} = 0.032\ [TMP] - 0.55 \quad (14)$$

$$FI_{91-3} = 0.047\ [TMP] - 1.20 \quad (15)$$

$$FI_{91-4} = 0.042\ [TMP] - 1.10 \quad (16)$$

The correlation coefficients for these equations were 0.90, 0.88, 0.95, and 0.94 respectively. The standard errors of estimate ranged from 0.22 (for equation 14) to 0.47 (for equation 13).

The TMP-axis intercepts, rounded to whole numbers, of the lines represented by these four equations were 20, 17, 26, and 26 respectively. This implies that it takes an initial concentration of 17 to 26 mg TMP/100 mL dodecane fuel to generate enough oligomer in 16 hours at 95°C to effect saturation of the fuel.

AI/FI Ratio - Figures 5 and 6 show the ratio of the AI (adherent insolubles) to the FI (filterable insolubles) for FY 90 and 91 respectively, as a function of the initial TMP concentration. Both the FY 90 and 91 ratios seem to be approaching asymptotic values of 0.5 to 0.6 respectively. The reciprocal FI/AI ratios shows the filterable insolubles approach a value 70 to 100 per cent more than the adherents.

Examination of figures 5 and 6 show that, when initial TMP concentrations are low (below 35 or 40 mg TMP/100 mL fuel), the scatter of data points around the trend curve is greater than it is at higher initial TMP concentrations. In particular, scatter is greatest when the initial TMP concentration is below about 25 mg/100 mL, i.e. the point where fuels are thought to be saturated with oligomer.

FINDINGS AND CONCLUSIONS

1. The components of total insolubles, viz. the adherent and filterable insolubles, are individually significant and can be obtained with a fair degree of repeatability and reproducibility at the higher TMP concentrations.

2. The quantity of adherent insolubles produced in dodecane to which various concentrations of 1,2,5-trimethylpyrrole have been added can be expressed as a linear function of the initial TMP concentration. The linear equation for the FY 91 data, equation 2, has a correlation coefficient of 0.98 and a standard error of estimate of 0.214.

3. Evidence is growing that filterable insolubles do not form until a fuel is saturated with an oligomer oxidation product that is the precursor to both adherent and filterable insolubles. An initial concentration of 20 - 25 mg TMP/100 mL of reference fuel seems to be required to reach the threshold for filterable insolubles formation in the 16 hour stress period used by Test Method D2274. The four analysts participating in the FY 91 program averaged only 0.03 - 0.09 mg filterable insolubles per 100 mL of reference fuel when the initial TMP concentration was below the threshold value. It is postulated that any filterable insolubles measured below the threshold value represents adherent insolubles that have been physically displaced from the glass-

ware, e.g. during rinsing with hydrocarbon solvent, or else oligomer that is adsorbed by the filter medium.

4. The quantity of filterable insolubles formed when the initial TMP concentration exceeds the threshold value appears to be a linear function of the TMP concentration. The FY 91 data were fitted by equation 12 with a correlation coefficient of 0.96 and a standard error of estimate of 0.25.

5. The AI/FI ratio becomes very consistent when initial TMP concentrations in the reference fuel exceeds 35 - 40 mg/100 mL FY 91 data yielded a ratio of about 0.6, so filterable insolubles were about 70% greater than adherent insolubles.

TECHNICAL REFERENCES

1. White, E.W., "A Study of Variables Affecting results Obtained in the ASTM D2274 Accelerated Stability Test," pp. 646-662 Proceedings 2nd International Conference on Long Term STorage Stabilities of Liquid Fuels 1986, San Antonio, TX.

2. White, E.W. and R. J. Bowen, "A Study of Variables Affecting Results Obtained in the ASTM D2274 Accelerated STability Test, Parts 2 & 3 - Effects of Selected Chemical and Physical Factors," pp. 659 - 686 Proceedings 3rd International Conference on Stability and Handling of Liquid Fuels, 1988, London, U.K.

3. Klinkhammer, M.D., E.W. White, and K.W. Flohr, "The Development of Reference Fuels for Use with the ASTM D2274 Test for Fuel Storage Stability," pp. 554 - 565, Ibid.

4. Klinkhammer, M.D. and E.W. White, "An Improved ASTM D2274 Reference Fuel System," pp. 605 - 619, Proceedings 4th International Conference on Stability and Handling of Liquid Fuels, 1991, Orlando, FL, USA

5. White, E. W. "A Fuel Stability Study: Filterable and Adherent Insolubles as Functions of Time," Preprint Paper -- 208th Amer. Chem. Soc. Meeting, Div. Fuel Chem., vol. 39 (#3), pp. 938 - 942, Washington, DC.

6. Castellan, G. W. Physical Chemistry (3rd Ed.), Addison-Wesley Publishing Company, Reading, MA, 1983, pp. 426 - 427.

ACKNOWLEDGMENTS: The authors thank those who conducted tests noted in this paper, -- R. Bowen, T. Dapp, J. Malcolm, D. Smith, and Dr. R. Venkatachalam, and, from ARTECH CORP., K. Flohr, R. Quimby, and J. Cowan. We also thank Dr. Bruce Friedman for the many calculations and correlation attempts used and unused for this paper. Although the work was funded by Office of Naval Research (Dr. A. Roberts, ONR 33) through CARDEROCKDIV's Shipboard Energy R&D Office (W. Stoffel) with R. Strucko as Project Manager, ideas and opinions expressed in this paper are those of the authors and do not necessarily represent those of the Navy.

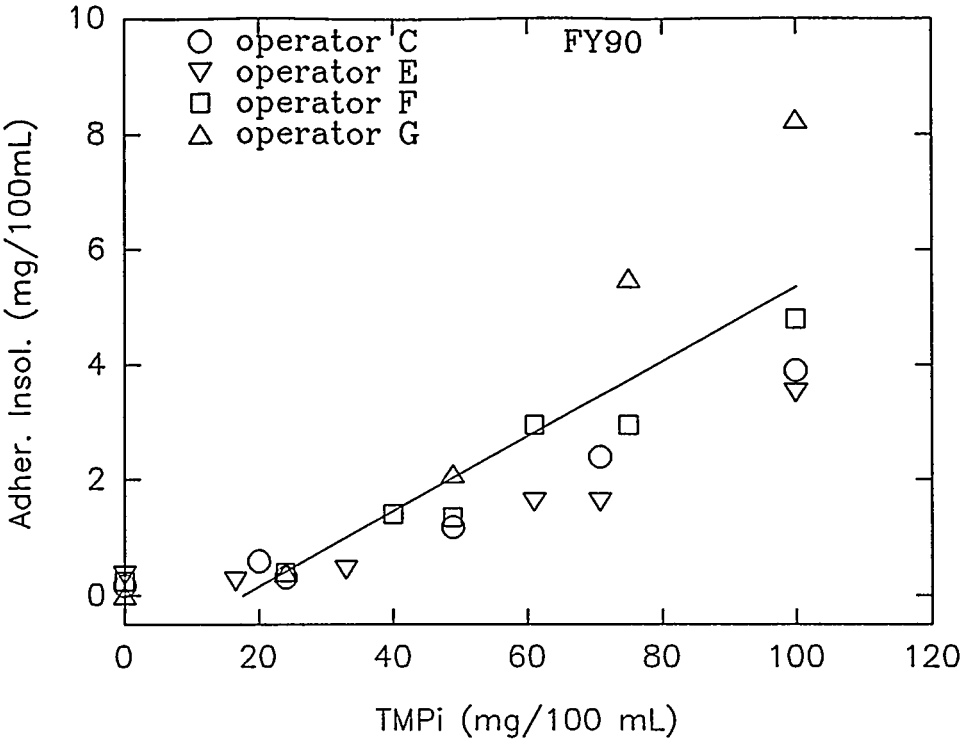

Figure 1. FY90 Adherent Insolubles as a Function of Initial 1,2,5 Trimethylpyrrole Concentration

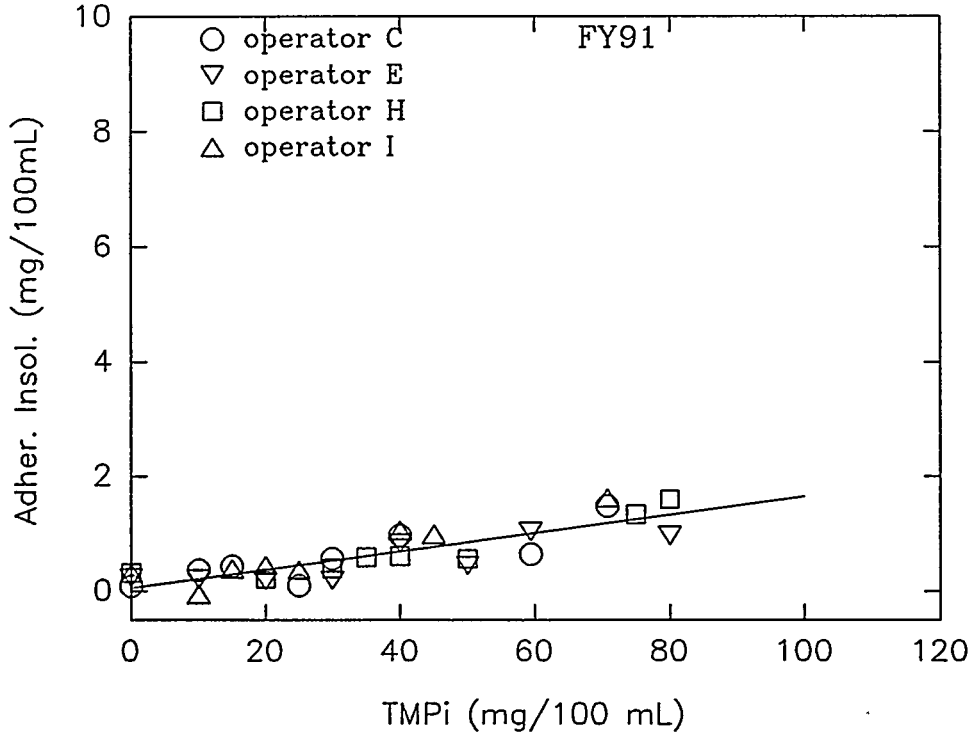

Figure 2. FY91 Adherent Insolubles as a Function of Initial 1,2,5 Trimethylpyrrole Concentration

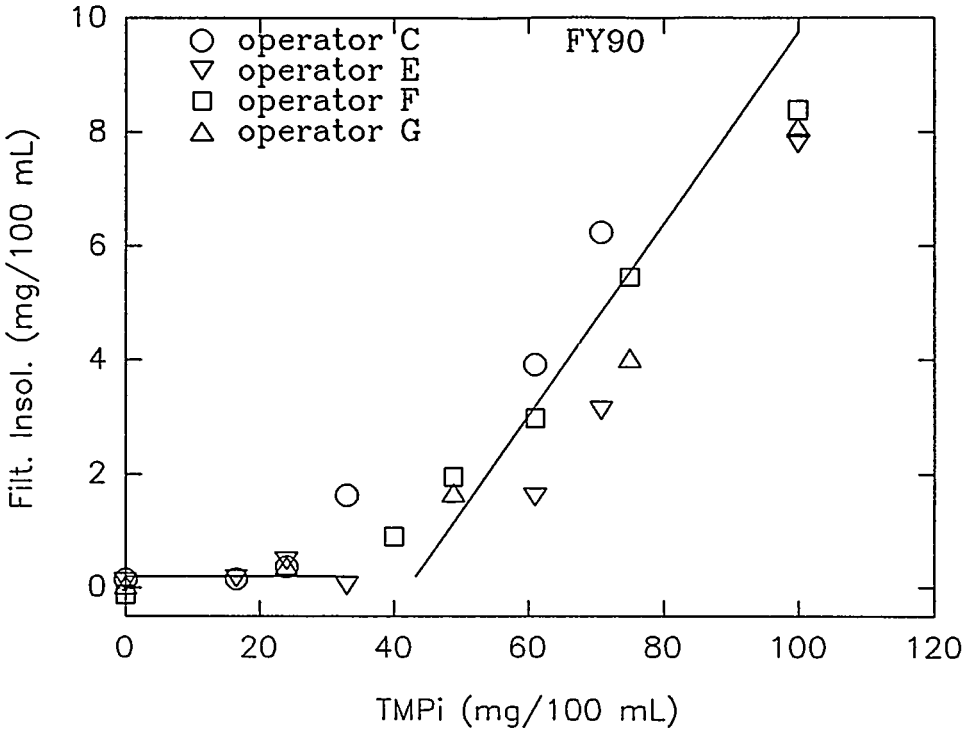

Figure 3. FY90 Filterable Insolubles as a Function of Initial 1,2,5 Trimethylpyrrole Concentration

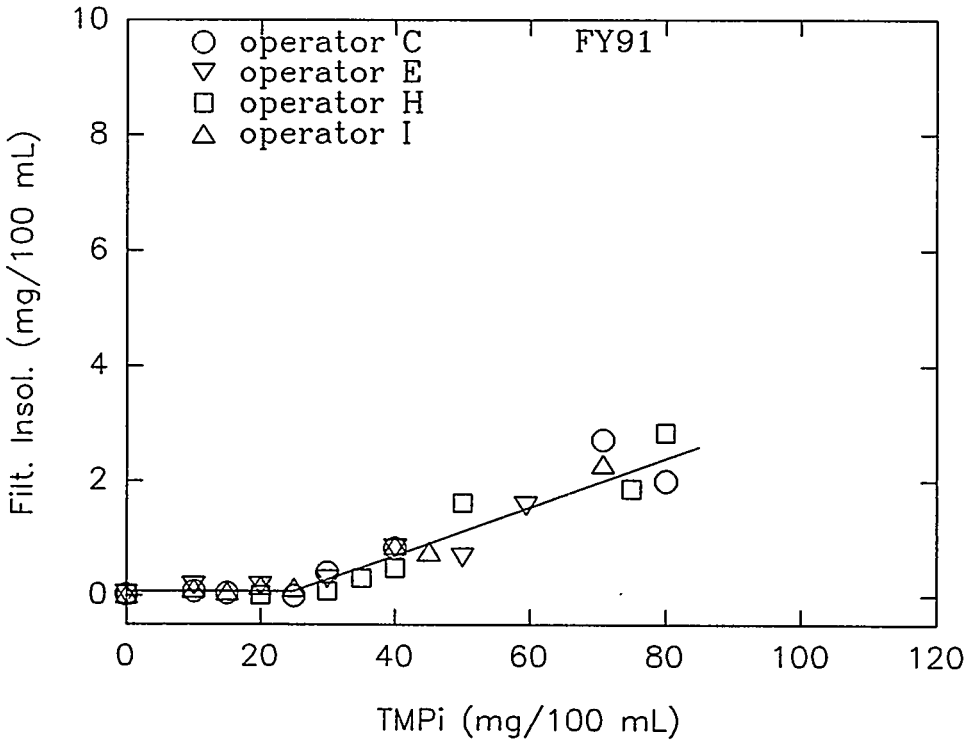

Figure 4. FY91 Filterable Insolubles as a Function of Initial 1,2,5 Trimethylpyrrole Concentration

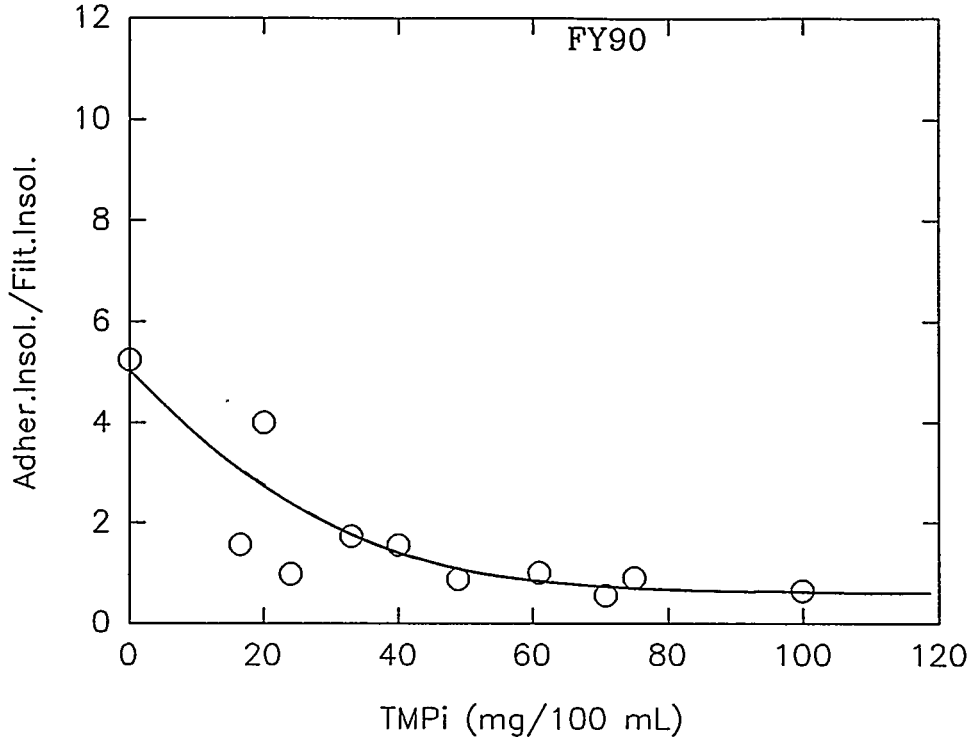

Figure 5. Ratio of Adherent to Filterable Insolubles as a Function of 1,2,5 Trimethylpyrrole Concentration for FY90

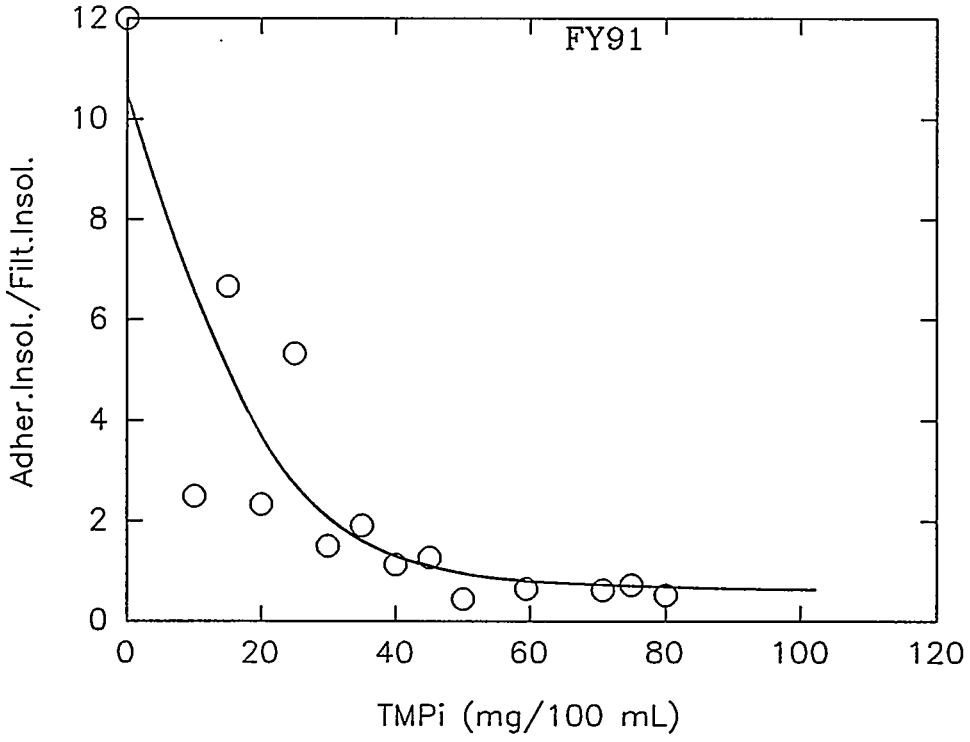

Figure 6. Ratio of Adherent to Filterable Insolubles as a Function of 1,2,5 Trimethylpyrrole Concentration for FY91

5th International Conference on
Stability and Handling of Liquid Fuels
Rotterdam, the Netherlands
October 4-7, 1994

REVISED PROCEDURE FOR THE MEASUREMENT OF PARTICULATE MATTER IN NAVAL JP5 AVIATION TURBINE FUEL (F44; AVCAT) USING THE CONTAMINATED FUEL DETECTOR (CFD).

Grier G McVea and Alan J Power

Airframes and Engines Division, Aeronautical and Maritime Research Laboratory (AMRL), 506 Lorimer Street, Fishermens Bend, Victoria, AUSTRALIA 3207

ABSTRACT

USA Military Specification MIL-D-22612 provides a procedure for measurement of particulate levels in Naval aviation gas turbine engine JP5 fuel (F44; RAN AVCAT) using the contaminated fuel detector (CFD). Evaluation of this procedure within the specification has revealed significant shortcomings in the application of the theoretical principles upon which the method is based. CFD measurements have been compared to gravimetric results from ASTM D2276, which provides accurate determination of concentrations of particulate matter in JP5. Inaccuracies evident in the CFD readings have been found to relate to the high sensitivity of the CFD to variations in fuel particulate extinction coefficients (ECs) (relating to fuel sediment colour) and to an error in the application of light transmittance theory in the recommended method. This report demonstrates that accurate CFD determination of JP5 particulate concentrations depends on spectrophotometric measurement of a narrow range of ECs of particulate matter. A range of fuel sediments derived from Australian naval ship and shore fuel storages was studied. It was observed that the CFD plot, which is in light transmittance mode, in theory provides a curved line graph against the gravimetric test results, whereas MIL-D-22612 describes a straight line graph. It was concluded that this must be an approximation. However, conversion of light transmittance data derived from the CFD into the reciprocal logarithm to give light absorbance data was shown to give a straight line graph which corresponded well with the gravimetric results. This relationship depended on construction of the graph on the basis of a narrow range of known particulate ECs. The conversion to absorbance gave improved correlation for JP5 particulate measurements with gravimetric procedures, using the CFD.

INTRODUCTION

The CFD, developed by the USN Aeronautical Engineering Laboratory (AEL) and adopted as Military Specification MIL-D-22612, provides a means for determining levels of particulate matter in JP5 aviation fuel when at sea. This ship-board instrument is also referred to as the AEL MK II or III. It was reported to AMRL that the CFD was not giving results consistent with those obtained from laboratory ASTM Method D 2276 for gravimetric measurements of fuel particulate. JP5 was being regarded as suspect, due to significantly higher fuel contamination values recorded by the CFD, and in some cases high purity fuel had been rejected on the basis of the CFD. Discrepancies between these values have been investigated by AMRL, with the objectives of (i) finding the reason for this lack of correlation, and (ii) possibly developing a revised method for more reliable operation of the CFD. Results of this research are reported here.

SUMMARY OF THE INITIAL INVESTIGATION FOR REVISED USE OF THE CFD

Theory of Light Measurements:

According to the combined Beer-Lambert law, the transmittance **T** is defined as the ratio of unabsorbed light irradiation **I** to the intensity of the incident irradiation $\mathbf{I_o}$.

Thus, $\mathbf{T} = \mathbf{I}/\mathbf{I_o}$; *(Equation 1)*

The absorbance **A** is the logarithm of the reciprocal of transmittance **T**.

Thus, $\mathbf{A} = \log 1/\mathbf{T} = \log \mathbf{I_o}/\mathbf{I} = -\log \mathbf{I}/\mathbf{I_o}$. *(Equation 2)*

These equations provide the basis for the investigation by AMRL into the reliability and accuracy of the procedure for field measurement of particulate contamination in Australian Naval aviation gas turbine fuel, using the CFD.

Light measurement Mode of the CFD:

It was not known at the initial stages of this investigation whether the CFD meter output was recording in transmittance or absorbance. Initially, optical measurements made by CFD Models EMSE 388R/390R (Cv International) were correlated experimentally with those from a visible spectrophotometer, to compare the CFD output with known light measurements. The transmittance mode was tested against *Equation 3* (derived from *Equation 1*), using neutral density (ND) filters.

Since the initial CFD set up output is 600 micro amps ($\mathbf{I_o}$), then

$$\%\mathbf{T} = \frac{\text{CFD } \textit{Meter Reading } (\mathbf{I}, \text{ micro amps}) \times 100}{(\mathbf{I_o}, 600 \text{ micro amps})} \qquad \textit{(Equation 3)}$$

From the two examples given below, it may be seen that %**T** calculated from the CFD readings for known neutral density (ND) filters corresponded very closely with the nominal values for %**T** quoted for the filters. These %**T** values also correlated well with those obtained using a uv/visible spectrophotometer. Similarly, it may also be seen that there was quite good correlation between the observed and calculated (*Equation 4*) values for absorbance **A**.

Visible Spectrophotometer (at 560 nm; Neutral Density (ND) Filters):

	Filter ND 0.1	Filter ND 0.2
Absorbance **A** (nominal)	0.1	0.2
% Transmittance **T** (nominal)	80	63
CFD Reading:(micro amps)	487	397
Calculated %**T**	81	66
Calculated **A***	0.092	0.180

{* **A** = log 100 / %**T**} *(Equation 4)*

In order to determine whether the output of the CFD was reading in **absorbance** or **transmittance**, concentrations of typical JP5 particulate contaminants in pre-filtered JP5 were measured by the CFD and plotted against concentration. It was observed that with a material possessing a relatively high extinction coefficient (ferric oxide), subtraction of CFD micro amp readings for top and bottom filters, as required by MIL-D-22612, gave a curved line graph. This result is shown in **Figure 1**.

This demonstrated that the CFD was reading in **transmittance**. Plots of transmittance versus concentration are curves, whereas plots of absorbance are linear. It was therefore concluded that a plot of CFD change in meter readings against the gravimetric results can only be an approximation, because the CFD plot provided a curved line graph against the gravimetric test results. In contrast, the CFD Technical Manual (per MIL-D-22612) requires the user to construct a calibration graph by drawing a straight line for CFD change in meter readings versus particulate concentration.

To enable the CFD to be used for quantitative measurement of aviation fuel particulate matter, the linear relationship between absorbance and concentration was adopted. In order to establish the degree of accuracy provided by the CFD, its output was compared with that obtained using a spectrophotometer, as in the above examples. It may be seen from the above data that differences between the spectrophotometer and CFD readings were found to be quite small. This may have resulted due to the spectrophotometer measurements being only one wavelength (560 nm), the wavelength in the visible spectrum where the absorbance of the ND filters corresponded exactly to 0.1 and 0.2 **A** units, respectively.

Variations in absorbance **A** of up to 10% were observed over the full visible spectral range (360-720 nm) of the filters, which is measured by the CFD. All spectrophotometer measurements cited in subsequent work to the initial study, described below, were made using a diode array instrument in the range 500-700 nm.

The approach following *Equation 2* was investigated in an attempt to derive a more precise means for use of the CFD. As described in the following section, it was found that a straight line graph for direct estimation of particulate matter in Australian JP5 could be obtained through conversion of CFD meter readings to absorbance values. It was concluded that the CFD 388R/390R Models were capable of making acceptably accurate optical measurements, when the CFD output was converted to the absorbance readings for the determination of particulate contamination in Australian JP5.

EVALUATION OF THE CFD FOR MEASUREMENT OF JP5 PARTICULATE LEVELS

The CFD Meter Reading/Absorbance Conversion Chart

The following section gives a detailed account of the research conducted for development of the **Revised CFD procedure (Table 2)** and the **Revised CFD Calibration Chart (Figure 2)**, which provide the basis for a more accurate method for use of the CFD for Australian JP5 aviation fuels. **Table 1** was prepared by conversion of CFD *Meter Readings* (μamp) to **%T** through substitution in *Equation 3*. Absorbance values **A** were then derived by substitution of **%T** into the expression log 100 / **%T** (*Equation 4*).

Optical Density Measurement Techniques

❑ **Effect of Fuel Filter Membrane Orientation:**

In order to determine the accuracy of CFD measurements, it was necessary to compare fuel particulate values derived using the CFD with those obtained from a calibrated spectrophotometer. Some obstacles were encountered in achieving this requirement, due to intrinsic incompatibility for filter membrane orientation with the CFD and HP8452A Diode Array uv/visible spectrophotometer used in this study.

The CFD is set up to use fuel-wet "transparentised" cellulose ester membrane filters (Millipore; pore size 0.65μm) placed horizontally in the optical measuring cell with the light transmission sourced vertically from below. In the spectrophotometer, however, these fuel-wet membranes cannot be physically measured horizontally because the light source is also horizontal. The fuel-wet membranes cannot be held vertically to the light source either, due to the draining effect of the fuel from the membrane. This causes loss of membrane transparency, as well as downward migration with the fuel of the collected particulates. These need to be distributed uniformly across the filter membrane surface for optical measurements to be made.

In addition, accurate spectrophotometric measurements of inorganic particulate suspensions in fuel cannot be made in liquid cells due to the formation of non-uniform suspensions caused by settling of the particulates in the measuring cell. However, a technique devised using Wratten neutral density calibration filters was found to be suitable for correlation of both the CFD and spectrophotometer optical density measurement methods.

❑ **Wratten Neutral Density Calibration Light Filters:**

Various sets of standard CFD Kodak Wratten calibration neutral density filters (NDFs) were used to correlate actual spectrophotometer absorbance values with those measured by the CFD. Light filter absorbance values were recorded by the spectrophotometer in the wavelength range 500-700 nm. Results from 12 pairs of membranes are given in **Table 3**. The nominal absorbance value of the CFD calibration NDFs, (colloidal carbon / dye dispersions in gelatin), are 0.1 and 0.2, respectively.

The spectrophotometer measurements of NDFs correlate with these values close to, or within $\pm$ 10%, which is in agreement with the Kodak manufacturing specified tolerances of NDFs. Conversion of the CFD meter readings into absorbance values, by the method described above, compared with the spectrophotometer readings, were all consistently lower in magnitude (**Table 3**). It may be seen from this Table that, for the CFD, the 0.1 NDFs (0.1**A**, 80%**T**) and 0.2 NDFs (0.2**A**, 63%**T**) were found to be between 21% and 25% and 14% and 17%, respectively, lower than those for the spectrophotometer. To establish a trend at the higher absorbance /lower transmission regimes, calculated combinations of 0.1 and 0.2 NDFs were sandwiched together to provide a range of up to 1.0**A**, 10%**T**. These results are given in **Table 4**, and show that with increasing absorbance,

the difference between the spectrophotometer readings and the CFD decreased progressively. The CFD measurements remained consistently lower than those derived by the spectrophotometer, with the closest reading between the two instruments represented by (1.0A, 10%T), which was 7.9%.

❑ **Capability of the CFD for JP5 Aviation Fuel Particulate Measurement:**

The following experimental procedures were designed to determine the degree of correlation between light absorbance measurements by the CFD and the spectrophotometer, to evaluate the capability of the CFD in accurately measuring JP5 aviation fuel particulate levels.

Each CFD Calibration Filter pack is labelled with an equivalent particulate gravimetric level (mg/L). Using these concentrations, and with the measured spectrophotometer absorbance values from the calibration filters, the Extinction Coefficients (ECs) were calculated. From 12 CFD Calibration Filter packs the variation in EC was from 0.030 to 0.035, representing a difference of 16.7%. These results are given in **Table 5**.

Using the same procedure as above, the calibration filters were measured for their absorbance characteristics with the CFD for comparison with the spectrophotometer measurements. The EC values obtained from CFD measurements varied from 0.028 to 0.032, representing a difference of 14.3%, which was lower than the spectrophotometer by 2.4%. These results are given in **Table 6**.

Comparison of the ECs determined by the spectrophotometer and CFD show quite good correlation ranging from 6.1 to 11.4%. These results are given in **Table 7**. All the measurements of optical density by the CFD have been shown to be in direct correlation with the spectrophotometer absorbance measurements.

Typical absorbance / wavelength scans of the calibration filters are given in **Figure 3**. These show a narrow band of absorption between 500 and 700 nm wavelengths, the majority of wavelengths being above their stated nominal absorbance values. These results indicate a working relationship between spectrophotometric and CFD absorbance measurements. Although, not exactly equivalent, it is considered to be a sufficiently accurate means for measuring absorbance versus concentration for materials which possess similar optical density characteristics.

❑ **Variations in Light Absorbance of differing JP5 Particulates using the CFD:**

The sensitivity of CFD absorbance measurements to the type of fuel particulate contaminant was examined by comparison of two distinct types of natural materials. Both silica dust (ACFTD) and red iron oxide are common contaminants of aviation fuel. There has been no evidence of the presence of organic particulate matter in Australian JP5.

Suspensions of 100 mg/L of these inorganic materials were prepared in pre-filtered (0.3μm) aviation turbine fuel and calculated portions of the fuel filtered through the CFD, so that the equivalent of 10, 4, 2 and 1 mg/L of particulate was deposited on the membranes. These results are shown in **Table 8**. They illustrate the large difference in absorbance characteristics between low and highly coloured

particulate materials. The Extinction Coefficient (EC) represented by absorbance/concentration is a means to compare differences in absorbance characteristics. The EC for ACFTD is 0.01 and Iron Oxide 0.195, respectively, indicating that the nature of particulate being measured by optical density techniques in the colour sensitive visible spectrum needs to be accurately defined. This is a factor to be considered in the use of the CFD to accurately determine aviation fuel particulates.

Determination of Extinction Coefficients of JP5 sediments

JP5 sediments from storage and distribution systems were obtained to determine the nature of particulates distributed in these fuels. Collected sediments were separated from the fuel by centrifuge, washed with hexane and dried in an oven at 100°C. Suspensions of the sediments were prepared in pre-filtered (0.3 micrometer) JP5 from weighed portions of the dried sediments.

Various aliquots were taken from these prepared suspensions to provide a range of concentrations for measurement of EC from the various sources of JP5 sediments. These JP5/sediment mixtures were passed through the CFD; the transmission meter readings were recorded from the top and bottom filters in accordance with the CFD operating procedure. The transmission readings obtained were converted into absorbance values, then the filters were washed with hexane, dried, weighed and the gravimetric amount of particulate matter was determined in accordance with ASTM D2276.

These results are given in **Table 9** and show a consistent narrow range of absorbance /concentration values for JP5 sediments which indicates that an optical density measuring technique can to be used for the reliable measurement of particulate matter in JP5.

The nature of the particulate matter in JP5 was examined under the microscope and was found to consist principally of siliceous matter, with some tank scale and rust particles. The tank scale and rust particles are the components responsible for raising the EC above that for siliceous matter. This variable mix of components gave rise to the narrow range of ECs between 0.035 and 0.048.

The difference in absorbance between top and bottom filters **(Table 9)** was used to construct the revised CFD calibration chart **(Figure 2)** by applying linear regression to obtain a line of best fit. The single straight line for absorbance versus concentration obtained by this method was found to be within the experimental reproducibility of ASTM D 2276.

USE OF THE REVISED CFD CALIBRATION CHART - (Figure 2)

A step-wise procedure has been developed to enable use of the CFD models EMSE 388R and 390R for reliable measurement of JP5 particulate matter in the field. An example of the use of this procedure is given in **Table 2,** with typical CFD values inserted.

Conversion of CFD direct μamp readings, which are in light transmittance, into the reciprocal logarithm to give light absorbance measurements, are readily translated from **Table 2**. This involves subtraction of top from bottom filter CFD values (**{T-B}** in **Table 2**) which may be derived from **Table 1**.

The **{T-B}** value in **Table 2** for CFD light absorbance **A** may then be directly correlated to JP5 fuel particulate contamination levels in mg/litre by cross reference to **Figure 2**. This is the figure which should be reported to the decision delegate for acceptance/rejection of the Naval aviation fuel. As indicated in **Table 2**, it is considered important to record the ship-board sampling point of the JP5 fuel to ensure that fuel to be delivered to Naval aircraft has been taken from post coalescer filtration.

CONCLUSIONS

1. Through re-evaluation of photometry laws which apply to the operation of CFD instruments, a revised method has been developed, based on **light absorbance** values for CFD measurement of fuel particulate concentrations, which provides accurate correlation with ASTM D 2276 gravimetric determinations of Australian JP5.

2. It has been determined from this study that the method prescribed in MIL-D-22612 for operation of the CFD is inconsistent with the laws of photometry, in that the output of the CFD is in **light transmittance**. Inherent inaccuracies in determining aviation fuel particulate matter, in the assumption of a linear relationship with transmittance, have been demonstrated by practical experimentation.

3. Conversion of CFD meter readings from light **transmittance** into **absorbance** values (**CFD Meter Reading / Absorbance Chart (Table 1)**) has been shown in this investigation to be consistent with the laws of photometry which apply to the operation of the CFD, provided that the extinction coefficients of the various fuel particulates fall within a narrow range.

4. A **Revised CFD Calibration Chart (Figure 2)** for the CFD has been constructed on the basis of the uniformity of the extinction coefficients observed for particulate matter in a range of JP5 fuels from Australian Naval sea and shore fuel storages. Reference to both **Figure 2** and **Table 1** is required for use of the **Revised CFD Procedure (Table 2)**.

5. For CFD Models 388R / 390R (Cv International), the photometric detection of particulate matter is very sensitive to the type and colour of fuel particulate material present. Variations in the colour and hence the extinction coefficients of particulates bear a direct relationship to the magnitude of light absorbance by the CFD. Because of this factor, the existing calibration curve (MIL-D-22612) supplied with the CFD (Model 388R) has been found to give very unreliable measurements for fuel particulate contamination for Australian JP5.

6. The revised method will enable increased reliability and confidence, both for the fuel manager and pilot, in the use of the CFD for field assessment of particulate contamination of Australian JP5 supplied to Naval aircraft.

ACKNOWLEDGMENT

Thanks are due to RAN CMDR M G Brice (IEP/ABCA/3 AUS Project Officer) for his assistance and sponsorship of this research project.

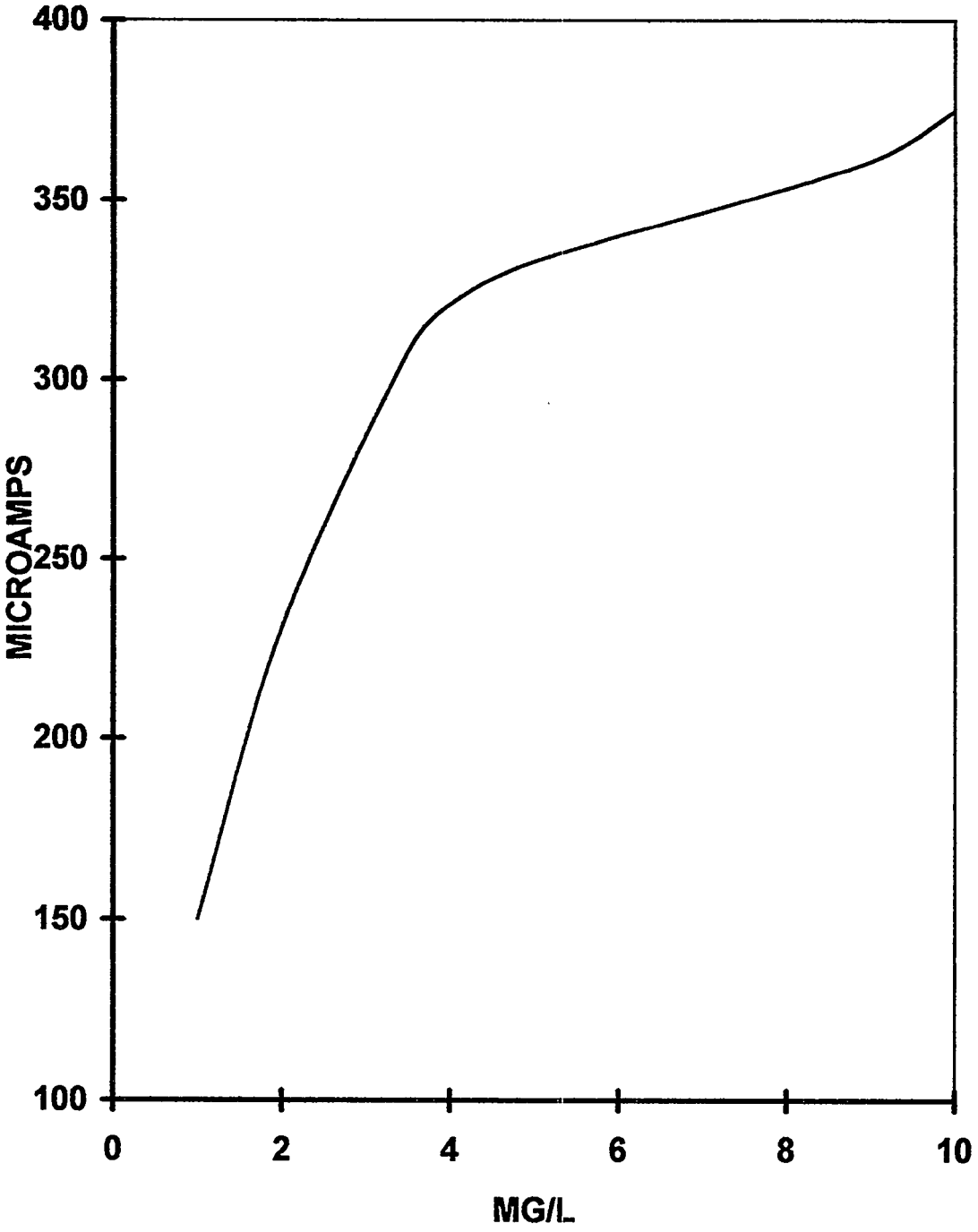

FIGURE 1

PLOT OF CFD CHANGE IN METER READINGS VS CONCENTRATION

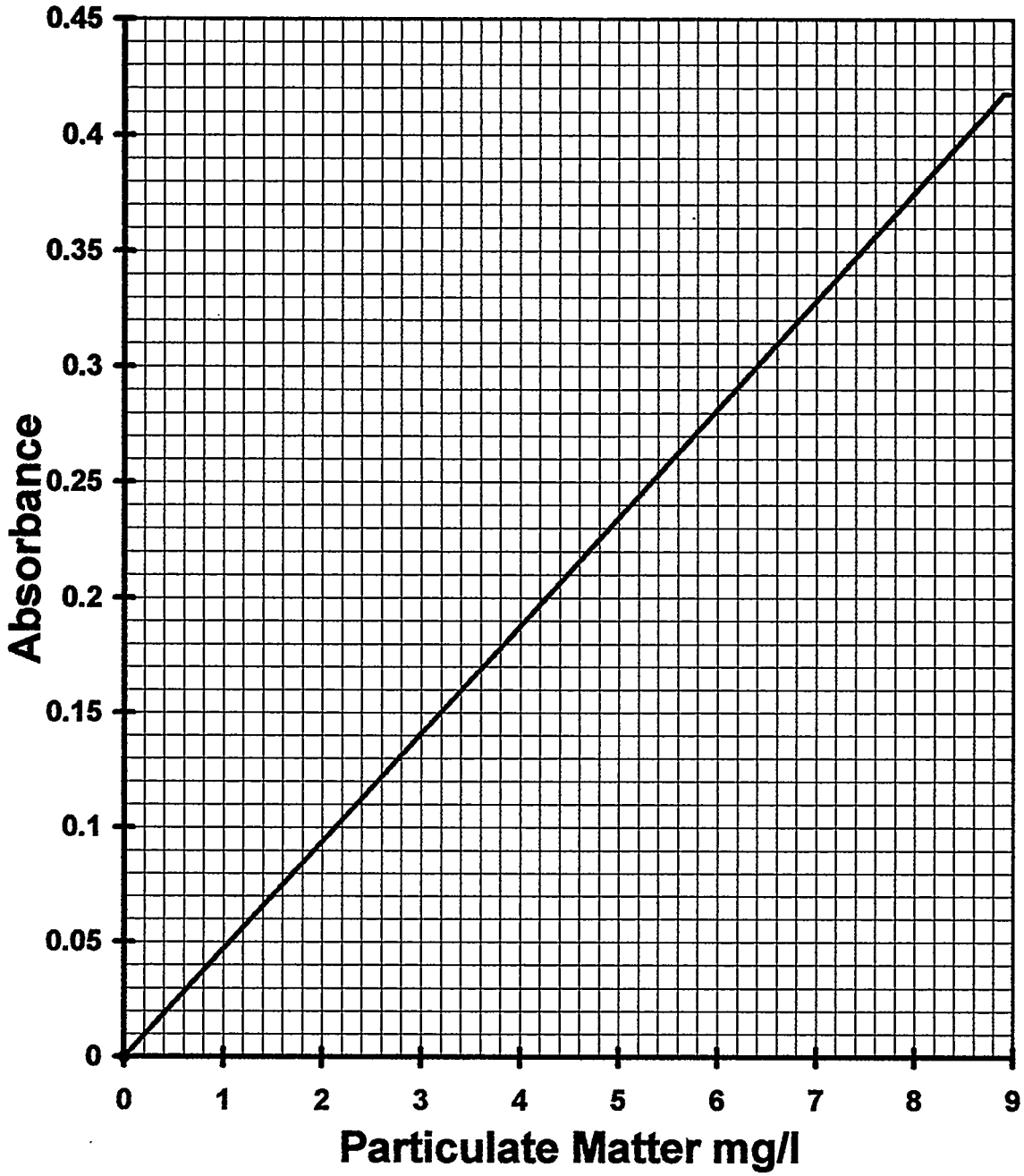

FIGURE 2

REVISED CFD JP 5 CALIBRATION CHART

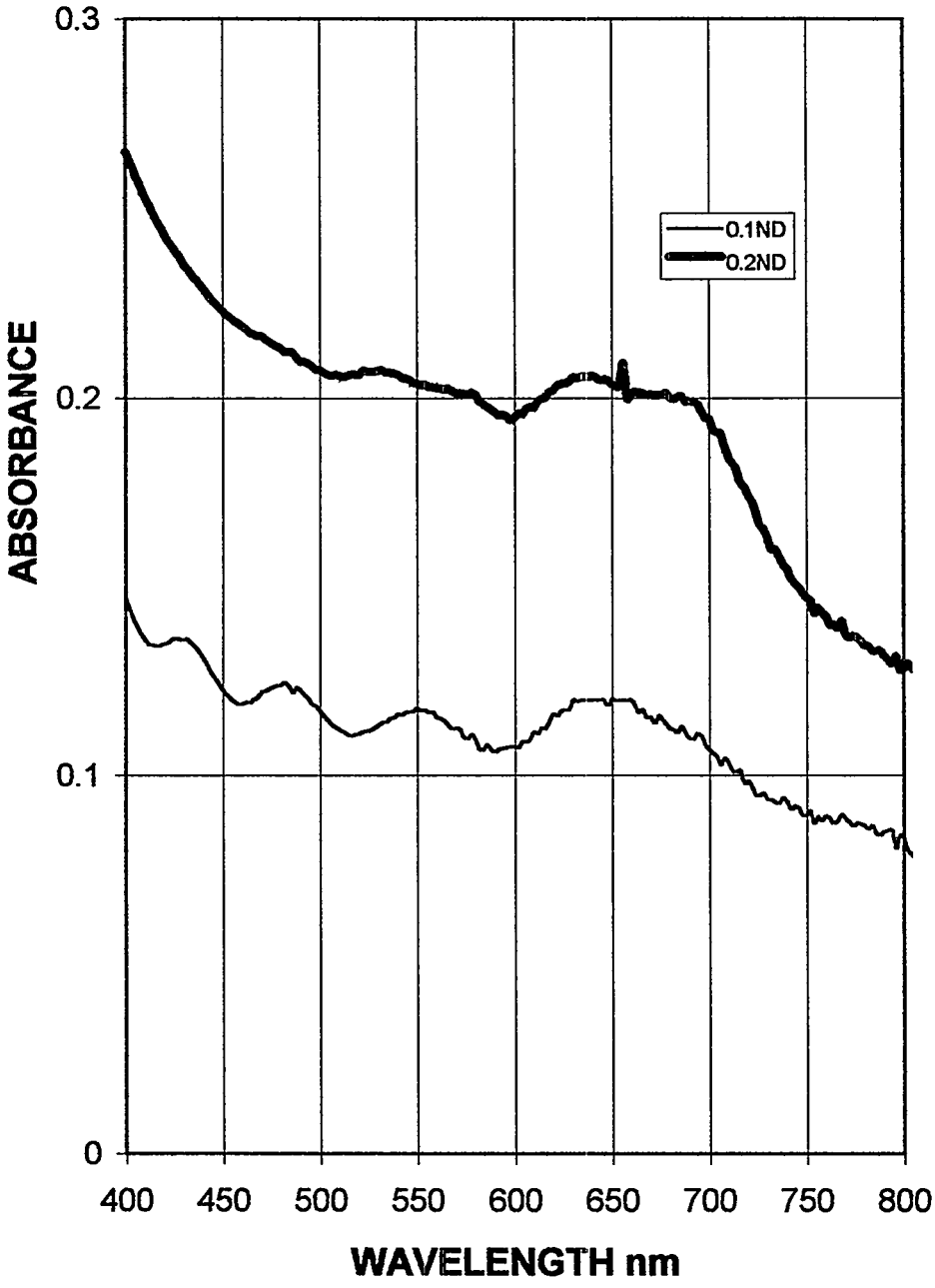

FIGURE 3

SPECTRA OF CALIBRATION NEUTRAL DENSITY FILTERS

Table 1

CFD Meter Reading / Absorbance Chart

CFD μamp reading	Absorbance	CFD μamp reading	Absorbance
500	0.080	441	0.134
499	0.080	440	0.135
498	0.081	439	0.136
497	0.082	438	0.137
496	0.083	437	0.138
495	0.084	436	0.139
494	0.085	435	0.140
493	0.086	434	0.141
492	0.087	433	0.142
491	0.087	432	0.143
490	0.088	431	0.144
489	0.089	430	0.145
488	0.900	429	0.146
487	0.091	428	0.147
486	0.092	427	0.148
485	0.093	426	0.149
484	0.094	425	0.150
483	0.095	424	0.151
482	0.095	423	0.152
481	0.096	422	0.153
480	0.097	421	0.154
479	0.098	420	0.155
478	0.099	419	0.156
477	1.000	418	0.157
476	0.101	417	0.158
475	0.102	416	0.159
474	0.103	415	0.160
473	0.104	414	0.161
472	0.105	413	0.163
471	0.105	412	0.164
470	0.106	411	0.165
469	0.107	410	0.166
468	0.108	409	0.167
467	0.109	408	0.168
466	0.110	407	0.169
465	0.111	406	0.170
464	0.112	405	0.171
463	0.113	404	0.172
462	0.114	403	0.173
461	0.115	402	0.174
460	0.116	401	0.175
459	0.117	400	0.176
458	0.118	399	0.178
457	0.119	398	0.179
456	0.120	397	0.180
455	0.120	396	0.181
454	0.121	395	0.182
453	0.122	394	0.183
452	0.123	393	0.184
451	0.124	392	0.185
450	0.125	391	0.186
449	0.126	390	0.187
448	0.127	389	0.189
447	0.128	388	0.190
446	0.129	387	0.191
445	0.130	386	0.192
444	0.131	385	0.193
443	0.132	384	0.194
442	0.133	383	0.195

Table 1 (continued)

CFD Meter Reading / Absorbance Chart

CFD µamp reading	Absorbance	CFD µamp reading	Absorbance
382	0.196	195	0.488
381	0.198	190	0.500
380	0.199	185	0.511
375	0.204	180	0.523
370	0.210	175	0.535
365	0.216	170	0.548
360	0.222	165	0.561
355	0.228	160	0.574
350	0.234	155	0.588
345	0.241	150	0.602
340	0.247	145	0.617
335	0.253	140	0.632
330	0.260	135	0.648
325	0.267	130	0.664
320	0.273	125	0.681
315	0.280	120	0.699
310	0.287	115	0.718
305	0.294	110	0.737
300	0.301	105	0.757
295	0.309	100	0.778
290	0.316	095	0.801
285	0.324	090	0.824
280	0.331	085	0.849
275	0.339	080	0.875
270	0.347	075	0.903
265	0.355	070	0.933
260	0.363	065	0.965
255	0.372	060	1.000
250	0.381	055	1.038
245	0.389	050	1.079
240	0.398	045	1.125
235	0.407	040	1.176
230	0.417	035	1.234
225	0.426	030	1.301
220	0.436	025	1.380
215	0.446	020	1.477
210	0.456	015	1.602
205	0.467	010	1.778
200	0.477	005	2.079

Table 2

Revised CFD Procedure

CFD JP5 Particulate Field Measurement HMAS SUCCESS

1. JP5 sampled from: CARGO HOLD **(eg. storage tank, coalescer, fuelling hose, pier etc)**

CFD Micro amp Recordings from 800 mL sample:

2. Record the micro amp output from the CFD for Top Filter (*T*): 431 *Top*

3. Record the micro amp output from the CFD for Bottom Filter (*B*): 479 *Bottom*

4. Use the *CFD Meter Reading/Absorbance Chart* (**Table 1**) to convert to Absorbance values.

5. Record Absorbance values of (*T*) and (*B*) and subtract (*B*) from (*T*) to obtain absorbance value corrected for the blank (Bottom filter).

Absorbance

(*T*) 0.144 *Top filter*

(*B*) 0.098 *Bottom filter*

Subtract (*T*) - (*B*) 0.046 {**T - B**}

(Change in Absorbance Value)

6. Use the revised JP5 **CFD Calibration Chart** (**Figure 2**) to correspond **Absorbance** {**T - B**} above with **Particulate Matter** 0.9 **mg/litre**.

7. REPORT: CFD recording of JP5 particulate: 0.9 **mg/litre** as in **6.** above.

Table 3

Comparison of Optical Density of CFD Calibration Filters

The nominal absorbance value of the CFD calibration NDFs are 0.1A* and 0.2A+, respectively.

Filter No	Spectrophotometer 500-700 nm (A)	CFD Meter Readings (µamp)	Change to Absorbance (A)	Difference %A
1.1*	0.1112	492	0.087	21.8
1.2+	0.2212	388	0.190	14.1
2.1	0.1104	494	0.085	23.0
2.2	0.2222	392	0.185	16.7
3.1	0.1106	492	0.087	21.3
3.2	0.2036	404	0.172	15.5
4.1	0.1091	492	0.087	20.3
4.2	0.2070	401	0.175	15.5
5.1	0.1064	496	0.083	22.0
5.2	0.2167	393	0.184	15.1
6.1	0.1136	489	0.089	21.7
6.2	0.2234	391	0.186	16.7
7.1	0.1196	486	0.092	23.1
7.2	0.2152	397	0.180	16.4
8.1	0.1126	491	0.087	22.6
8.2	0.2043	403	0.173	15.3
9.1	0.1085	495	0.084	22.6
9.2	0.2049	402	0.174	15.1
10.1	0.1075	498	0.081	24.7
10.2	0.2053	403	0.173	15.7
11.1	0.1041	497	0.082	21.2
11.2	0.2087	401	0.175	16.2
12.1	0.1105	493	0.086	22.2
12.2	0.2213	390	0.187	15.5

Table 4

Comparison of Spectrophotometer / CFD Absorbance Measurements

Nominal Absorbance (A)	Nominal Transmission (%T)	Spectro-Photometer 500-700 nm (A)	CFD Meter Reading (μamp)	Change to Absorbance (A)	Difference %A
0.1	80	0.1106	491	0.087	21.34
0.2	63	0.2036	403	0.173	15.03
0.3	50	0.3142	325	0.267	15.02
0.4	40	0.4106	263	0.358	12.81
0.5	32	0.5212	211	0.454	12.89
0.6	25	0.6318	163	0.566	10.42
0.8	16	0.8485	102	0.770	9.25
1.0	10	1.0707	62	0.986	7.91

Table 5

Extinction Coefficients Determined From CFD Calibration Filters using Visible Spectrophotometer Absorbance Measurements

Filter No	Spectrophotometer (500-700 nm) A	Difference (0.2ND-0.1ND) A	Labelled Equivalent Gravimetric Level (mg/L)	Extinction Coefficient (Abs/Conc)
1.1	0.1112	0.1100	3.68	0.030
1.2	0.2212			
2.1	0.1104	0.1118	3.60	0.031
2.2	0.2222			
3.1	0.1106	0.0930	2.66	0.035
3.2	0.2036			
4.1	0.1091	0.0979	2.84	0.035
4.2	0.2070			
5.1	0.1064	0.1103	3.37	0.033
5.2	0.2167			
6.1	0.1136	0.1098	3.48	0.032
6.2	0.2234			
7.1	0.1196	0.0956	3.15	0.030
7.2	0.2152			
8.1	0.1126	0.0917	2.77	0.033
8.2	0.2043			
9.1	0.1085	0.0964	3.00	0.032
9.2	0.2049			
10.1	0.1075	0.0978	3.04	0.032
10.2	0.2053			
11.1	0.1041	0.1046	3.11	0.034
11.2	0.2087			
12.1	0.1105	0.1108	3.62	0.031
12.2	0.2213			

Table 6

Extinction Coefficients Derived from Wratten CFD Calibration Filters using CFD Meter Readings Converted to Absorbance

Filter No	CFD Meter Readings (μamps)	Change To Absorbance	Difference (0.2NA-0.1NA) (A)	Labelled Equivalent Gravimetric Level (mg/L)	Extinction Coefficient (Abs/Conc)
1.1	492	0.087	0.103	3.68	0.028
1.2	388	0.190			
2.1	494	0.085	0.100	3.60	0.028
2.2	392	0.185			
3.1	492	0.087	0.085	2.66	0.032
3.2	404	0.172			
4.1	492	0.087	0.088	2.84	0.031
4.2	401	0.175			
5.1	496	0.083	0.101	3.37	0.030
5.2	393	0.184			
6.1	489	0.089	0.103	3.48	0.030
6.2	391	0.186			
7.1	486	0.092	0.088	3.15	0.028
7.2	397	0.180			
8.1	491	0.087	0.086	2.77	0.031
8.2	403	0.173			
9.1	495	0.084	0.090	3.00	0.030
9.2	402	0.174			
10.1	498	0.081	0.091	3.04	0.030
10.2	403	0.173			
11.1	497	0.082	0.093	3.11	0.030
11.2	401	0.175			
12.1	493	0.086	0.101	3.62	0.028
12.2	390	0.187			

Table 7

Comparison of Calibration Wratten Filter Extinction Coefficients from Spectrophotometer and CFD Measurements

Filter No	Spectrophotometer Extinction Coefficient (Abs/Conc)	CFD Extinction Coefficient (Abs/Conc)	% Difference
1.1	0.030	0.028	6.7
1.2			
2.1	0.031	0.028	9.7
2.2			
3.1	0.035	0.032	8.6
3.2			
4.1	0.035	0.031	11.4
4.2			
5.1	0.033	0.030	9.1
5.2			
6.1	0.032	0.030	6.3
6.2			
7.1	0.030	0.028	6.7
7.2			
8.1	0.033	0.031	6.1
8.2			
9.1	0.032	0.030	6.3
9.2			
10.1	0.032	0.030	6.3
10.2			
11.1	0.034	0.030	11.8
11.2			
12.1	0.031	0.028	9.7

Table 8

Extinction Coefficients of Typical Fuel Inorganic Contaminants

SOURCE	GRAVIMETRIC CONCENTRATION	CFD METER READINGS TRANS	CHANGE TO ABS	CFD METER READINGS TRANS	CHANGE TO ABS	DIFFERENCE	EXTINCTION COEFFICIENT
		TOP FILTER (T)	TOP FILTER (T)	BOTTOM FILTER (B)	BOTTOM FILTER (B)	(T-B)	
	(mg/L)	Microamps	Absorbance	Microamps	Absorbance	Absorbance	(Abs/Conc)
ACFTD‡	1.0	377	0.202	386	0.192	0.010	0.010
	2.0	370	0.210	388	0.190	0.020	0.010
	4.0	358	0.225	391	0.186	0.039	0.010
	10.0	320	0.273	402	0.174	0.099	0.010
							mean 0.010
IRON OXIDE	1.0	239	0.400	389	0.189	0.212	0.212
	2.0	161	0.571	392	0.185	0.386	0.193
	4.0	069	0.939	390	0.187	0.752	0.188
	10.0	005	2.079	380	0.199	1.880	0.188
							mean 0.195

‡ ACFTD - Air Cleaning Fine Test Dust (siliceous dust)

Table 9

Extinction Coefficients JP5 Fuel Sediments

Source	Gravimetric Sediment Concentration	CFD Meter Readings T	Change to A	CFD Meter Readings T	Change to A	Difference	Extinction Coefficient
	(mg/L)	TOP FILTER (T) Microamps	TOP FILTER (T) Absorbance	BOTTOM FILTER (B) Microamps	BOTTOM FILTER (B) Absorbance	(T - B) Absorbance	(Abs/Conc)
Shore Storage	0.3	386	0.192	395	0.182	0.010	0.0333
	0.5	377	0.202	392	0.185	0.017	0.0340
	0.9	363	0.219	391	0.186	0.033	0.0367
	2.0	319	0.274	391	0.186	0.088	0.0440
	3.5	275	0.339	394	0.183	0.156	0.0446
	5.8	219	0.438	389	0.189	0.249	0.0429
							mean 0.039
Ship Stowage	0.4	382	0.196	394	0.183	0.013	0.0325
	1.0	364	0.217	393	0.184	0.033	0.0330
	1.6	344	0.242	397	0.180	0.062	0.0388
	3.2	299	0.303	397	0.180	0.123	0.0384
							mean 0.036
Ship Stowage	0.2	390	0.187	396	0.181	0.006	0.0300
	0.5	378	0.201	396	0.181	0.020	0.0400
	0.9	364	0.217	393	0.184	0.033	0.0367
	1.8	330	0.260	393	0.184	0.076	0.0444
							mean 0.038
Ship Stowage	0.4	368	0.213	396	0.181	0.011	0.0320
	0.7	374	0.205	396	0.181	0.024	0.0343
	1.0	364	0.217	394	0.183	0.034	0.0340
	2.1	329	0.261	395	0.182	0.079	0.0376
							mean 0.035
Ship Tanker	0.4	380	0.199	395	0.182	0.017	0.0425
	1.0	352	0.232	392	0.185	0.047	0.0470
	1.2	340	0.247	392	0.185	0.062	0.0517
	2.8	286	0.323	394	0.183	0.140	0.0500
	5.0	224	0.427	394	0.183	0.244	0.0488
	8.9	146	0.615	394	0.183	0.432	0.0485
							mean 0.048

resulting from oxidation polymerisation processes. We have shown experimentally that by the long term control on the rust and deposit formation in the fuel tanks, the rust amounts to 2 kg./10 m^3, and that of deposits to 5 kg/10 m^3. The latter ratio was taken into account during our investigations.

The purpose of the present paper is to evaluate quantitatively the effect of rust and tanks' deposits on the oxidation processes and the storage term of motor gasoline containing catalytic cracking fraction (CCF) on the basis of a method developed by us in a cycle of studies [5,6,8,9].

EXPERIMENTAL

The studies were carried out with commercially available gasoline A-86 containing 50% vol. CCF and 0,02 % wt.ionol (added to the CCF) at five different temperatures. The oxidative stability of A-86 was determined in an autoclave apparatus under pressure [6]. The oxidation stability was evaluated by the following kinetic parameters: induction period, maximal rate of oxidation (W_{max}), maximal amount of absorbed oxygen, the concentration of hydroperoxides [7] and acids [8]. The storage terms of the gasoline under study were determined with the help of the cited above method.

The rust and the deposits were isolated from iron tanks, where gasoline has been stored for a long time and they were added to the tested A-86 in concentrations of 0,2 gr./l ml. and 0,5 gr./l.. respectively. The analysis of the rust showed that it contains mainly oxides of Fe (III), and small amounts of Fe(II) oxides. The deposits contain less than 2 % mass Pb, and consist mainly of polymeric oxygen containing products.

RESULTS AND DISCUSSION

In Figure 1 is shown the experimental curve, describing the absorption of oxygen by A-86 (without any additives), in an autoclave installation. The kinetic curve is typical for the three types of oxidation carried out - pure gasoline, in the presence of rust and deposits, respectively. The curve is characterised by three macrokinetic stages: 1 - induction period (τ_{ind}); 2 - stage of intensive oxygen absorption , where inflexion point is observed and from it one can determine both the induction period and the maximum rate of oxygen absorption (W_{max}); 3 - stage of autoretardation in the system. The latter is characterised by occurring of termination steps of the oxidation process, and there are measured the maximal amount of absorbed oxygen and the content of oxygen-containing compounds. The increase of the temperature results in decrease of the amount of the absorbed oxygen (see Tables 1 & 2). This can be explained by the intensive gas evolution

5th International Conference
on Stability and Handling of Liquid Fuels
Rotterdam, the Netherlands
October 3-7, 1994

EFFECT OF METAL OXIDES AND TANKS' DEPOSITS ON THE OXIDATIVE STABILITY OF GASOLINE

Slavi K. Ivanov*[1], Margarita I. Boneva[2], Zhetcho D. Kalitchin*[1],
Petko T. Georgiev[1], and Setrak K. Tanielyan[3]

[1] - SciBulCom, Ltd., P.O.Box 249, 1113 Sofia, Bulgaria.
[2] - Institute of Organic Chemistry, Bulgarian Academy of Sciences, 1113, Sofia, Bulgaria.
[3] - Seton Hall University, South Orange, New Jersey 07079-2694, USA.

ABSTRACT

The present investigation is devoted to assessment of the influence of species isolated from fuel tanks and tank bottoms on the oxidative stability of gasoline. The aim of the paper is to be evaluated quantitatively the effect of rust and tank' deposits on the oxidation processes and the storage terms of motor gasoline containing catalytic cracking fraction on the basis of a method developed by us earlier. As a result of the theoretical model and the experiments is found that the deposits decrease the chemical stability of gasoline containing 50 % fraction from catalytic cracking, while the rust has no significant influence on this parameter. Correction coefficients are calculated and introduced, taking into account the influence of deposits and rust on the predicted storage terms.

INTRODUCTION

The liquid phase oxidation processes are strongly accelerated by traces of metal species [1-4]. These metal contaminations may enter the fuel from variety of sources, as via railway tanks, distribution system, pipelines, storage tanks, etc. The acceleration of the oxidation process under their action results in reducing of the fuel storage terms. However, a quantitative evaluation of this effect is lacking in the literature. This problem is expected to become more urgent in the future due to the usage of petroleum-derived fuels containing catalytically cracked stocks.

Of special interest with respect to the fuel oxidative stability is the influence of species isolated from the fuel tank bottoms. The deposits can reasonably be assumed to originate from complex reactions involving both the tetraethyl lead decomposition leading to the formation of high molecular organic lead compounds with lower solubility in the fuel and deposited on the bottom and partially on the tank's wall, and deposits

at higher temperatures and thus the maximal oxygen absorbed appears to be the difference between its real value and that of the evoluted gas. The analysis of the three macrokinetic stages proves undoubtedly, that for prediction of storage terms, only the first stage (τ_{ind}) should be considered. The second period is not appropriate because it consists of two concurrent processes - oxygen absorption and desorption of gases resulting from the thermal decomposition of the oxygen containing compounds during oxidation, mainly decarboxylation of carboxylic acids. The comparison of the kinetic curves of Figure 2 with Figure 3, confirms that only the dependence of the induction period (τ_{ind}) is exponential and obeys the Arrhenius equation. This fact also shows that the experiments are carried out in the kinetic region and they are not influenced by the diffusion factors. The dependencies of the maximal rate from the temperature do not satisfy this equation. The same applies to the maximal amount of absorbed oxygen and the concentration of oxygen containing compounds. The appearance of extrema in the kinetic curves in the presence of rust and deposits (Figures 4, 5, Tables 1, 2) does not allow the application of these dependencies for prediction purposes. The data from the study of the effect of the rust and deposits on the induction period are summarised in Figure 2. The results show that their presence leads to a decrease of the induction period whereby the effect of the deposits is more pronounced. For instance, τ_{ind} for the pure A-86 at 383 K is 500 min., while for A-86 + 0,2 gr./l. rust it is 420 min and for A-86 + 0,5 gr./l. deposit it is 380 min With the increase of the temperature the effect of these two factors on the duration of the induction period decreases (for instance, at 403 K under the influence of the rust it is decreased by 10 min., and of the deposits by 25 min). It should be pointed out that the character of the A-86 dependence of τ_{ind} on the temperature does not change, when there are added rust and sediments. The kinetic curves are only shifted to the left.

The results of the study of the rust and deposits effect on the maximal rate of oxidation are given in Figure 3. At temperatures up to 383 K this parameter is not practically affected by their presence. However, the rise of the temperature leads to a significant increase in W_{max} , under the influence of these two factors. Thus, at 398 K W_{max} for pure A-86 is $5{,}8.10^{-5}$ mol/l.sec., for A-86 + rust - $7{,}7.\ 10^{-5}$ mol/l.sec., and for A-86 + deposits - $8{,}2.10^{-5}$ mol/l.sec.

Of a particular interest for us was to follow the influence of rust and deposits on the hydroperoxide concentration in the oxidate (Figure 4). The curve 3 in Figure 4 reveals that deposits addition to the gasoline leads to increase of the hydroperoxide

concentration. The latter reaches its maximum at 385 K afterwhich it decreases following a S-shape dependence. Above 398 K the hydroperoxide concentration in the oxidates obtained in the presence of deposits is lower than that of the pure gasoline and in the presence of rust. The presence of maximum in the dependence of the hydroperoxides concentration versus the temperature, in the presence of lead containing deposits can be explained by two consecutive processes: formation of hydroperoxides resulting from the initiation step of the oxidative process and their decomposition. Obviously the action of Pb(II) found in these deposits can be expressed as follows:

$$Pb(II) + 2ROOH \longrightarrow Pb(IV) + 2RO^{\cdot} + 2\,{}^{-}OH \xrightarrow{\text{deposits}} 2HO^{\cdot}$$

This process increases the initiation rate and also the concentration of the hydroperoxides. At certain temperature, obviously prevails the process of thermal deactivation of the formed radicals and a gas is evoluted:

$$Pb(II) + 2ROOH \longrightarrow Pb(IV) + 2ROOR + 2\,{}^{-}OH \xrightarrow{\text{deposits}} 2H_2O_2 \rightarrow \tfrac{1}{2}\,O_2 + H_2O$$

Therefore the experimentally registered decrease of the amount of absorbed oxygen is caused by the evolution of gases: O_2 , CO_2 , H_2 , and hydrocarbons.

Quite interesting dependence was observed following the change of the acid number of the oxidates with the temperature in the presence of rust and deposits (see Figure 5). The kinetic curves for pure gasoline and the sample with deposits are similar as the acid number decreases with the increase of the oxidation temperature attaining a constant value above 398 K. The addition of rust leads to a quite different dependence, characterised by a minimum at 385 K, after which it increases with the rise of the temperature. The decrease of the concentration of the formed carboxylic acid with the increase of the temperature is explained by their decarboxylation with evolution of CO_2 and intensive esterification . Obviously in the presence of rust the processes of formation of carboxylic acids are more intensive compared with the processes of decarboxylation and esterification and a maximum in their concentration is observed with the change of the temperature.

The other data needed for prediction of the storage terms of A-86 and for evaluation of the rust and deposits influence on it are given in Tables 1 and 2.

The chemical stability (τ_{ch}), expressed in years can be determined by equation (1):

$$\tau_{ch} = \tau_o \cdot e^{Ei/RT} \qquad (1)$$

where: τ_{ch} is the preexponential factor;

E_i is the activation energy of the initiation process;

T is the temperature in Kelvin.

As it is shown in Table 1, the chemical stability of the gasoline in the presence of rust at the real storage temperature (the average temperature in Bulgaria is 284 K) shows a tendency to increase. Therefore, the storage terms in real conditions will not be influenced by the steel tanks without anticorrosion cover .

An interesting fact is observed - from one side the induction periods are increased in the presence of rust and from the other side the activation energy is also increased. It can be explained with existence of the following two concurrent processes:

a) at low temperature - deactivation of the radicals

$$RO_2^{\cdot} + Fe(II) \longrightarrow RO_2^{-} + Fe(III)$$

b) at higher temperature, decomposition of the radicals with evolution of gas, with no change of the initiation rate

$$RO_2^{\cdot} + Fe(II) \longrightarrow R^{\cdot} + Fe(III) + O_2^{-}$$

The deposits have strongly expressed destabilising action and the storage terms in real conditions for A-86 is decreased from 3,2 years down to 1,5. Therefore, the tanks should be thoroughly cleared from deposits before they are filled with gasoline.

For exact assessment of the influence of rust and sediments we have introduced the coefficients k_r and k_s respectively:

$$k_r = \tau_r / \tau_{ch} \qquad \text{and } k_s = \tau_s / \tau_{ch}$$

where: τ_r is the chemical stability in the presence of rust;

τ_s is the chemical stability in the presence of deposits;

τ_{ch} is the chemical stability (determined by equation 1).

From the data in Tables 1 and 2 are obtained the following values: $k_r = 1,2$ and $k_s = 0,5$. The presence of deposits in the gasoline decreases the storage terms twice.

The coefficients obtained can be used successfully for prediction of the real storage terms of gasolines. The full equation for the calculations is as follows:

$$\tau_{real} = \tau_{ch} \cdot k_D \cdot (k_r \cdot k_s \cdot k_m \cdot k_{dw}) \qquad (2)$$

where: τ_{real} is the real term of storage;

τ_{ch} is the theoretically determined term of gasoline storage, where the different factors are not taken into account;

k_D is the diffusion factor (for our studies it is 1.66 [8]);

$k_r \cdot k_s \cdot k_m \cdot k_{dw}$ are coefficients taking into account the influence of the rust, deposits, metals and the drain water, respectively, on the storage terms [8,9].

Depending on the metal with which the gasoline comes into contact the coefficient k_m has different values k_{Zn}, k_{Fe}, etc.

When the gasoline is stored in steel tanks, partially covered by rust τ_{real} is determined by the expression:

$$\tau_{real} = \tau_{ch} \cdot k_D \cdot (k_r \cdot a + k_m \cdot b)\, k_s \cdot k_{dw} \qquad (3)$$

where: a and b are the coefficients taking into account the part of the tank covered with rust.

In our studies we have measured that this part of the surface of the tanks is 80%, i.e. a = 0,8 and b = 0,2.

CONCLUSIONS

The influence of rust and deposits on the oxidation stability of gasoline A-86 containing 50 % CCF has been studied. It was found out that the deposits decrease the chemical stability of gasoline, while the rust has no influence on it. The correction coefficients taking into account the influence of rust and deposits have been used for prediction of the real storage terms of gasoline.

REFERENCES

(1) Emanuel, N.M.; Denisov, E.T.; Maizus, Z.K. *Chain reactions of the oxidation of hydrocarbons in liquid phase*, Nauka, Moskva, 1965, p.375.

(2) Evmenenko, N.E.; Gorohovatsky, Ia.B.; Tzepalov, V.F. *Neftekhimia*, **1970**, *10*, 226.

(3) Kovalev, G.I.; Gogitudze, L.D.; Kuranova, V.I.; Denisov, E.T. *Neftekhimia*, **1979**, *19*, 237.

(4) Colcough, T., *Ind. Eng. Chem. Res.*, **1988**, *26*, 1987.

(5) Ivanov, S.K.; Tanielyan, S.K.; Ivanov, A.; Georgiev, P.T. *Khimiya i Industriya*, **1984**, *56*, 438..

(6) Tanielyan, S.K.; Ivanov, S.K.; Tsonkovski, I.M. *Khimiya i Industriya*, **1985**, *57*, 13.

(7) Kruzhalov B.D.; Golovalenko B.I., *Combined synthesis of phenol and acetone*, Moskva, 1963, p.63 (Russ).

(8) Kalitchin, Zh. K; Boneva, M.I.; Ivanov, S.K.; Georgiev, P.T.; Tanielyan, S.K. *5th International Conference on Stability and Handling of Liquid Fuels*, Rotterdam, the Netherlands, Oct.3-7, 1994.

(9) Ivanov, S.K.; Georgiev, P.T.; Tanielyan, S.K.; Kalitchin, Zh.D.; Boneva, M.I.; Hinkova, M.K. *Ropa a Uhlie*, **1986**, *28*, 746 (Chec.)

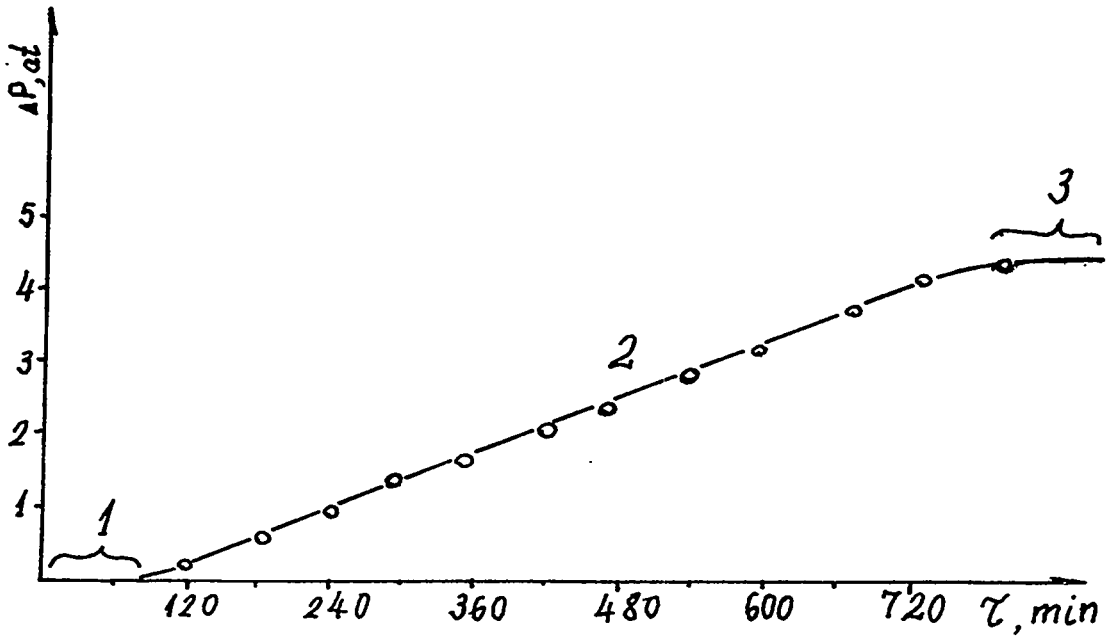

Figure 1. Kinetic curve of oxidation of gasoline A-86 at 385 K. 1- induction period; 2 - maximum rate of oxygen absorption; 3 - autoretardation.

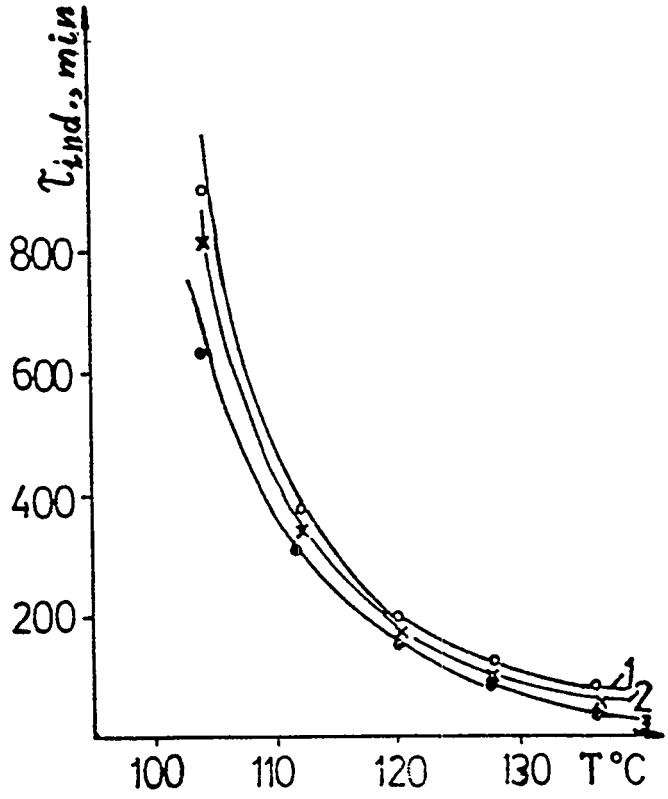

Figure 2. Change of the induction period of gasoline A-86, containing 50 % CCF at different oxidation temperatures: 1 - base gasoline A-86; 2-gasoline A-86 + 0,2 gr./l. rust; 3-gasoline A-86 + 0,5 gr./l. deposits.

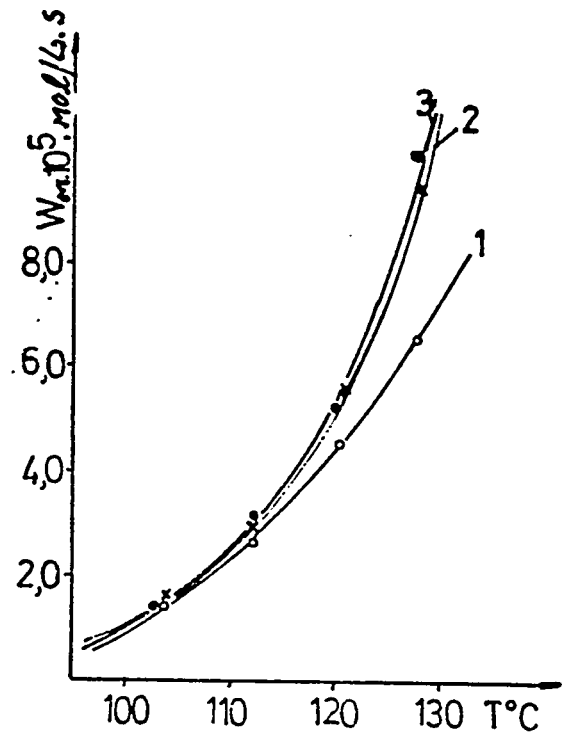

Figure 3. Change of the maximal rate of oxidation of gasoline A-86, containing 50 % CCF at different oxidation temperatures: 1 - base gasoline A-86; 2-gasoline A-86 + 0,2 gr./l. rust; 3 - gasoline A-86 + 0,5 gr./l. deposits.

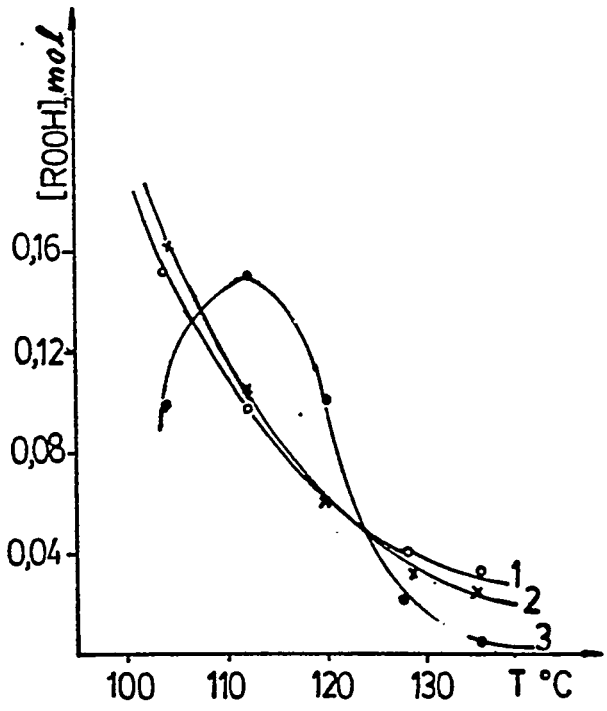

Figure 4. Change of the hydroperoxide concentration of gasoline -86, containing 50 % CCF at different oxidation temperatures: 1 - base gasoline A-86; 2-gasoline A-86 + 0,2 gr./l. rust; 3 - gasoline A-86 + 0,5 gr./l. deposits.

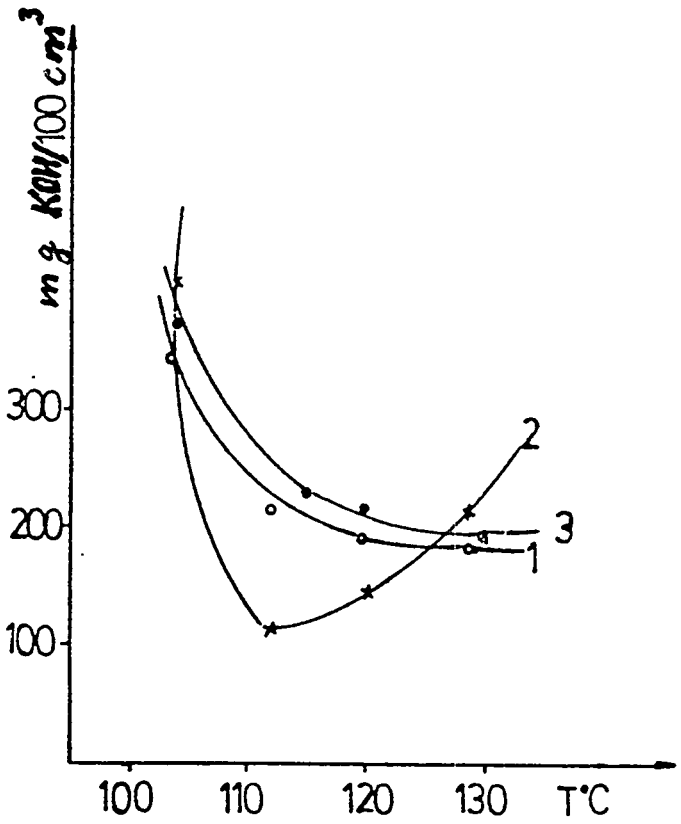

Figure 5. Change of the acid number of gasoline A-86, containing 50 % CCF at different oxidation temperatures: 1 - base gasoline A-86; 2-gasoline A-86 + 0,2 gr./l. rust; 3 - gasoline A-86 + 0,5 gr./l. deposits.

Table 1.
Predicted storage terms of gasoline A-86 containing 50 % CCF in the presence of rust

Temp. K	Abs. O_2 mol/l.	Neutr. O-containing compn. Mol %	Added amount gr./l	Activation energy kcal/mol	Preexponential $lg\tau_o$	Chemical stability τ_{ch} years
377	0,47	54,9	0,0	18,180	-17,90	3,2
385	0,37	69,2	0,2	19,410	-19,65	4,1
393	0,37	72,9	0,2			
401	0,32	72,9	0,2			
409	0,24	75,8	0,2			

Table 2.
Predicted storage terms of gasoline A-86 containing 50 % CCF in the presence of deposits

Temp. K	Abs. O_2 mol/l.	Neutr. O-containing compn. Mol %	Added amount gr./l	Activation energy kcal/mol	Preexponential $lg\tau_o$	Chemical stability τ_{ch} years
377	0,48	65,4	0,0	18,180	-17,90	3,2
385	0,38	47,9	0,2	17,04	-16,63	1,5
393	0,30	52,7	0,2			
401	0,24	71,2	0,2			
409	0,18	86,1	0,2			

5 th International Conference
on Stability and Handling of Liquid Fuels
Rotterdam, The Netherlands
October 3-7, 1994

Improving Storage Stability of Gasoline Using Elevated Antioxidant Concentrations

Seth Sommer [*1], David Luria[2], Jacob Sufrin, Arthur Weiss, Max Shuftan[3], Itamar Lavie[4].

[1]"DELEK" - The Israel Fuel Corporation LTD, P.O. Box 50250, Tel Aviv, Israel 61500;
[2]The Israeli Ministry of Energy, The Fuel Authority, P.O. Box 33541, Haifa, Israel 31334;
[3]The Israeli Defense Forces, Military P. O. 02306, Israel;
[4]Bromine Compounds LTD, P.O. Box 180, Be'er Sheva, Israel, 84101.

Absract
The purpose of this study was to examine the feasibility of increasing storage-stability of gasoline by blending it with elevated concentrations of standard antioxidants, normally added at low concentrations to gasolines. It was thought that, by raising the concentration of these additives in the gasoline from 25 ppm to 100 ppm, the storage stability of the fuel can be improved. In this study, two types of antioxidants (an aromatic diamine type and an alkylphenol type), and a mixture of the two, were added at different concentrations to two different gasoline blends. The various blends were stored in drums, simulating tank storage conditions, for a period of 25 months. Samples were drawn at varying intervals over the test duration and tested for Existent Gum, Potential Gum, Induction Period and other properties (according to standard ASTM test procedures). It was found that raising the concentrations of the aromatic amine antioxidant adversely effected the storage stability of the gasoline blends, whereas elevated conentrations of the alkylphenol antioxidant indeed improved the gasoline's stability.

Introduction

The Israel Military, as many other militaries, maintains equipment, materials and supplies in strategic "readiness" for prolonged periods. Any improvement in the storage stability of materials, such as fuels, would be logistically and economically advantageous to the Military, allowing longer storage intervals, with lower maintenance and handling costs.

Due to the high content of oxidation-prone crackate streams in gasoline, this distillate has poor storage stablity. It is generally accepted that gasoline should not be stored for periods longer than six to eight months, as the gum content in the fuel rises above tolerable levels if stored for longer intervals. As such, the Israeli Military specifies a special grade of gasoline to be used in long-term storage applications. This grade is inherently more stable, being comprised of leaded, straight-run gasoline, containing little to no FCC crackate. Over the past few years, it has become more difficult for the local petroleum companies to meet this specification, due to the ever increasing octane demand of the Israeli car-pool and stability problems with "civilian" gasoline grades. For this and other logistics reasons, the Military preferred to divert to using more widely available civilian gasoline grades in all their applications. It was, therefore, suggested that the use of antioxidant additives in civilian gasolines may provide these fuels with the storage stability required for Military applications.

By law, all civilian gasoline grades marketed in Israel must adhere to one of two Israeli Standards (one governs leaded grades, the other unleaded grades).[1,2] If the Military sought to add an antioxidant to civilian gasoline which

is not presently approved for use by the Israeli Standard, it would require the amendment of the standard to include that antioxidant type. For this reason, the Military preferred to limit this study to standard, approved antioxidants. These antioxidants are usually added at a concentration of 15-30 ppm to gasoline blends during their production. The purpose of this study was to determine the effect of elevated antioxidant concentration on storage stability.

Method

The study was performed in two stages. The objective of the first, preliminary stage was to determine which antioxidants and what concentrations show the best feasibility to succeed in the primary stage of the study. During this stage, samples of a single gasoline blend containing varying concentrations of two antioxidants, and a mixture of the two, were tested for gum content and oxidation stability (Induction Period). Optimal additive treat levels were determined.

The primary stage of the study consisted of real-time storage of two leaded gasoline blends (representative of gasolines produced in Israel) containing two antioxidant at several concentrations. The gasoline specimens were stored in drums simulating tank storage. Samples were drawn at varying intervals over a 25 month period. Several chemical and physical properties were determined for these samples.

Preliminary Stage - Experimental

For this stage, a laboratory gasoline blend was prepared containing 80 % (vol) FCC crackate and 20 % (vol) straight- run gasoline. The blend contained no anti-knock compound. A minimal amount of approximately 6 ppm antioxidant was added to these streams during their manufacture, unfortunately the exact type and concentration could not be ascertained. Two antioxidants were added to this base blend, as follows:

An aromatic diamine:	N,N-diisopropyl-p-phenylene diamine	1)
An alkylphenol blend:	55% 2,4-dimethyl-6-tert.butylphenol	
	45% butylated phenols	2)

Three series of samples were tested: the first contained increasing concentrations of the aromatic diamine additive; the second, increasing concentrations of the alkylphenol additive; the last, a 1:1 mixture of the two additives at increaing concetrations. Additive concentrations tested were: 0, 10, 25, 50, 90, and 150 ppm (vol). These concentrations represent the antioxidant added to each sample and do not include the estimated 6 ppm already in the distillate streams.

The samples required 3-5 hours to prepare, during which they were kept at room temperature. After preparation, they were refrigerated at 3°C until tested. All samples were tested for Existent Gum (in accordance with ASTM D-381)[3] and Induction Period (in accordance with ASTM D-525)[3]. All test results were determined twice.

Preliminary Stage - Results

Figure 1 shows test results of Existent Gum found in the samples, as a function of rising antioxidant content. All results were rounded to the nearest whole mg/100 ml. The results plotted are averages of two determinations. The drawn lines represent linear regressions performed using the least-squares method. All series show a trend towards increased gum content with rising antioxidant concentration. This trend is strongest for the aromatic diamine additive, and weakest for the alkylphenol additive.

Figure 2 shows Induction Periods found for the samples, as a function of rising antioxidant concentration. Each sample was tested twice, with a time lapse of approximately two months between determination (due to the abundance of samples, limited number of test beds and the length of the test). Both results are plotted in the figure. The lines drawn represent second order polynomial regression performed using the least-squares method. The second determination of Induction Period was higher than the first (i.e. the result increased after the sample was stored for two months) for all but two samples (representing 89.2% of all results). All series show a rise in Induction Period with increasing antioxidant content.

Preliminary Stage - Discussion

From the results found for the gum content of all samples it is apparent that the time elapsed between the drawing of the distillate streams from the refinery and the preparation of the samples (whereupon the antioxidant was added and the samples refrigerated) sufficed for gasoline oxidation, and thus the relative high gum content in all samples. Nonetheless, the researchers were surprised by the apparent increase in gum content with rising antioxidant concentrations. It is also apparent that the alkylphenol additive gave generally better gum results than the aromatic diamine additive, or the mixture.

For the single antioxidant series (excluding the mixture), the Induction Period reached its maximum value of 1,200 minutes at a concentration of 90 ppm. For the mixture, this value was reached only at the maximum treat tested: 150 ppm. The rise in Induction Period for samples stored two months may be credited to the partial oxidation of the samples over this short storage interval. As functional groups in the distillate oxidize, fewer groups are available for further reaction, and, therefore, the distillate shows improved results.

Based upon the results of this preliminary stage, it was decided that only the aromatic diamine and the alkylphenol antioxidants would be tested in the primary stage, the mixture of the two would not. The concentrations to be tested would be: 25 ppm (corresponding to the additive level used today in civilian gasolines), 100 ppm (instead of 90 ppm, as the concentration giving best overall results in the preliminary stage) and 75 ppm (half the maximum

concentraion tested in the preliminary stage). Higher concentrations would not be tested, as the preliminary stage shows a possible detrimental effects of evelated antioxidant content on gum formation.

Primary Stage - Experimental

For preparation of test specimens for this stage, two distillate streams were used: FCC crackate and raffinate. These streams were received from the refinery containing a minimal antioxidant content of approximately 6 ppm (the exact type and concentration could not be ascertained). To both streams, 0.15 g/l Et_4Pb was added (the only anti-knock conpound tested in this study).

Using these streams, two gasoline blends were prepared. Gasoline A contained 70 % (vol) FCC crackate and 30 % (vol) raffinate. This blend represented a "more stable" gasoline. Gasoline B was comprised of 80 % (vol) FCC crackate and 20 % (vol) raffinate, and represented a "less stable" blend. Both are indicative of Israeli civilian gasoline. Specimens were prepared containing these two blends, and the two antioxidants (the aromatic diamine and the alkylphenol) at three different concentrations, as mentioned (these concentrations represent the antioxidant added to the estimated 6 ppm already in the distillate streams). Table 1 lists all specimens prepared, their composition and their identification code, as assigned to each in the study.

Specimens were prepared in new drums on location at the storage site. The volume of each drum was 190 litres. Duplicates drums of each were prepared. The drums were vented to the atmosphere via a 120 cm long, 1.5" diameter pipe, capped with a "T" connection to prevent rain water from entering. This long pipe allowed for natural ventilation and aeration, without excess evaporation (in fact, very little evaporation loss was noted over the entire 25 month period). In this manner, tank storage simulation was achieved. All drums were stored outdoors, exposed to direct sunlight and rain from October 1990 through November 1992.

Every drum was sampled (i.e. each gasoline specimen was sampled twice) at the following intervals: upon preparation ("zero" sample), 1, 3, 6, 9, 12, 18, and 25 months after preparation. Samples were 1 or 2 litres in volume, and were drawn from the bottom third of the drum. The drums were not mixed before sampling. The following laboratory tests were performed on each sample: Copper Strip Corrosion (in accordance with ASTM D-130)[3], Bromine Number (in accordance with ASTM D-1159)[3], Induction Period (in accordance with ASTM D-525)[3], Existent Gum (in accordance with ASTM D-381)[3] and Potential Gum (in accordance with ASTM D-873)[3]. Additionally, the "zero" , 12 and 25 month samples were tested for Density (in accordance with ASTM D-1298)[3], Distillation Range (in accordance with ASTM D-86)[3] and Research Octane Number (in accordance with ASTM D-2699)[3]. An additional sample was scheduled for 30 months, but was canceled due to 25 month results.

Primary Stage - Results

Copper Strip Corrosion

None of the specimens showed any corrosion tendency toward Copper. Even after 25 months of storage, all samples gave a Copper Strip Corrosion Standard Rating of 1.

Bromine Number

All Bromine Number results obtained are shown in Figures 3 and 4 as functions of storage time. All results were rounded to the nearest whole number. Figure 3 contains results for specimens containing Gasoline A and Figure 4 contains results for specimens containing Gasoline B. The drawn lines represent linear regressions performed using the least-squares method.

Although results obtained show great fluctuation and no apparent functional correlation, all show a definite, downwards trend towards reduced Bromine Number over prolonged storage periods. No difference was noted between the specimens containing different antioxidants or concentrations, however a distinction was noted between specimens of different gasoline blends: results for specimens containing Gasoline B were generally higher than for Gasoline A. This is consistent with the higher FCC crackate content of Gasoline B.

As Bromine Number is an indication of aliphatic unsaturation in the distillate[4], it would appear that double bond oxidation, giving rise to gum products, corresponds to a drop in Bromine Number. Although gum content of the various specimens was different, the reduction in their Bromine Number was similar. This would suggest different mechanisms of gum formation in the various specimens.

Induction Period

All results obtained for Induction Period of all specimens are tabulated in Table 2. Fluctuations in these results were also great, especially for specimens containing the alkylphenol antioxidant. Nonetheless, all specimens gave good results even after 25 months storage, well above the 240 minutes minimum required by the Israeli Standards[1,2]. For the aromatic diamine antioxidant, all specimens containing 75 ppm or more gave a maximum 1,200 minutes result throughout the storage period. For the alkylphenol additive, the specimen containing 75 ppm antioxidant and Gasoline B dropped from this maximum value after about 12 months, although still giving a high 1,100 minute result for the remainder of the storage period. All other specimens containing 75 ppm or more retained their maximum value throughout the study.

From these results it is apparent that the aromatic diamine antioxidant has a more possitive effect on Induction Period than the alkylphenol additive. Nonetheless, no correlation was found between gum content and Induction Period, suggesting that this test is not suitable for predicting storage stability of distillates.

Existent Gum and Potential Gum

Figures 5-8 show all results obtained for the Existent Gum content of all test specimens as a function of storage time. All results were rounded to the nearest whole mg/100ml. Figure 5 shows results for specimens containing Gasoline A and the aromatic diamine antioxidant; Figure 6, specimens containing Gasoline A and the alkylphenol antioxidant; Figure 7, specimens containing Gasoline B and the aromatic diamine antioxidant; Figure 8, specimens containing Gasoline B and the alkylphenol antioxidant. All specimens display a consistent increase in Existent Gum as a function of storage period.

All results obtained for "zero" samples were outside or equal to the Israeli Standard limit of 5 mg/100ml[1,2]. Once again, this would suggest partial oxidation of distillate streams during blend preparation, and prior to antioxidant introduction.

Results obtained for Potential Gum for all specimens as a function of storage time are shown in Figures 9-12, where Figure 9 shows results for specimens containing Gasoline A and the aromatic diamine antioxidant, Figure 10 for specimens containing Gasoline A and the alkylphenol antioxidant, Figure 11 for specimens containing Gasoline B and the aromatic diamine antioxidant and Figure 12 for specimens containing Gasoline B and the alkylphenol antioxidant. All results were rounded to the nearest whole mg/100ml. Here, too, the Potential Gum of all specimens increase consistently over the entire test duration.

The statistical treatment of these results made use of second order polynomial regression (applying the least-squares method). The following two criteria were applied to determine whether a given result should be accepted or rejected from the regression: 1) if the Existent Gum content of a particular sample was higher or equal to the Potential Gum found for that sample, both Existent and Potential Gum results were disregarded; 2) if a large, unexplained deviation was found between results of the two duplicate samples of a given specimen, the result with the greater diversion was disregarded. After disregarding all results meeting either of these two criteria, the remaining results were regressed polynomially. The resulting regression lines are plotted in Figures 5-12. Tables 3 and 4 contain the corresponding equations for these lines. The Correlation Coefficients (also given in Tables 3 and 4) are generally high, showing good agreement with the regression order chosen.

Results obtained for Existent and Potential Gums in both samples taken from specimen coded 123 after 1 and 6 months storage deviated greatly from the general trend of the other samples. Disregarding these results improved the Correlation Coefficient from R^2=0.216 and R^2=0.143, respectively, to R^2=0.767 and R^2=0.725. No explanation could be given for these deviations. It was, therefore, decided to disregard these results for further discussions. Tables 3 and 4 note both equations and coefficients.

Primary Stage - Discussion

As neither Copper Strip Corrosion, Bromine Number nor Induction Period were able to differentiate between "more-stable" and "less-stable" gasolines, this discussion focuses primarily on the gum forming tendency of the specimens. It is safe to assume that stable fuels will form less gum during storage than less-stable fuels. It is further assumed that "real" gasoline blends containing same antioxidant type and content as the test specimens will form gum at a similar rate as those measured in this study.

As stated, the gum contents found for "zero" samples taken from all specimens were significantly higher than those normally found in Israeli gasolines. This is ascribed to the manner in which the specimens were prepared and the stage at which antioxidant was introduced into them. Had antioxidants been added to the blends at the refinery during manufacture, it is believed that gum content of the specimens would have been closer to those normally found in civilian gasolines. The accepted industry averages today for all gasoline grades produced in Israel are 3 mg/100ml for Existent Gum and 8 mg/100ml for Potential Gum (based on results from all batches produced in Israel throughout 1992).

Assuming these "zero" values for all specimens, and the gum formation rates measured for each, the maximum storage periods until gum contents become unacceptable were calculated for all. In these calculation, it was assumed that gasoline would be "unacceptable" for automotive applications if its Existent Gum content would be 7 mg/100ml or higher, or its Potential Gum content would be 15 mg/100ml or higher. Tables 3 and 4 also show the calculated month in which the specimen becomes "unacceptable" by these criteria (using the above industry averages as "zero" sample values).

Gasoline specimen "breakdown" was defined as the maximum storage period in months whereupon its Existent Gum content reaches 7 mg/100ml or its Potential Gum content reaches 15 mg/100ml, the earlier of the two (assuming industry averages for "zero" sample gum contents). The calculated "breakdown" months for all specimens are shown in Figure 13, as a function of rising antioxidant concentration. The Figure shows clearly that elevating the concentration of the alkylphenol antioxidant from 25 to 100 ppm raised the storage stability of Gasoline A from 16 to 22 months (a raise of 37.5%) and of Gasoline B from 14 to 19 months (a raise of 26.3%). Conversely, elevated concentrations of the aromatic diamine antioxidant caused a drop in storage stability: for Gasoline A from 15 to 8 months (a drop of 46.7%), and for Gasoline B from 18 to 11 months (a drop of 38.9%). These results clearly confirms the findings of the Preliminary Stage of the study: raising the concentration of an antioxidant may cause a drop in gasoline storage stability. Additionally, the alkylphenol type additive was more active in improving storage stability than the aromatic diamine type. Another important trend is noted: storage

stability values for the aromatic diamine antioxidant in Gasoline B were generally higher than those for Gasoline A, while for the alkylphenol antioxidant the opposite was found (i.e. values for Gasoline A were higher than for Gasoline B). This is consistent with the accepted practice whereby aromatic diamines are considered more active in distillates with high olefin content[5]. Garrett[6] states that alkylphenols retard the rate of hydroperoxide formation in gasolines for periods exceeding normal storage life, and are, therefore, more suitable for prolonged storage applications. The findings of this study seem to confirm this statement.

Conclusions

Raising the concentration of an alkylphenol antioxidant in two different gasoline blends from 25 ppm to 75 and 100 ppm indeed prolonged the maximum storage interval for these blends by an average of 32%. Raising the concentration of an ariomatic diamine additive in the same blends produced the opposite effect: an apparent drop in storage stability by an average of 43%. Although the latter additive improved the oxidation stability of the blends, as measured by Induction Period, it was the former type that was more effective at inhibiting gum formation over prolonged storage intervals. This trend was found also for blends with particularly high olefin content (above 30%).

Although many sources state that a mixture of the two types usually produce more desirable effects[5,6], the findings of this study did not justify this practice. The researchers believe, however, that the 1:1 proportion tested in this study may not have been optimal, and suggest to continue studying other ratios containing more alkylphenol and less aromatic diamine antioxidant.

In general, Induction Period results improved with storage time, suggesting that this characteristic may rise as fuel oxidizes. As such, Induction Period may be used as an indication of oxidation stability of a fuel sample, but should not be used in follow-up programs. Similarly, Bromine Number results were not indicative of the gum-forming tendency of fuel samples. This is probably due to the inability to differentiate between olefin types or gum formation mechanisms using Bromine Number results alone.

Before any antioxidant system is added to a particular blend, laboratory and short-term storage trials should be run in order to ascertain that the system indeed produces the desirable effect and does not impair storage stability.

Acknowledgements

The researchers wish to express their gratitude to Dr. Brauch and Mrs. R. Brukman of Oil Refineries LTD. for providing raw materials for the preparation of the study specimens, to Dr. A. Lavie and her staff at the Chemical Testing Laboratories of the Technion Research and Development Foundation for performing all laboratory tests,

and especially to Ms. A. Vanunu and Mr. Z. Lavie of the IDF for their hard work sampling the specimens, correlating samples and tabulating results.

References

(1) Israeli Standard 90: "Automotive Gasoline: Leaded Gasoline", The Israeli Standards Institue, Jul. 1993.

(2) Israeli Standard 1499: "Automotive Gasoline: Unleaded Gasoline", The Israeli Standards Institue, May 1993.

(3) *1994 Annual Book of ASTM Standards*, Sec. 05, 1994.

(4) Owen, K., Coley,T.*Automotive Fuels Handbook* Society of Automotive Engineers, Inc., Warrendale PA, 1990, p. 181.

(5) same, pp. 188-190.

(6) Garrett, T.K. *Automotive Fuels and Fuel Systems. Vol. I: Gasoline* Society of Automotive Engineers, Inc., Warrendale PA, Pentech Press, London, 1991, pp. 19-20.

Specimen Identification Code	Gasoline Blend	Antioxidant Type	Antioxidant Concentration
111	A	Aromatic Diamine	25
112	A	Aromatic Diamine	75
113	A	Aromatic Diamine	100
121	A	Alkylphenol	25
122	A	Alkylphenol	75
123	A	Alkylphenol	100
211	B	Aromatic Diamine	25
212	B	Aromatic Diamine	75
213	B	Aromatic Diamine	100
221	B	Alkylphenol	25
222	B	Alkylphenol	75
223	B	Alkylphenol	100

Table 1: All specimens prepared for follow-up in Primary Stage, their composition and Identification Code.

Specimen ID Code	Storage Interval (months)															
	0		1		3		6		9		12		18		25	
111	>1200	>1200	1200	1150	1200	>1200	1200	1200	>1200	>1200	>1200	>1200	>1200	1170	>1200	1100
112	>1200	>1200	>1200	>1200	>1200	>1200	1200	1200	>1200	>1200	>1200	>1200	>1200	>1200	>1200	>1200
113	>1200	>1200	>1200	>1200	>1200	>1200	1200	1200	>1200	>1200	1100	>1200	>1200	>1200	>1200	>1200
121	970	>1200	1190	1170	>1200	>1200	1200	1100	1080	1120	>1200	>1200	1050	1020	1080	1150
122	>1200	>1200	>1200	>1200	>1200	>1200	>1200	1200	>1200	>1200	>1200	>1200	1170	1170	>1200	>1200
123	>1200	>1200	>1200	>1200	>1200	1200	1200	>1200	>1200	>1200	>1200	>1200	>1200	>1200	>1200	>1200
211	>1200	>1200	970	990	930	930	>1200	1200	>1200	>1200	>1200	>1200	900	>1200	820	>1200
212	>1200	>1200	>1200	>1200	>1200	>1200	>1200	>1200	>1200	>1200	>1200	>1200	>1200	>1200	>1200	>1200
213	>1200	>1200	>1200	>1200	>1200	>1200	1080	>1200	>1200	>1200	>1200	>1200	>1200	>1200	>1200	>1200
221	>1200	>1200	>1200	900	900	870	1200	1200	>1200	>1200	>1200	1090	900	900	1050	950
222	>1200	>1200	>1200	>1200	>1200	1080	1200	1140	1200	>1200	>1200	1040	>1200	970	>1200	1020
223	>1200	>1200	>1200	>1200	>1200	1050	1200	1200	1200	>1200	>1200	>1200	>1200	>1200	>1200	>1200

Table 2: Induction Period (minutes) for all specimens in Primary Stage as a function of months stored. ">1200" indicates that no breakdown occured up to the maximum test duration of 1200 minutes.

Specimen ID Code	Second Order Polynomial Regression Equation	Correlation Coefficient	Breakdown Month
111	y=5.8939 - 0.10358x + 0.022886x^2	R^2=0.804	16
112	y=5.6699 + 0.28908x + 0.0088794x^2	R^2=0.803	11
113	y=10.658 - 1.0665x + 0.096247x^2	R^2=0.840	14
121	y=5.2273 + 0.042207x + 0.012316x^2	R^2=0.890	17
122	y=5.5652 + 0.0098620x + 0.0072923x^2	R^2=0.639	24
123*	y=10.330 - 0.70831x + 0.031009x^2	R^2=0.216	28
123*	y=5.6656 - 0.25221x + 0.020742x^2	R^2=0.767	22
211	y=7.1287 - 0.11005x + 0.01513x^2	R^2=0.851	21
212	y=7.1777 - 0.042440x + 0.019505x^2	R^2=0.835	16
213	y=7.4807 - 0.22134x + 0.013575x^2	R^2=0.940	11
221	y=5.5586 - 0.12215x + 0.029537x^2	R^2=0.918	14
222	y=5.9097 - 0.12196x + 0.021760x^2	R^2=0.965	17
223	y=6.0643 - 0.12515x + 0.013248x^2	R^2=0.895	23

Table 3: Regression equation and Correlation Coefficient obtained for rate of Existent Gum formation as a function of time stored, where 'y' is Existent Gum content and 'x' is storage period in months. The 'Breakdown Month' is the month in which the calculated Existent Gum content would reach or exceed 7 mg/100ml (assuming 'zero' sample gum content equaled 3 mg/100ml). *For specimen '123', two values are provided: the first includes 1 and 6 month samples, the second disregards these results.

Specimen ID Code	Second Order Polynomial Regression Equation	Correlation Coefficient	Breakdown Month
111	y=9.2436 + 0.28748 + 0.012881x^2	R^2=0.808	15
112	y=9.3093 + 0.43761x + 0.0099171x^2	R^2=0.896	13
113	y=11.858 + 0.21725x + 0.084628x^2	R^2=0.752	8
121	y=8.9224 - 0.092352x + 0.035170x^2	R^2=0.957	16
122	y=8.6054 - 0.15052x + 0.012539x^2	R^2=0.749	19
123*	y=16.866 - 0.77351x + 0.035516x^2	R^2=0.143	29
123*	y=10.607 - 0.23984x + 0.025316x^2	R^2=0.725	23
211	y=11.619 - 0.061249x + 0.018284x^2	R^2=0.819	18
212	y=12.749 - 0.13952x + 0.017722x^2	R^2=0.814	17
213	y=13.855 + 0.38922x + 0.0039838x^2	R^2=0.843	16
221	y=9.4525 + 0.22931x + 0.020604x^2	R^2=0.843	14
222	y=9.4888 + 0.42808x + 0.0042304x^2	R^2=0.825	15
223	y=9.8293 + 0.023803x + 0.019027x^2	R^2=0.784	19

Table 3: Regression equation and Correlation Coefficient obtained for rate of Potential Gum formation as a function of time stored, where 'y' is Potential Gum content and 'x' is storage period in months. The 'Breakdown Month' is the month in which the calculated Potential Gum content would reach or exceed 15 mg/100ml (assuming 'zero' sample gum content equaled 8 mg/100ml). *For specimen '123', two values are provided: the first includes 1 and 6 month samples, the second disregards these results.

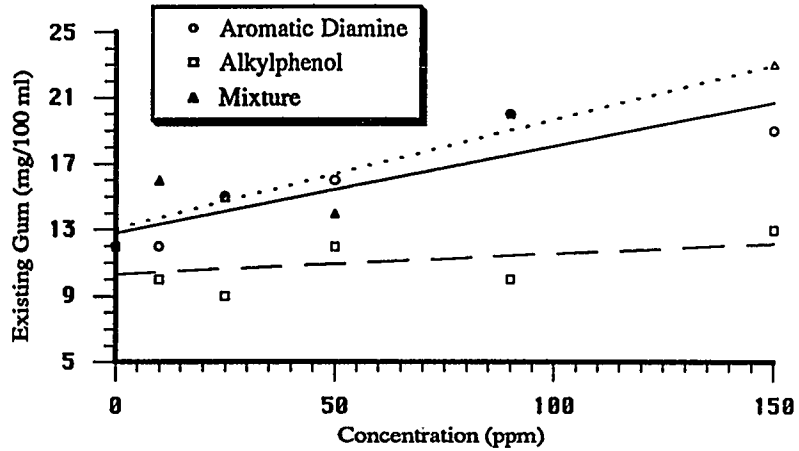

Figure 1: Existent Gum as a function of increasing antioxidant content of gasoline samples in Preliminary Stage.

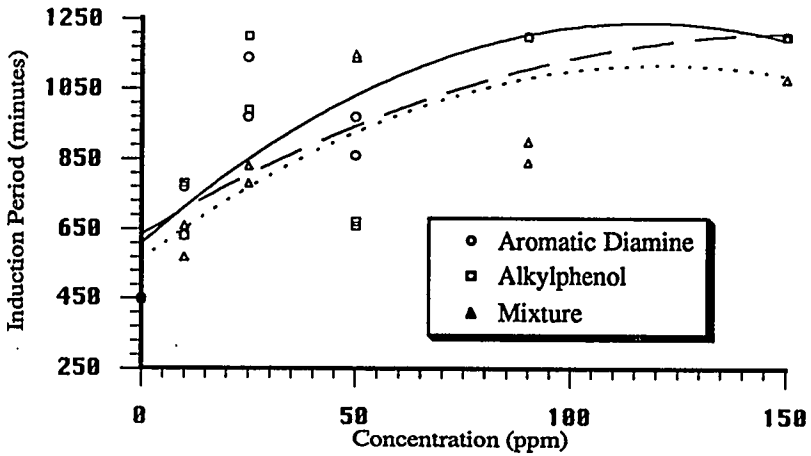

Figure 2: Induction Period as a function of increasing antioxidant of gasoline samples in Preliminary Stage.

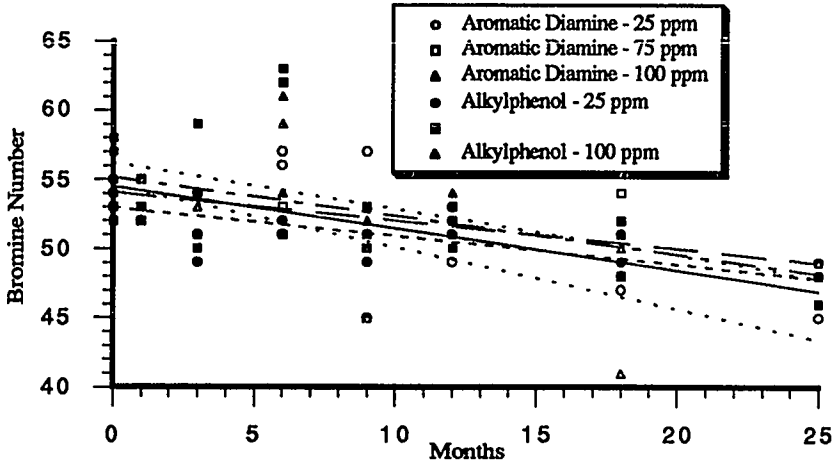

Figure 3: Bromine Number for all specimens containing Gasoline A, as a function of months stored.

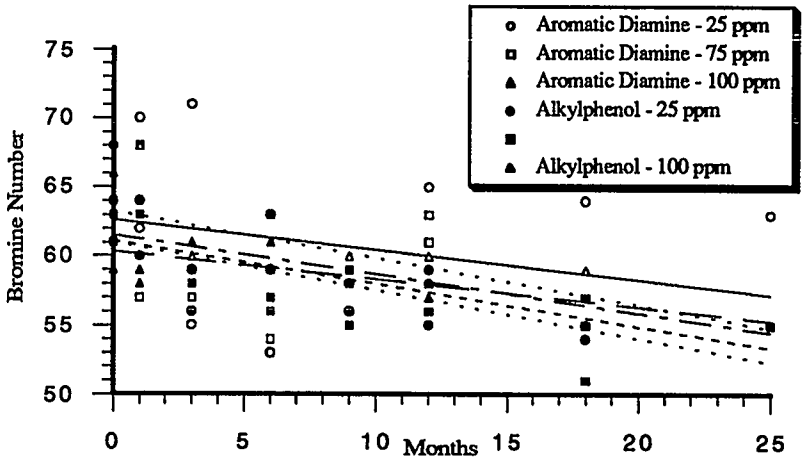

Figure 4: Bromine Number for all spcimens containing Gasoline B, as a function of months stored.

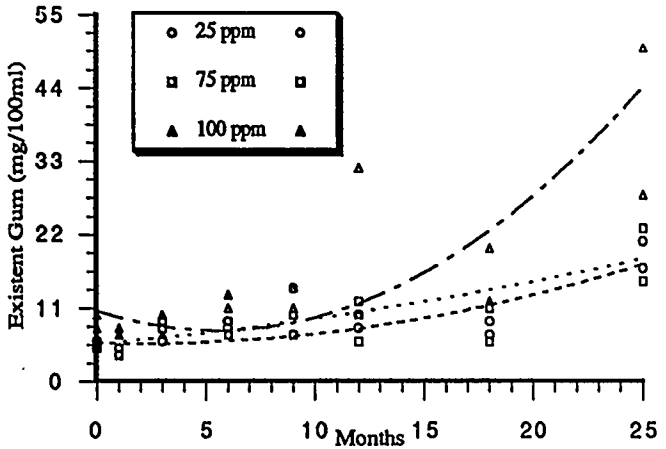

Figure 5: Existent Gum found in specimens containing Gasoline A and the aromatic diamine antioxidant, as a function of months stored.

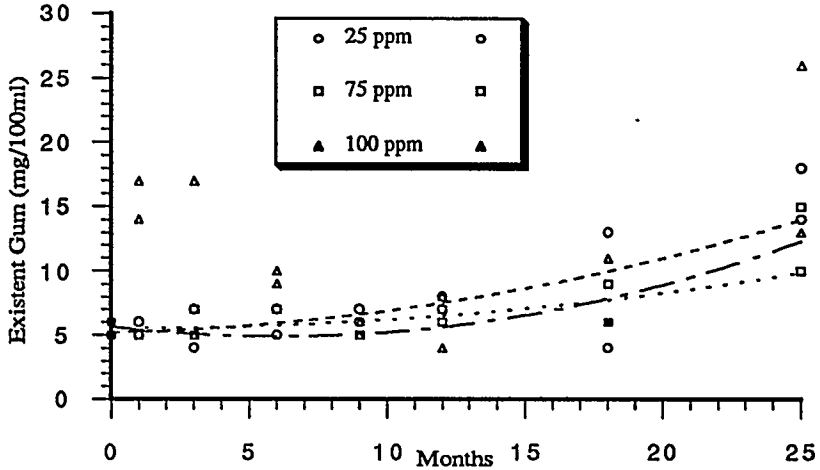

Figure 6: Existent Gum found in specimens containing Gasoline A and the alkylphenol antioxidant, as a function of months stored.

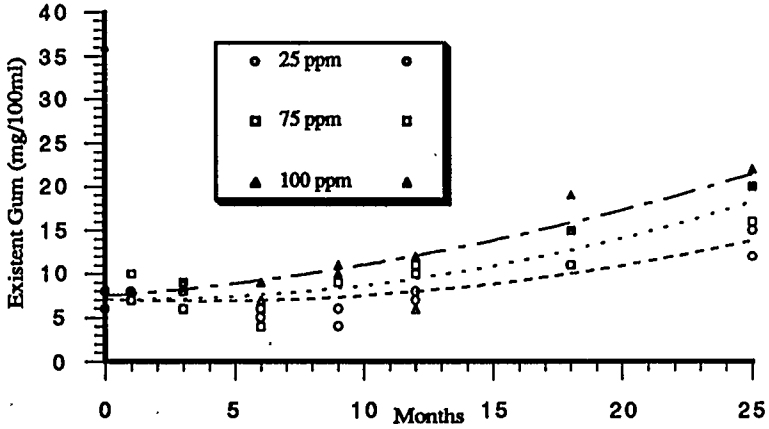

Figure 7: Existent Gum found in specimens containing Gasoline B and the aromatic diamine antioxidant, as a function of months stored.

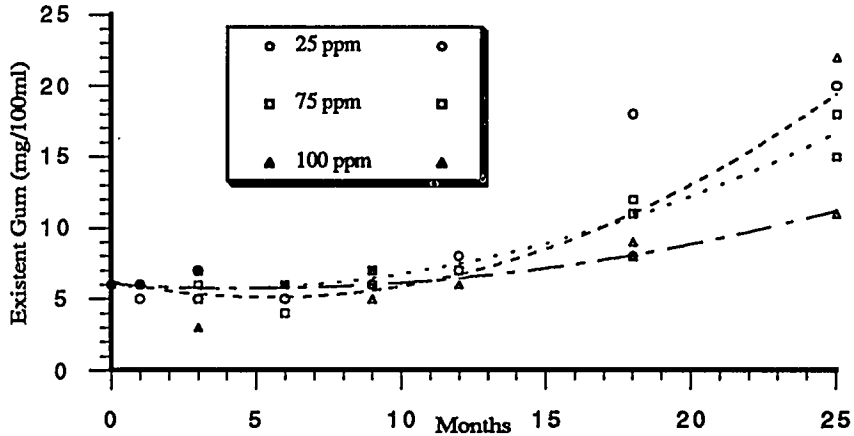

Figure 8: Existent Gum found in specimens containing Gasoline B and the alkylphenol antioxidant, as a function of months stored.

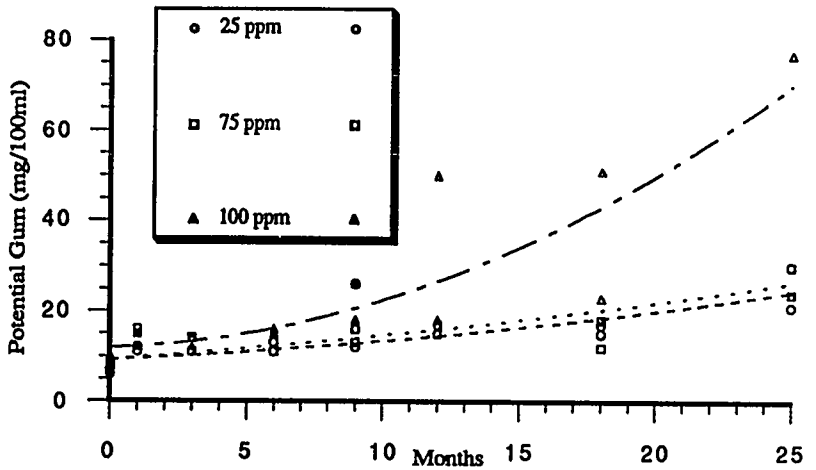

Figure 9: Potential Gum found in specimens containing Gasoline A and the aromatic diamine antioxidant, as a function of months stored.

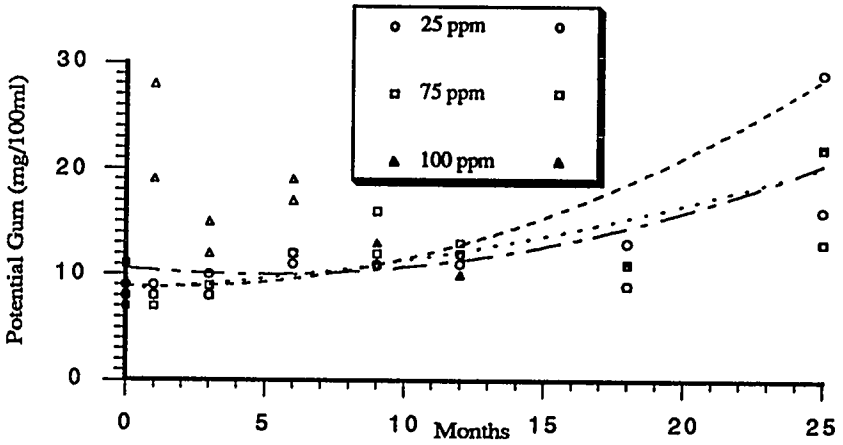

Figure 10: Potential Gum found in specimens containing Gasoline A and the alkylphenol antioxidant, as a function of months stored.

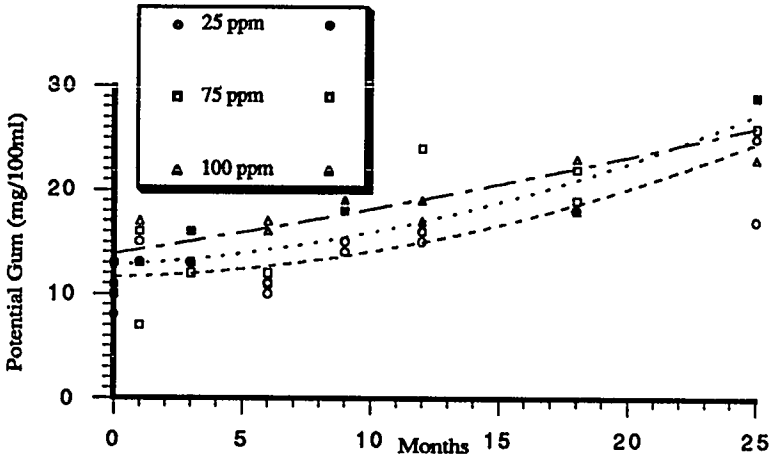

Figure 11: Potential Gum found in specimens containing Gasoline B and the alkylphenol antioxidant, as a function of months stored.

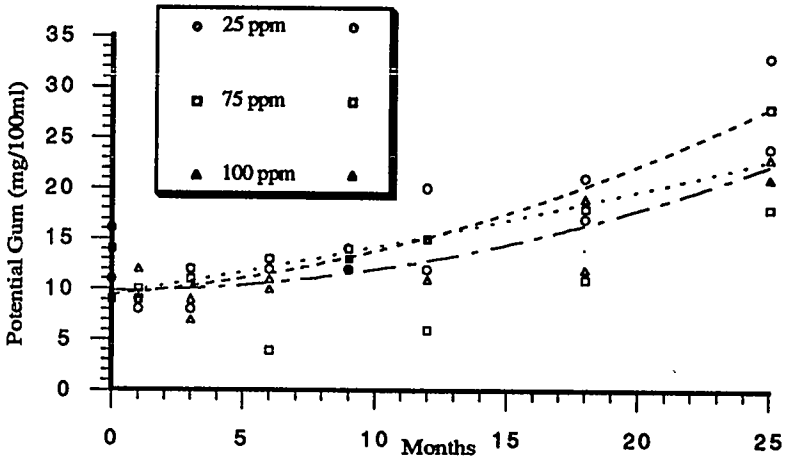

Figure 12: Potential Gum found in specimens containing Gasoline B and the alkylphenol antioxidant, as a function of months stored.

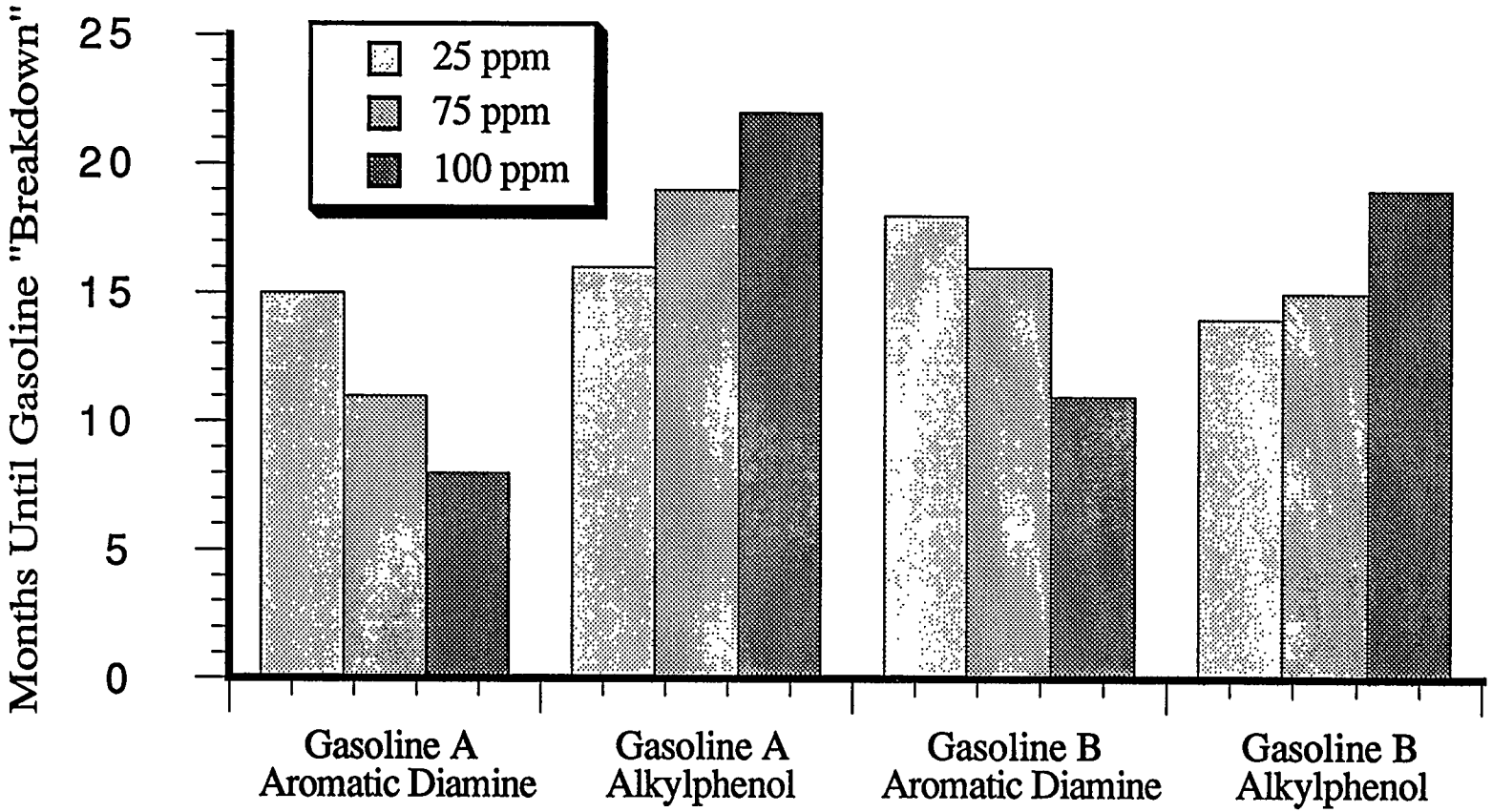

Figure 13: Calculated storage month wherein the gasoline specimen would "breakdown" and be rendered unacceptable for automotive usage.